

PDF hosted at the Radboud Repository of the Radboud University Nijmegen

The following full text is a publisher's version.

For additional information about this publication click this link.

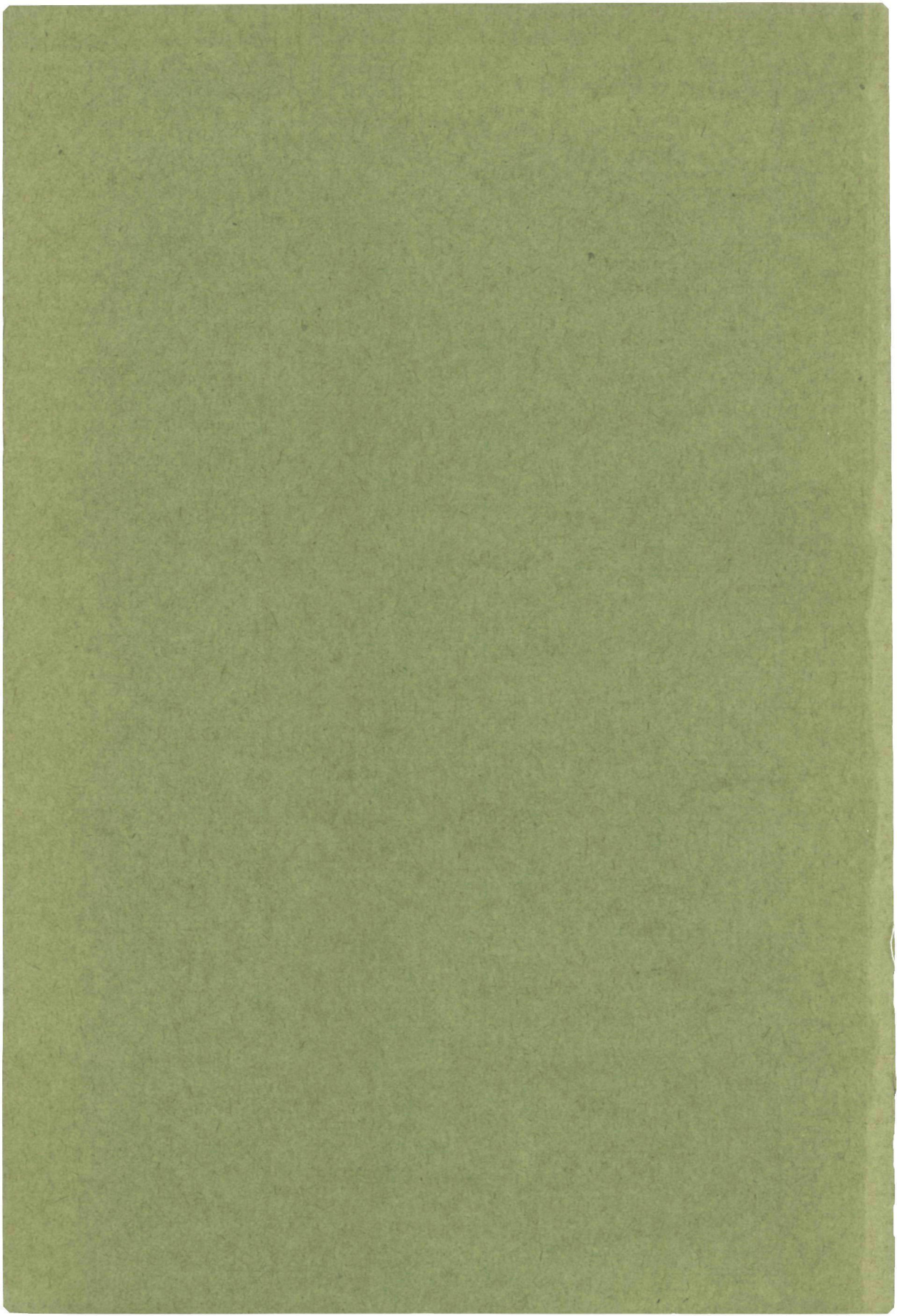
<http://hdl.handle.net/2066/148069>

Please be advised that this information was generated on 2017-12-05 and may be subject to change.

2630

AB INITIO CALCULATIONS OF
INTERMOLECULAR FORCES
AND
RELATED PROPERTIES

R.M. BERNS



AB INITIO CALCULATIONS OF
INTERMOLECULAR FORCES
AND
RELATED PROPERTIES

R.M. BERNS

Promotor: Prof.dr.ir. A. van der Avoird
Co-referent: Dr.ir. P.E.S. Wormer

AB INITIO CALCULATIONS OF INTERMOLECULAR FORCES AND RELATED PROPERTIES

Proefschrift

ter verkrijging van de graad van doctor in de wiskunde en natuurwetenschappen aan de Katholieke Universiteit te Nijmegen, op gezag van de Rector Magnificus Prof. Dr. P.G.A.B. Wijdeveld, volgens besluit van het College van Decanen in het openbaar te verdedigen op vrijdag 16 oktober 1981 des namiddags te 2.00 uur precies

door

Rutgerus Mathias Berns
geboren te Heerlen



Graag wil ik allen bedanken die bijgedragen hebben in de totstandkoming van dit proefschrift. In het bijzonder:

- (ex-)medewerkers en (ex-)studenten van de afdeling Theoretische Chemie
- medewerkers van het Universitair Rekencentrum
- medewerkers van afdelingen Illustratie, Fotografie en Reproductie
- Monique Bongers-de Bie voor het verzorgen van het type-werk.

aan mijn overleden vader,
mijn moeder

C O N T E N T S

<u>CHAPTER I</u>	General introduction and summary	1
<u>CHAPTER II</u>	N_2-N_2 interaction potential from ab initio calculations, with application to the structure of $(N_2)_2$. (J. Chem. Phys. <u>72</u> , 6107 (1980))	5
	1) Introduction	6
	2) Ab initio calculations and results	7
	3) Analytical representation of the interaction potential	13
	a- Spherical expansion	13
	b- Atom-atom representation of the ab initio potential	17
	c- Spherical expansion of the ab initio potential by numerical integration	18
	4) Applications of the N_2-N_2 interaction potential, comparison with experimental data	23
	a- Isotropic potential	23
	b- N_2 crystal properties	26
	c- Stability	26
	References	32
<u>CHAPTER III</u>	Comparison of electron gas and ab initio potentials for the N_2-N_2 interactions. Application in the second virial coefficient*. (to appear in J. Chem. Phys., January 1982)	34
	1) Introduction	35
	2) Theoretical and computational aspects	36
	1- Monomer electron density	36
	2- The interaction energy in the electron gas approach	37
	3- Representation in terms of a spherical expansion	41
	4- The second virial coefficient	43

*) This paper will also be part of the thesis by M.C. van Hemert

	3) Discussion	44
	References	54
<u>CHAPTER IV</u>	Lattice dynamics of solid N ₂ with an ab initio intermolecular potential. (J. Chem. Phys. <u>73</u> , 5305 (1980))	56
	1) Introduction	57
	2) Methods and potential	57
	3) Results	61
	4) Conclusions	68
	References	70
<u>CHAPTER V</u>	Lattice dynamics of the ethylene crystal with interaction potentials from ab initio calculations. (J. Chem. Phys. <u>69</u> , 5288 (1978))	71
	1) Introduction	72
	2) Ab initio calculations of the ethylene-ethylene interaction	74
	a- Procedure and results	74
	b- Conclusions	80
	3) Analytic fit by atom-atom potentials	84
	a- Fitting procedure and results	84
	b- Conclusions	94
	4) Lattice dynamics calculations on the ethylene crystal	98
	a- Procedure and results	98
	b- Conclusions	104
	References	110
<u>CHAPTER VI</u>	Dynamical and optical properties of the ethylene crystal; self-consistent phonon calculations using an ab initio intermolecular potential. (To appear in J. Chem. Phys.)	115
	1) Introduction	116
	2) Methods and potential	117
	1- Intermolecular potential	117
	2- Self-consistent phonon method, implementation	118

	for molecular crystals	
	3- Raman intensities	123
	4- Infrared intensities	125
	3) Results and discussion	127
	4) Conclusions	135
	References	136
<u>CHAPTER VII</u>	Ab initio calculations of the collision- induced dipole in He-H ₂ : I) A Valence Bond approach (J. Chem. Phys. <u>69</u> , 2102 (1978))	138
	1) Introduction	139
	2) Theory	140
	3) Computations	150
	4) Results and discussion	152
	Appendix	156
	References	159
<u>CHAPTER VIII</u>	MACINTOS: The many atom configuration inter- action program for orthogonal spin orbitals	161
	1) Introduction	162
	2) Theory	163
	3) Generation of a list of configurations	165
	4) Reordering the list configurations	165
	5) Generation of spin symmetry coefficients	166
	6) Generation of orthogonalization matrix	167
	7) Sorting of two-electron spin-symmetry coefficients	167
	8) Construction of H-matrix	168
	9) Orthogonalization of H-matrix	169
	10) Diagonalization of H-matrix	169
	11) Back transformation of eigenvectors to original basis	169
	12) Construction of the first order density matrix and natural orbitals	170
	13) Calculation of energy contributions	170
	14) Example	171
	References	172

<u>CHAPTER IX</u>	Finite field configuration interaction calculations on the distance dependence of the hyperpolarizabilities of H ₂ (submitted for publication)	175
	1) Introduction	176
	2) Computations	178
	3) Results and discussion	181
	4) Conclusion	192
	Appendix	193
	References	194
<u>CHAPTER X</u>	A comparison of different CI methods for the calculation of polarizabilities: the Be atom and CN ⁻ anion as example (to be published)	196
	1) Introduction	197
	2) Method	198
	3) Results	200
	1- The Be atom	200
	2- The CN ⁻ ion	201
	4) Conclusions	202
	References	204
<u>SAMENVATTING</u>		206
<u>CURRICULUM VITAE</u>		209

GENERAL INTRODUCTION AND SUMMARY

In the study of molecular gases, liquids and solids knowledge of the intermolecular potentials is basic. These intermolecular potentials are a function of the distance between the molecules involved and the orientation of these molecules with respect to each other.

In the past, potentials were exclusively obtained from experiment, by assuming a model potential, e.g. of the Lennard-Jones or Buckingham (atom-atom) type, with a limited number of parameters, chosen such that the experimental data was well reproduced. This data was obtained from experiments such as molecular beam scattering, molecular beam spectroscopy, collision induced IR absorption, pressure induced line broadening and from bulk properties (virial coefficients, transport properties). In several cases, however, this approach produced potentials which, whilst describing some experimental data quite well, did not reproduce experiments not included in the fitting. This could be due to either an inaccurate representation of the potential, the experiment may be sensitive to a different region of the potential than the measurements used in the fit, or to some deficiencies, in the models used for the experimental interpretation. In order to solve this problem, one must find other sources to obtain more information about the potential.

Nowadays, it is possible to obtain fairly accurate intermolecular potentials, by approximately solving the Schrödinger equation, applying so called ab initio quantum mechanical methods. This is not only due to theoretical improvements in the quantum chemical methods, but also to the increased power of modern computers. Still, rather small systems such as N_2-N_2 and $C_2H_4-C_2H_4$ are on the border of computational possibilities.

In this thesis the Schrödinger equation is solved in the Born-Oppenheimer approximation: i.e. the electronic equation is solved for a fixed nuclear geometry; varying the nuclear geometry yields the intermolecular potential. Model potential parameters can then be obtained by fitting a model potential of the atom-atom type to the results of ab initio calculations for a number of orientations and distances (for nitrogen and ethene in chapters II and V respectively). Next, these model potentials can be used, for example, in lattice dynamics calculations on molecular solids for comparison with experimental data (chapters IV, V and VI).

These (atom-atom) model potentials have the disadvantage that

they are difficult to improve systematically. Another analytical representation of the intermolecular potential, the so called spherical expansion, does not have this drawback. The potential is expanded in angular functions, depending on the orientations of the molecules; the expansion coefficients depend only on the intermolecular distance. These (Fourier) coefficients can be expressed as angular integrals over the intermolecular potential multiplied by angular functions and calculated by numerical integration techniques (Gauss type quadratures) (for the N_2 -dimer in chapter II and III).

The ab initio calculations are very expensive, even for rather small systems (for the $(N_2)_2$ potential: 3 hours on IBM 370/158 for each geometry). Evaluation of cheaper, but still accurate methods is important for obtaining intermolecular potentials for larger systems. One of these methods, the so called Gordon-Kim method, based on the expressions in the electron-gas theory of atoms and molecules, is tested on the nitrogen dimer (chapter III).

In a number of phenomena, not only is the intermolecular potential important, but also the effect of molecular collisions on other properties. For example, in the interpretation of collision induced IR absorption spectra (CIA) of dense gases, a knowledge of the dipole moment is required. This dipole occurs whenever two or more unlike or more than two like atoms are interacting. Just as the intermolecular potential, it is a function of the intermolecular distance and the orientations of the molecules. To calculate this interaction dipole accurately is even more difficult than the evaluation of the intermolecular potential and, so, only small systems can be considered. In chapter VII the interaction dipole for the HeH_2 system is calculated. The collision induced IR absorption in this system is believed to be responsible for the greenhouse effect on the heavy planets, which have an atmosphere containing mainly helium and hydrogen.

For large separations the intermolecular potential can be approximated by the multipole expansion. The terms in this expansion depend only on the properties of the molecules involved: permanent and transition multipole moments and polarizabilities. In other words, one can reduce the problem of calculating the potential in the long range region to the determination of the separate monomer properties. The calculation of these properties is mostly done at the Hartree-Fock (independent particle) level of accuracy. In some cases, the results are not sufficiently accurate, however, to obtain reliable intermolecular

potentials and more sophisticated methods are necessary.

One of these methods for obtaining the effects of electron correlation is the Configuration Interaction (CI) method. The wavefunction is written in terms of (spin adapted) configuration functions and the variational solutions of the Schrödinger equation are obtained by diagonalization of the Hamiltonian matrix. For larger molecules the method becomes rather complicated. For example, not all of the spin-symmetry coefficients, necessary for the construction of the Hamiltonian matrix from the molecular integrals, can simultaneously be kept in the main storage of the computer; neither can the molecular integrals. Furthermore, the complete H-matrix does not fit into main storage during its construction and diagonalization and obtaining all eigenvalues and eigenvectors becomes impossible. This implies that special techniques are necessary to avoid severe computational problems. In chapter VIII a computer program is described, which has been developed for large scale CI calculations.

As an application of the CI method, the hyperpolarizabilities of hydrogen are calculated as a function of the internuclear distance (in chapter IX). The calculation is performed at the "full CI" level (i.e. including all singlet configurations which can be constructed within the given orbital basis). Because the hyperpolarizabilities are highly sensitive to the quality of the basis set, large bases are needed and, even for this two electron system, the full CI calculation is not an easy job.

For many-electron systems full CI becomes impractical: The expansion of the wavefunction has to be shortened. This can be accomplished either by using a better molecular orbital basis (natural orbitals) or by truncating the configuration space, or both. There are, of course, several methods of doing this, each with advantages and drawbacks. In chapter X two are investigated: The Iterative Natural Orbital (INO) method with a configuration space containing all single and double excitations from the Hartree-Fock ground state and INO with a "first-order" wavefunction (containing all single excitations from a full CI space, which is generated by the valence orbitals). Tests are performed on the Be atom, where the electron correlation effects on the polarizability are relatively large. Next the methods are used to calculate the polarizability of the CN^- ion.

For more details about the problems treated and the results obtained, the reader is referred to the individual chapters, which have their own abstracts, introductions and conclusions.

N_2-N_2 interaction potential from ab initio calculations,
with application to the structure of $(N_2)_2$ [†]

Rut M. Berns and Ad van der Avoird

Institute of Theoretical Chemistry

University of Nijmegen

Toernooiveld, Nijmegen

The Netherlands

Abstract

The short range electrostatic and (first order) exchange contributions to the N_2-N_2 interaction energy have been calculated ab initio as a function of the N_2 orientations and the distance (139 geometries). Using a numerical integration procedure, the results have been represented analytically in the form of a spherical expansion. At $R = 0.3$ nm this expansion is accurate to better than 0.5% if we include the first 18 independent terms, to 2% if we truncate after $L_A=L_B=4$ and to 16% if we truncate after $L_A=L_B=2$. In combination with the long range multipole expansion results (electrostatic R^{-5}, R^{-7}, R^{-9} terms, dispersion R^{-6}, R^{-8}, R^{-10} terms) calculated by Mulder et al., this yields an anisotropic N_2-N_2 interaction potential in the region of the Van der Waals minimum, which can be fairly well represented also by a site-site model. The potential is in good agreement with the available experimental data for the gas phase and for the ordered (α and γ) crystal phases of solid N_2 . The structure of the Van der Waals molecule $(N_2)_2$ is discussed; its energy is lowest for the crossed structure: $\Delta E_m = 1.5$ kJ/mol, $R_m = 0.35$ nm (for the isotropic potential the well characteristics are: $\Delta E_m = 0.75$ kJ/mol, $R_m = 0.417$ nm). The (staggered) parallel and the T-shaped structures are slightly higher in energy. The internal N_2 rotation barriers vary from 0.2 kJ/mol (17 cm⁻¹) to values comparable with the dissociation energy.

[†] Supported in part by the Netherlands Foundation for Chemical Research (SON) with financial aid from the Netherlands Organization for the Advancement of Pure Research (ZWO)

1. Introduction

Knowledge of the intermolecular interaction potential is basic for understanding the properties of molecular gases, liquids and solids. In principle, this interaction potential can be derived from experimental sources. In practice one has to introduce model potentials with a limited number of parameters and then to fit these parameters to the experimental data. For nitrogen much work has been done in this direction (see [1,2]) using gas phase data (virial coefficients, viscosity data) as well as solid state properties (from X-ray diffraction, IR, Raman and nuclear resonance spectroscopy, neutron scattering). Model potentials which have been used [1,2] are molecular ones, isotropic or elliptical, and atom-atom potentials, with distance dependent functions mostly of the Lennard-Jones (12-6) or Buckingham (exp-6) type. Sometimes, these have been supplemented with the electrostatic quadrupole-quadrupole interaction [2]. In spite of all these efforts, there is still no N_2-N_2 interaction potential available at present that is universal, in the sense that it fits all the different experimental data. Especially, the anisotropy of the potential, its dependence on the relative N_2-N_2 orientations, has not been established unequivocally.

Another way to determine the N_2-N_2 interaction potential is by ab initio calculations. Such calculations, which yield the anisotropic interactions, have been performed by Mulder et al. [3] in the long range region where the interaction potential can be expanded as a multipole series, i.e. in powers of the distance R . Here, we report results for shorter distances, including the physically important region around the Van der Waals minimum. These have been obtained from ab initio calculations which avoid the multipole expansion of the interaction operator and which take the intermolecular exchange into account (in first order). The results are given for a set of intermolecular distances and molecular orientations, but, also, we present two analytical representations of the interaction potential. The first one is a spherical expansion in terms of the angles describing the molecular orientations. Such an expansion is obtained directly in the long range if one substitutes a spherical multipole expansion into the Rayleigh-Schrödinger perturbation expressions for the interaction energy [4,5]; in the short range a fitting or

numerical integration procedure is required, which we describe. Also, we discuss the convergence of this spherical expansion. The second approximate representation of the ab initio results is in the form of an atom-atom potential.

2. Ab initio calculations and results

The interaction energy between two N_2 molecules A and B has been calculated in a general space fixed coordinate system as a function of the orientations, described by the polar coordinates $\underline{\omega}_A = (\theta_A, \phi_A)$ and $\underline{\omega}_B = (\theta_B, \phi_B)$, and the distance vector $\vec{R} = (R, \underline{\Omega}) = (R, 0, \phi)$. In order to simplify the calculations, we have chosen a special frame with the z-axis along \vec{R} ($0 = \phi = 0$) and molecule B in the xz plane ($\phi_B = 0$), and we have varied only the "internal" coordinates, $R, \theta_A, \theta_B, \phi_A$. The energy has been calculated up to second order in perturbation theory.

a. The first order interaction energy, including exchange, is defined as:

$$\begin{aligned} \Delta E^{(1)}(\underline{\omega}_A, \underline{\omega}_B, \vec{R}) = & \langle A \psi_0^A \psi_0^B | H^{AB} | A \psi_0^A \psi_0^B \rangle \\ & - \langle \psi_0^A | H^A | \psi_0^A \rangle - \langle \psi_0^B | H^B | \psi_0^B \rangle \end{aligned} \quad (1)$$

The nitrogen monomer wave functions ψ_0^A and ψ_0^B have been taken as ground state Hartree-Fock MO-LCAO functions (Slater determinants). The N-N distance was fixed at the experimental value of 0.1094 nm [6]. The operators H^{AB} , H^A and H^B are the dimer and monomer hamiltonians, respectively; A is the normalized anti-symmetrizer of the dimer. For the expansion of the MO's the AO basis set D of Mulder et al. [3], including two d-type polarization functions, has been used. This large basis is necessary in order to obtain reliable molecular multipole moments [3].

This first order energy $\Delta E^{(1)}$ can be separated into an electrostatic component, $\Delta E_{elec.}^{(1)}$, defined by (1) with the operator A replaced by the identity, and an exchange component defined as:

$$\Delta E_{exch.}^{(1)} = \Delta E^{(1)} - \Delta E_{elec.}^{(1)}$$

For large intermolecular distances one can approximate $\Delta E_{\text{elec}}^{(1)}$ by a power series in R by substituting the multipole expansion for the interaction operator $V_{\text{H}^{\text{A}}\text{H}^{\text{B}}}^{\text{AB}}$:

$$\Delta E_{\text{mult.}}^{(1)} = \sum_n C_n(\omega_{\text{A}}, \omega_{\text{B}}, \Omega) R^{-n}$$

with $n=5, 7, 9, \text{etc.}$ Actually, this expansion is an asymptotic series. The deviation $\Delta E_{\text{pen.}}^{(1)} = \Delta E_{\text{elec.}}^{(1)} - \Delta E_{\text{mult.}}^{(1)}$ is due to the penetration between the charge clouds of the two nitrogen molecules, which increases exponentially with decreasing distance.

b. The second order interaction energy, without exchange, is defined as:

$$\Delta E^{(2)} = \sum_{a, b \neq 0, 0} \frac{|\langle \psi_0^{\text{A}} \psi_0^{\text{B}} | V^{\text{AB}} | \psi_a^{\text{A}} \psi_b^{\text{B}} \rangle|^2}{E_0^{\text{A}} - E_a^{\text{A}} + E_0^{\text{B}} - E_b^{\text{B}}} \quad (2)$$

The second order exchange energy has been neglected as it is rather small in the region around the Van der Waals minimum for those cases where it has been evaluated [7]. The excited monomer wave functions, ψ_a^{A} and ψ_b^{B} , are constructed by exciting one electron to a virtual ground state Hartree-Fock MO; the energy differences in the denominator are replaced by orbital energy differences. This choice is sometimes called the uncoupled Hartree-Fock perturbation method [8]. The same method and some other perturbation methods have been applied to the long range $\text{N}_2\text{-N}_2$ interaction energy by Mulder et al. [3], who also discussed the quantitative defects of these methods. The second order energy can be separated into an induction and a dispersion part:

$$\begin{aligned} \Delta E^{(2)} &= \sum_{a, b \neq 0, 0} \dots \\ &= \sum_{\substack{a \neq 0 \\ b=0}} \dots + \sum_{\substack{a=0 \\ b \neq 0}} \dots + \sum_{\substack{a \neq 0 \\ b \neq 0}} \dots \\ &= \Delta E_{\text{ind. A}}^{(2)} + \Delta E_{\text{ind. B}}^{(2)} + \Delta E_{\text{disp.}}^{(2)} = \Delta E_{\text{ind.}}^{(2)} + \Delta E_{\text{disp.}}^{(2)}. \end{aligned}$$

For large intermolecular distances one can again substitute the multipole expansion for V^{AB} and obtain the series:

$$\Delta E_{\text{mult.}}^{(2)} = \sum_n C_n(\underline{\omega}_A, \underline{\omega}_B, \underline{\Omega}) R^{-n}$$

with $n=6,8,10$, etc. The charge penetration effect is defined by the difference:

$$\Delta E_{\text{pen.}}^{(2)} = \Delta E^{(2)} - \Delta E_{\text{mult.}}^{(2)}$$

For the calculation of the second order energy the MO's have been expanded in the basis G' of Mulder et al. [3] which contains d and f type atomic polarization functions. The addition of f functions to the first order basis D , but, also, a somewhat different optimization of the orbital exponents, is necessary in order to ensure approximate completeness of the excited state wave functions, ψ_a^A and ψ_b^B [3,9].

The first order interaction energy and its components have been calculated, in first instance, for 6 orientations and several distances of the N_2 molecules in the dimer (34 different geometries). The results are listed in table 1 and plotted for two parallel N_2 molecules as a function of distance in fig. 1. From these results we observe that the first order penetration and exchange effects are quite important already at the Van der Waals minimum. (This minimum lies at $R = 0.413$ nm for the isotropic potential, see below, and at $R = 0.36$ nm for the parallel dimer, see fig. 1). This conclusion agrees with the penetration effect calculations by Ng et al. [10].

The second order interaction energy has been calculated for 10 geometries only, see table 2 and fig. 1. We have found, just as Mulder et al. [3], that the induction energy can be neglected with respect to the dispersion energy. The second order penetration energy is much smaller than the corresponding first order contribution. Therefore, the second order energy can be well represented by the dispersion multipole series, $\Delta E_{\text{mult.,disp.}}^{(2)}$. Mulder et al. [3] have pointed out, however, that the dispersion multipole coefficients obtained by the uncoupled Hartree-Fock perturbation method (but al-

Table 1: First order interaction energy contributions

geometry ^{a)} $\theta_A, \theta_B, \phi_A$ R [nm]	$\Delta E^{(1)}$ ^{b)} [kJ mol ⁻¹]	$\Delta E^{(1)}$ ^{b)} exch. [kJ mol ⁻¹]	$\Delta E^{(1)}$ ^{b)} elec. [kJ mol ⁻¹]	$\Delta E^{(1)}$ ^{c)} mult. [kJ mol ⁻¹]
90 ^o , 90 ^o , 0 ^o				
0.331	3.991	4.481	-0.490	0.375
0.357	1.562	1.564	-0.002	0.259
0.384	0.640	0.531	0.109	0.187
0.410	0.291	0.176	0.115	0.139
0.437	0.154	0.056	0.098	0.105
90 ^o , 90 ^o , 90 ^o				
0.331	3.519	4.154	-0.635	0.134
0.357	1.331	1.461	-0.130	0.096
0.384	0.505	0.499	0.006	0.071
0.410	0.201	0.166	0.035	0.053
0.437	0.089	0.054	0.035	0.040
45 ^o , 45 ^o , 0 ^o				
0.331	15.619	21.689	-6.070	-0.649
0.357	5.753	7.985	-2.232	-0.467
0.384	1.975	2.855	-0.880	-0.337
0.410	0.588	0.992	-0.404	-0.246
0.437	0.109	0.335	-0.226	-0.182
45 ^o , 135 ^o , 0 ^o				
0.331	27.187	35.132	-7.945	1.391
0.357	10.440	12.508	-2.068	0.889
0.384	4.045	4.340	-0.295	0.593
0.410	1.625	1.469	0.156	0.409
0.437	0.706	0.484	0.222	0.291
0 ^o , 0 ^o , 0 ^o				
0.331	104.589	142.630	-38.041	4.177
0.357	43.925	55.629	-11.704	2.525
0.384	15.959	18.882	-2.923	1.601
0.410	6.299	6.600	-0.301	1.057
0.437	2.586	2.249	0.337	0.721
0.463	1.152			
0.489	0.582			
0.516	0.340			
0.542	0.224			
0 ^o , 90 ^o , 0 ^o				
0.331	17.515	24.113	-6.598	-0.747
0.357	6.345	8.718	-2.373	-0.533
0.384	2.133	3.067	-0.934	-0.384
0.410	0.613	1.050	-0.437	-0.280
0.437	0.099	0.349	-0.250	-0.208

continued

- a) Coordinate system described in text; data for 105 additional orientations have been calculated at $R = 0.3$ nm (see table 4)
- b) Monomer MO's and integrals calculated with the ATMOL3 program. We thank dr. M.F. Guest, Daresbury Laboratory, UK, for making this program available to us and mr. J. van Lierop for assistance with the implementation. Interaction energies evaluated with the program COULEX written by P.E.S. Wormer, Nijmegen. GTO basis set 9s, 5p, 2d contracted to 4s, 3p, 2d. (basis D of ref. [3])
- c) Obtained from the multipole moments of ref. [3], calculated in the same basis D

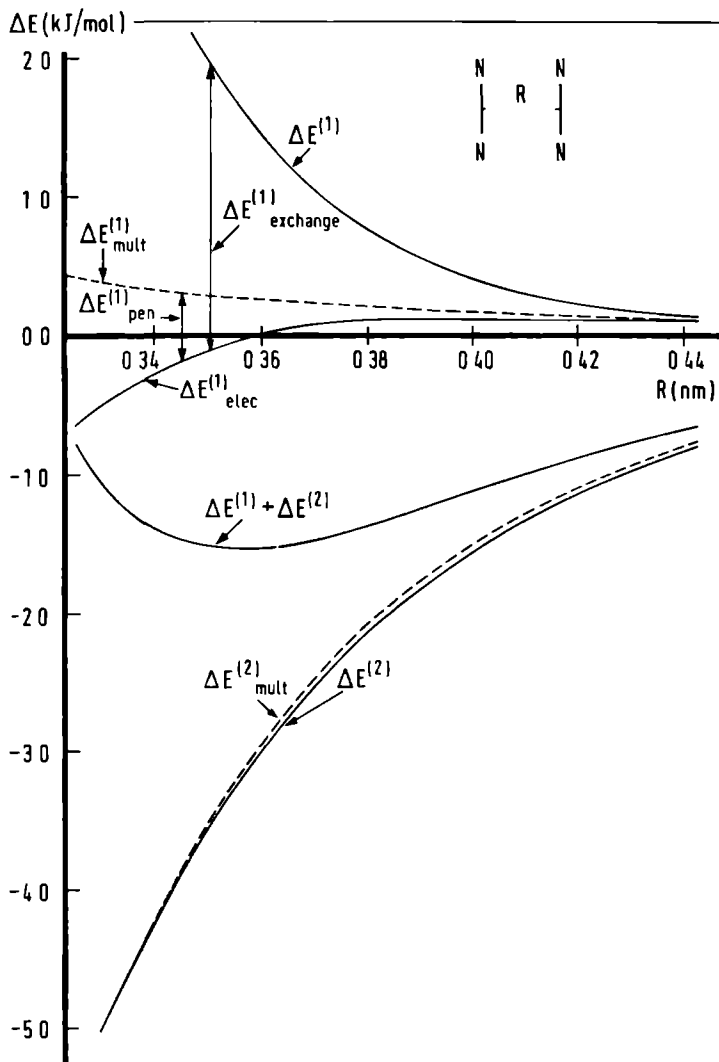


Fig. 1. Different contributions (as defined in the text) to the interaction energy between two parallel N_2 molecules; ab initio results, see tables 1 and 2.

so by other perturbation methods starting from Hartree-Fock monomer wave functions) are rather inaccurate for N_2-N_2 . Using accurate semi-empirical data for C_6 and for the dipole polarizability (from dipole oscillator strength distributions) in combination with their ab initio results, they have made better estimates for the higher multipole coefficients C_8 and C_{10} and the corresponding anisotropy factors. From here on, we shall use the latter results ([3], table 6) in order to represent the second order N_2-N_2 interaction energy.

The total, first plus second order, interaction energies have been plotted in fig. 2.

3. Analytical representation of the interaction potential

a. Spherical expansion

The dependence of the (anisotropic) interaction potential between two molecules A and B on the orientations of these molecules can be explicitly expressed in the form of a spherical expansion [11-13]. For two identical homonuclear diatomic molecules this expansion reads:

$$\Delta E(\underline{\omega}_A, \underline{\omega}_B, \vec{R}) = (4\pi)^{3/2} \sum_{L_A \geq L_B} \sum_{L} V_{L_A, L_B, L}(R) (2 - \delta_{L_A, L_B}) \times \\ (L_A, L_B, L \text{ even}) \\ \frac{1}{2} \left[A_{L_A, L_B, L}(\underline{\omega}_A, \underline{\omega}_B, \underline{\Omega}) + A_{L_B, L_A, L}(\underline{\omega}_A, \underline{\omega}_B, \underline{\Omega}) \right] \quad (3a)$$

with the angular functions given by:

$$A_{L_A, L_B, L}(\underline{\omega}_A, \underline{\omega}_B, \underline{\Omega}) = \sum_{M_A, M_B, M} \begin{pmatrix} L_A & L_B & L \\ M_A & M_B & M \end{pmatrix} Y_{L_A, M_A}(\underline{\omega}_A) Y_{L_B, M_B}(\underline{\omega}_B) Y_{L, M}(\underline{\Omega}) \quad (3b)$$

The functions $Y_{L, M}(\underline{\omega})$ are spherical harmonics [14] which are coupled with the aid of a Wigner 3-j symbol $\begin{pmatrix} L_A & L_B & L \\ M_A & M_B & M \end{pmatrix}$ to a scalar. I.e., the angular functions $A_{L_A, L_B, L}$ are invariant under rotations of the total system [13]. The expansion coefficients $V_{L_A, L_B, L}$, which are functions of the distance only, completely determine the orientational dependence of the intermolecular interaction potential.

Table 2: Second order interaction energy contributions

geometry ^{a)} $\theta_A, \theta_B, \phi_A$ R [nm]	$\Delta E_{\text{ind.}}^{(2)}$ ^{b)} [kJ mol ⁻¹]	$\Delta E_{\text{mult., ind.}}^{(2)}$ ^{c)} [kJ mol ⁻¹]	$\Delta E_{\text{disp.}}^{(2)}$ ^{b)} [kJ mol ⁻¹]	$\Delta E_{\text{mult., disp.}}^{(2)}$ ^{c)} [kJ mol ⁻¹]
90 ^o , 90 ^o , 0 ^o				
0.331	-0.070	-0.015	-5.045	-5.046
0.357	-0.018	-0.009	-3.074	-3.009
0.384	-0.007	-0.005	-1.931	-1.877
0.410	-0.003	-0.003	-1.250	-1.216
0.437	-0.002	-0.002	-0.833	-0.813
90 ^o , 90 ^o , 90 ^o				
0.331	-0.066	-0.019	-4.606	-4.654
45 ^o , 45 ^o , 0 ^o				
0.331	-1.462	-0.042	-10.162	-10.099
45 ^o , 135 ^o , 0 ^o				
0.331	-2.858	-0.076	-12.528	-11.417
0 ^o , 0 ^o , 0 ^o				
0.331	-17.996	-0.312	-24.899	-19.314
0 ^o , 90 ^o , 0 ^o				
0.331	-1.250	-0.097	-10.033	-9.629

a) Coordinate system defined in text

b) Monomer MO's and integrals calculated with the IBMOL package written by E. Clementi and coworkers; interaction energies with a program written by R.M. Berns, Nijmegen, which is a modification of the program written by T.P. Groen, Utrecht. GTO basis 9s, 5p, 2d, 1f contracted to 4s, 3p, 2d, 1f (basis G' of ref. [3])

c) Obtained from the multipole coefficients in table 4 of ref. [3], which have been calculated with the same basis G'

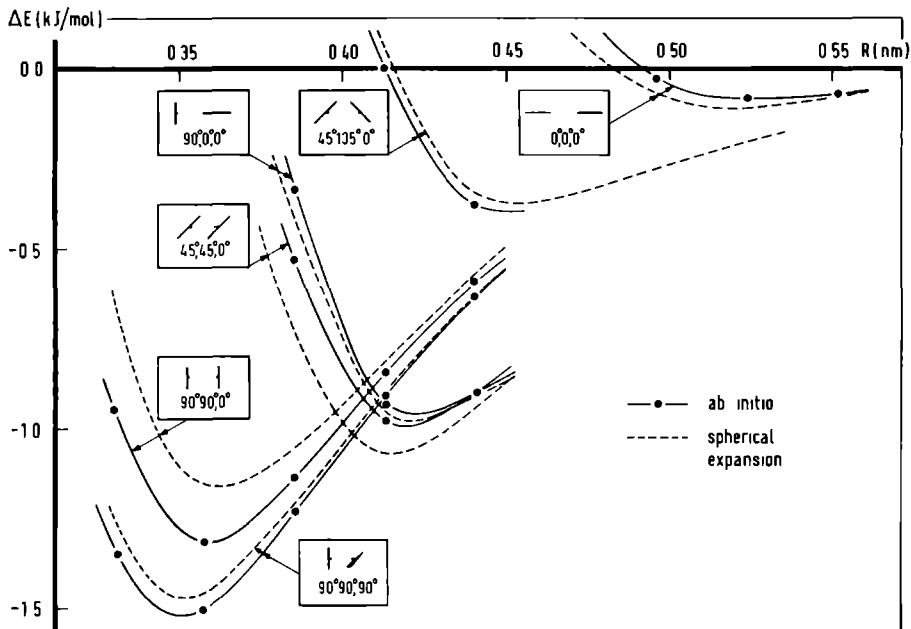


Fig. 2. Total interaction energy at 6 different orientations.
 "Ab initio": first order energy from table 1, second order energy from the dispersion multipole coefficients of ref. [3] (table 6), see our table 5.
 Spherical expansion see table 5.

For a given potential $\Delta E(\underline{\omega}_A, \underline{\omega}_B, \vec{R})$ they can be expressed as:

$$V_{L_A, L_B, L}(R) = (4\pi)^{-3/2} \int d\underline{\omega}_A \int d\underline{\omega}_B \int d\underline{\Omega} A_{L_A, L_B, L}(\underline{\omega}_A, \underline{\omega}_B, \underline{\Omega}) \Delta E(\underline{\omega}_A, \underline{\omega}_B, \vec{R}) \quad (4)$$

Here, we have used the orthonormality of the angular functions $A_{L_A, L_B, L}$. Since $A_{0,0,0} = (4\pi)^{-3/2}$ and $\int d\underline{\omega}_A \int d\underline{\omega}_B \int d\underline{\Omega} = (4\pi)^3$ it is obvious that $V_{0,0,0}(R)$ is just the isotropic potential.

In the long range, where the multipole expansion for V^{AB} can be used, the first and second order interaction energies, $\Delta E_{\text{mult.}}^{(1)}$ and $\Delta E_{\text{mult.}}^{(2)}$, are easily obtained in the form (3). All one has to do is use an expansion of V^{AB} in terms of spherical multipoles [4]; in first order this leads directly to the result (3), in second order some angular momentum recoupling has to be done [4,5]. In both cases, the expansion coefficients $V_{L_A, L_B, L}(R)$ are simply powers of R^{-1} then, multiplied by constant coefficients $C_n^{L_A, L_B, L}$, which contain the properties of the systems A and B (multipole moments in first order, multipole transition moments and excitation energies in second order). These multipole coefficients have been calculated for N_2-N_2 by Mulder et al. [3]. So, the present paper only deals with the spherical expansion of the (ab initio) calculated short range interactions, $\Delta E_{\text{pen.}}^{(1)}$ and $\Delta E_{\text{exch.}}^{(1)}$.

At first we have tried a procedure which has been used for H_2 -He [15,16] and H_2 - H_2 [17]. From the interaction energy calculated for five different orientations (at a given distance R) we have computed the first five spherical expansion coefficients: $V_{0,0,0}$, $V_{2,0,2}$, $V_{2,2,0}$, $V_{2,2,2}$, $V_{2,2,4}$. This simply involves the solution of a system of five simultaneous linear equations. The results for the sixth orientation have been used as a check on the accuracy of the expansion coefficients. This procedure has been repeated for different choices of orientations, but the results were always poor. So we concluded that, either the spherical expansion is far from having converged with these first five terms, or the applied procedure is not numerically stable (if the remaining terms in the expansion are small but not negligible), or both. In order to investigate these questions we have proceeded as follows.

b. Atom-atom representation of the *ab initio* potential

The interaction energy between the two N_2 molecules has been approximated by an atom-atom potential:

$$\Delta E^{AB} = \sum_{i \in A} \sum_{j \in B} V_{ij}$$

with V_{ij} being dependent only on the distance r_{ij} between the atoms:

$$V_{ij}(r_{ij}) = q_i q_j r_{ij}^{-1} - C_{ij} r_{ij}^{-6} + A_{ij} \exp(-B_{ij} r_{ij})$$

The electrostatic interaction potential, which is added to the Buckingham (exp-6) potential, depends on the charges q_i, q_j of the atoms. It is obvious that this model as such cannot represent the electrostatic interaction between N_2 molecules, since the atomic charges should be zero. Therefore, we have chosen for a generalized atom-atom (site-site) model with two positive and two negative charges (of equal magnitude) placed symmetrically on the N-N axis. Also the force centers of the exponential and the r^{-6} site-site potentials have been allowed to shift (independently) along the N-N axes. The (three parameter) point charge model could in principle represent the first three non-zero multipole moments of N_2 ; in fact, it can do this only if they satisfy the relation:

$Q_{2,0} Q_{6,0} \leq (Q_{4,0})^2 \leq \frac{4}{3} Q_{2,0} Q_{6,0}$, which does not hold for the calculated multipole moments of N_2 [3]. We have fitted the site-site potential parameters to the *ab initio* results, calculated for six orientations and six distances $0.30 \leq R \leq 0.44$ nm. The fits have been performed in three separate steps, just as for ethylene [18], in order to avoid correlation between the fit parameters.

- (1) The charges $q = q_+ = -q_-$ and the position parameters z_+ and z_- have been found by fitting $\sum_i \sum_j q_i q_j r_{ij}^{-1}$ to $\Delta E_{\text{mult.}}^{(1)}$, calculated up to R^{-9} terms inclusive, using the multipole moments of ref. [3], (mean deviation 6.5% for 36 points).
- (11) The parameter $C = C_{N-N}$ and the positional parameter of the r^{-6} force centers have been found by fitting $\sum_i \sum_j C r_{ij}^{-6}$ to $\Delta E_{\text{mult.}}^{(2)}$, calculated up to R^{-10} terms inclusive from the multipole coefficients of ref. [3], table 6, (mean deviation 6.3%, or 9.7% if the force centers were fixed on the nuclei).

(111) The sum of the short range contributions $\Delta E_{\text{pen.}}^{(1)}$ and $\Delta E_{\text{exch.}}^{(1)}$, emerging from the present ab initio calculations, has been fitted by the exponential site-site potential $\sum_i \sum_j A \exp(-B r_{ij})$. Both short range components indeed appear to behave as an exponential. This has yielded the parameters $A = A_{\text{N-N}}$ and $B = B_{\text{N-N}}$ (mean deviation 9.2%); the optimum positions of the force centers practically coincide with the nuclear positions, in this case.

The results have been listed in table 3. We conclude that for $\text{N}_2\text{-N}_2$ the generalized atom-atom (site-site) potential forms a rather good representation of the ab initio results (see also figs. 3 and 4). Especially for the short range interactions the fit is much better than for the ethylene case [18]. Possibly this is due to the effect of the nitrogen lone pair electrons balancing the effects of chemical bonding on the charge distribution. (The fact that the intermolecular interaction is not an additive (isotropic) atom-atom interaction is caused, of course, by the chemical bonding). Also for a much larger set of orientations where the $\text{N}_2\text{-N}_2$ interaction potential has been calculated ab initio (see below), the site-site potential yields a rather good description of the anisotropy (see next section, table 4).

c. Spherical expansion of the ab initio potential by numerical integration

Since the site-site potential yields a rather good description of the ab initio calculated $\text{N}_2\text{-N}_2$ potential, we can now use the first in order to obtain a reliable spherical expansion of the latter. First, we have made a spherical expansion of the site-site potential. For this known potential the expansion coefficients can be obtained from formula (4), by performing the angular integration. This integration can be considerably simplified:

- using the invariance of ΔE and $A_{L_A, L_B, L}$ under rotations of the total system. This reduces the integration to the three "internal" angles $\theta_A, \theta_B, \phi_A$ ($0 = \phi = \phi_B = 0$). The angular functions can be written as:

$$A_{L_A, L_B, L} = \left[\frac{(2L_A + 1)(2L_B + 1)(2L + 1)}{64\pi^3} \right]^{\frac{1}{2}} \sum_{M_A=0}^{L_B} \int_{M_A=0}^{L_B} (2 - \delta_{M_A, 0}) (-1)^{M_A} \times$$

$$\left[\frac{(L_A - M_A)! (L_B - M_A)!}{(L_A + M_A)! (L_B + M_A)!} \right]^{\frac{1}{2}} \begin{pmatrix} L_A & L_B & L \\ M_A & -M_A & 0 \end{pmatrix} P_{L_A}^{M_A}(\cos\theta_A) P_{L_B}^{M_A}(\cos\theta_B) \cos M_A \phi_A$$

Table 3. Atom-atom potential fitted to the "ab initio" data

Parameters	I	II
	fit for $0.33 < R < 0.44$ nm	fit for $0.30 < R < 0.44$ nm
Electrostatic:		
charges ^{a)} $q=q_+=-q_-$	0.373 e ^{b)}	0.379 e ^{b)}
positions ^{a)} z_+, z_- [nm]	$\pm 0.0847, \pm 0.1044$	$\pm 0.0848, \pm 0.1041$
Short range repulsion:	A [kJ mol ⁻¹]	770000
(exchange + penetration)	B [nm ⁻¹]	40.37
force centers ^{a)} z_{SR} [nm]	± 0.0547	± 0.0547
Dispersion:	C [kJ mol ⁻¹ nm ⁶]	0.001511(0.001407) ^{d)}
force centers z_D [nm]	± 0.0471	

a) Molecular multipole moments calculated with this point charge model:

$$Q_{2,0} = -4.449 \cdot 10^{-40} \text{ C m}^2, \quad Q_{4,0} = -8.046 \cdot 10^{-60} \text{ C m}^4, \quad Q_{6,0} = -11.063 \cdot 10^{-80} \text{ C m}^6$$

ab initio [3]:

$$Q_{2,0} = -4.487 \cdot 10^{-40} \text{ C m}^2, \quad Q_{4,0} = -9.233 \cdot 10^{-60} \text{ C m}^2, \quad Q_{6,0} = -6.129 \cdot 10^{-80} \text{ C m}^6$$

b) $e = 1.602 \cdot 10^{-19} \text{ C}$

c) Optimized force centers $z_{SR} = \pm 0.0554$ nm practically coincide with the nuclear positions $z_N = \pm 0.0547$ nm

d) In parentheses: optimized parameter C if the force centers are fixed on the nuclei, $z_D = \pm 0.0547$ nm

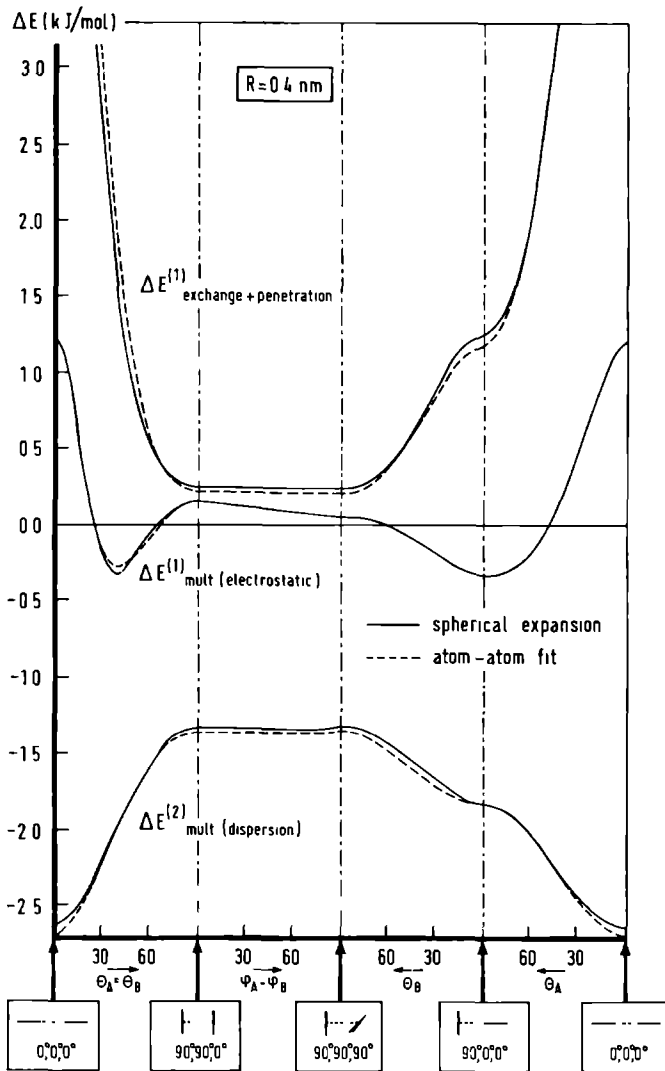


Fig. 3. Orientational dependence of different long range (multipole) and short range (penetration plus exchange) contributions to the interaction energy, at $R = 0.4 \text{ nm}$. Spherical expansion, see table 5. Atom-atom potential I of table 3.

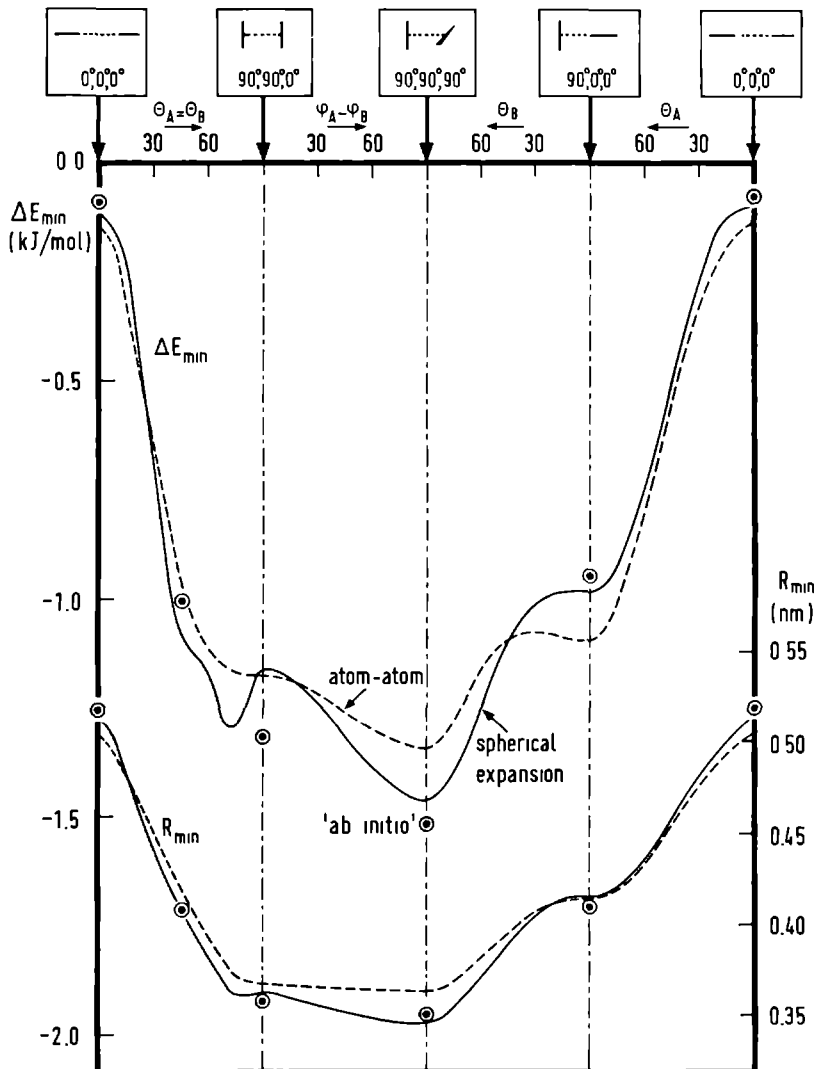


Fig. 4. Orientational dependence of the Van der Waals minimum. The well depth ΔE_{\min} and equilibrium distance R_{\min} have been obtained by varying R for each orientation $\theta_A, \theta_B, \phi_A$. "Ab initio", spherical expansion and atom-atom potentials defined as in figs. 2 and 3.

where the P_L^M are associated Legendre functions [14].

- using the symmetry properties of the system. This reduces the integration intervals.

Since the angular functions depend only on $\cos\theta_A$, $\cos\theta_B$ and $\cos\phi_A$ (the function $\cos M_A \phi_A$ can easily be expanded as a function of $\cos\phi_A$) and the volume element is $d(\cos\theta_A)d(\cos\theta_B)d\phi_A$ one can substitute $\eta_A = \cos\theta_A$, $\eta_B = \cos\theta_B$ and $\zeta_A = \cos\phi_A$ and obtain the integral:

$$V_{L_A, L_B, L}(R) = 8\pi^{\frac{1}{2}} \int_0^1 d\eta_A \int_0^1 d\eta_B \int_{-1}^1 d\zeta_A (1-\zeta_A^2)^{-\frac{1}{2}} \times$$

$$A_{L_A, L_B, L}(\eta_A, \eta_B, \zeta_A) \Delta E(\arccos \eta_A, \arccos \eta_B, \arccos \zeta_A; R)$$

This integral is very suitable for numerical integration. The best method for our purpose (which is to apply it to ab initio results) is one of the Gaussian integration techniques, since these give the highest accuracy with the smallest number of integration points [19]. For Legendre functions it is best to choose the Gauss-Legendre modification. (Parker et al. [20] have used this technique in a one-dimensional integration required to obtain the Ar-CO potential.) We have used the formula's 25.4.30 and 25.4.38 of ref. [21]. Since we only have to find the spherical expansion of the short range contributions $\Delta E_{\text{pen.}}^{(1)}$ and $\Delta E_{\text{exch.}}^{(1)}$ (see section 3a), we have applied this integration method to the exponential part of the site-site potential, section 3b, term (111). Some experimentation with the grid and with the expansion length has led to the conclusions that:

- the first 18 terms in the spherical expansion are necessary to represent the short range potential to an accuracy better than one percent in each point.
- the required number of integration points for $(\eta_A, \eta_B, \zeta_A)$ is (6,6,5).

Next we have performed ab initio calculations of $\Delta E^{(1)}$ (formula (1)) at these grid points [21]. (Using the full symmetry their number can be further reduced from 180 to 105.) The intermolecular distance for which we have chosen to do this is $R = 0.3$ nm, since this distance is relevant both for beam scattering experiments and for solid state properties [2]. The expansion coefficients which

result from the numerical integration of the ab initio points are given in table 4.

We observe that the short range coefficients $V_{L_A, L_B, L}^{SR}$ indeed decrease with increasing L_A and L_B ; the expansion is convergent. Most of the terms with $L_A, L_B = 4, 4$ and $6, 2$ are less than one percent of the isotropic coefficient $V_{0, 0, 0}^{SR}$. For fixed L_A, L_B the coefficients increase with increasing L . The 18 term expansion deviates less than 0.5% from the ab initio results; truncation of the series after $L_A, L_B = 4, 4$ leads to an error of 2%; truncation after $L_A, L_B = 2, 2$ to 16% error.

If one wants to determine the distance dependence of the expansion coefficients $V_{L_A, L_B, L}^{SR}(R)$ this procedure should be repeated for a set of distances R . The ab initio calculations are rather expensive, however, (about 3 hours of IBM 370/158 CPU time per point) and so we have instead used a different, more approximate method. We have assumed that all expansion coefficients $V_{L_A, L_B, L}^{SR}$ of the short range energy have the same exponential distance dependence:

$$V_{L_A, L_B, L}^{SR}(R) = \tilde{V}_{L_A, L_B, L}^{SR}(R) = V_{L_A, L_B, L}^{SR}(R_0) \exp[A - B_1(R - R_0) - B_2(R - R_0)^2]$$

with $R_0 = 0.3$ nm. The parameters A , B_1 and B_2 have been optimized by fitting the spherically expanded $\tilde{\Delta E}^{(1)}$ with the coefficients given by $\tilde{V}_{L_A, L_B, L}^{SR}(R)$ to the ab initio values of $\Delta E_{pen}^{(1)} + \Delta E_{exch}^{(1)}$ calculated for six orientations and six distances $0.3 \leq R \leq 0.44$ nm. The accuracy of the fit is 7%; the results (see table 5), in combination with the long range results [3], yield a fairly good representation of the ab initio calculations for the N_2-N_2 interaction potential (see figs. 2 and 4).

4. Applications of the N_2-N_2 interaction potential; comparison with experimental data

a. Isotropic potential

Our calculated isotropic N_2-N_2 potential, $V_{0, 0, 0}(R)$, can be compared with some empirical isotropic potentials from gas phase virial coefficients, viscosity data and from solid state properties [22]. Since the latter have only been determined in the simplified

Table 4. Spherical expansion coefficients (formula 4) of the short range (penetration and exchange) interaction energy

L_A, L_B, L	$v_{L_A, L_B, L}^{SR}$ [kJ mol ⁻¹] at R = 0.3 nm	
	ab initio ^{a)}	atom-atom ^{b)}
0,0,0	44.258	49.769
2,0,2	23.871	26.936
2,2,0	2.947	3.674
2,2,2	-4.734	-5.794
2,2,4	13.154	14.667
4,0,4	4.309	3.551
4,2,2	0.314	0.380
4,2,4	-0.732	-0.701
4,2,6	3.151	2.520
4,4,0	0.005	0.010
4,4,2	-0.006	-0.015
4,4,4	0.026	0.033
4,4,6	-0.131	-0.107
4,4,8	1.035	0.573
6,0,6	0.389	0.264
6,2,4	0.011	0.018
6,2,6	-0.057	-0.049
6,2,8	0.399	0.250

a) Calculated by numerical integration from the ab initio data for a grid of 180 (105 independent) orientations (AO basis, see table 1)

b) Same as a), for the repulsive part of the atom-atom potential II (table 3, exponential term)

Table 5. Spherical expansion of the complete interaction potential (formula 3)

$$V_{L_A, L_B, L}^{SR}(R) = v_{L_A, L_B, L}^{SR}(0.3) \exp\{-0.00153 - 35.6(R-0.3) - 20.5(R-0.3)^2\} \\ + C_{L_A+L_B+1}^{L_A, L_B, L} R^{-(L_A+L_B+1)} + C_6^{L_A, L_B, L} R^{-6} \\ + C_8^{L_A, L_B, L} R^{-8} + C_{10}^{L_A, L_B, L} R^{-10}$$

R in nm;

$v_{L_A, L_B, L}^{SR}(0.3)$ from table 4, ab initio

Long range (multipole) coefficients ^{a)}					
L_A, L_B, L	Electrostatic		Dispersion		
	$C_{L_A+L_B+1}^{L_A, L_B, L}$	L_A+L_B+1	$C_6^{L_A, L_B, L}$	$C_8^{L_A, L_B, L}$	$C_{10}^{L_A, L_B, L}$
	[kJ mol ⁻¹ nm ^{L_A+L_B+1}]		[kJ mol ⁻¹ nm ⁶]	[kJ mol ⁻¹ nm ⁸]	[kJ mol ⁻¹ nm ¹⁰]
0,0,0	-		-4.231 10 ⁻³	-2.946 10 ⁻⁴	-2.239 10 ⁻⁵
2,0,2	-		-1.815 10 ⁻⁴	-5.277 10 ⁻⁵	-5.974 10 ⁻⁶
2,2,4	1.849 10 ⁻³		-3.638 10 ⁻⁵	-4.932 10 ⁻⁶	-1.219 10 ⁻⁶
2,2,2	-		-4.505 10 ⁻⁶	1.026 10 ⁻⁶	3.692 10 ⁻⁷
2,2,0	-		-3.764 10 ⁻⁶	-6.098 10 ⁻⁷	-2.256 10 ⁻⁷
4,2,6	7.655 10 ⁻⁵		-	-	-
4,4,8	6.078 10 ⁻⁶		-	-	-
6,2,8	8.465 10 ⁻⁷		-	-	-

^{a)} Note that the long range multipole coefficients $C_n^{L_A, L_B, L}$ defined in this paper are different from the $C_n^{L_A, L_B, M}$ of ref. [3]; the two definitions are, of course, related by a simple linear transformation

forms of Lennard-Jones (12-6) or Buckingham (exp-6) potentials we shall not compare the shape of the potentials but only their main characteristics: the scattering diameter (σ), the equilibrium distance (R_m) and the well depth (ΔE_m). The results listed in table 6 show that the agreement is good, so that we expect our calculated potential to explain quantitatively the experimental bulk data (at least those which have been used to determine the empirical potential parameters).

b. N₂ crystal properties

Our site-site potential fitted to the ab initio data (section 3b) has been used to calculate the equilibrium structure and the cohesion energy of the ordered (α and γ) phases of solid N₂. The results, unit cell dimension $a = 0.561$ nm for the cubic α -phase, cohesion energy 6.43 kJ/mol (corrected for the zero-point lattice vibrations), and $a = 0.403$ nm, $c = 0.500$ nm for the tetragonal γ -phase, are in good agreement with the experimental data [1,2], $a = 0.564$ nm, heat of sublimation (at 0°K) 6.92 kJ/mol for α -N₂, $a = 0.396$ nm, $c = 0.510$ nm for γ -N₂. Also the phonon frequencies at various wave vectors, obtained from harmonic or self-consistent phonon lattice dynamics calculations using our non-empirical site-site potential, agree nicely with the experimental data. Further details will appear in a forthcoming paper [23], which is concerned with the properties of solid N₂ in the α and γ phases and their temperature and pressure dependence.

c. Stability and structure of (N₂)₂

In the gas phase at 77°K stable N₂ dimers, so-called Van der Waals molecules, have been observed and their infrared spectrum has been measured [24]. In spite of this knowledge of the spectrum, the structure of this N₂ dimer has not been established. Mainly on the basis of favourable quadrupole-quadrupole interactions a T-shaped equilibrium structure ($\theta_A=90^\circ$, $\theta_B=\phi_A=0^\circ$) has been proposed [24]. Addition of the higher multipole interactions plus the anisotropic dispersion interactions from ab initio calculations gives further support for the stability of this T-shaped complex, but also suggests another possible structure of equal stability, the staggered parallel one ($\theta_A=\theta_B=45^\circ$, $\phi_A=0^\circ$) [3]. A more approximate model including the short range repulsion [25] predicts a T-shaped

Table 6. Characteristics of the isotropic potential

	σ [nm]	R_m [nm]	ΔE_m [kJ mol ⁻¹]
Calculated $V_{0,0,0}(R)$ (table 5)	0.376	0.417	0.748
Lennard-Jones (12-6) from virial coefficients (ref. [22], page 209)	0.370	0.415	0.793
Lennard-Jones (12-6) from viscosity data (ref. [22], page 209)	0.368	0.413	0.763
Buckingham (exp-6) from virial coefficients and crystal data (ref. [22], page 181)	0.363	0.404	0.947
Buckingham (exp-6) from viscosity data (ref. [22], page 181)	0.362	0.401	0.844

or a crossed ($\theta_A = \theta_B = \phi_A = 90^\circ$) $(N_2)_2$ structure, but if the molecular shape parameters are somewhat modified the outcome is a T-shaped or a staggered parallel structure [26]. Beam deflection measurements [27], which are sensitive to the dipole moment of the molecular complex, have not demonstrated the existence of such a dipole on $(N_2)_2$. Several possible $(N_2)_2$ structures must have a zero dipole, however, because of symmetry (for instance, the staggered parallel one and the crossed one) and for the remaining structures (such as the T-shaped) the interaction induced dipole may be too small to be detectable.

With our quantitative knowledge of the anisotropic N_2-N_2 interaction potential, including both the long range and the short range contributions, we can make somewhat more definite remarks on the N_2 dimer structure and confront these with the available experimental information. To this end we have studied the potential surface of $(N_2)_2$ as a function of the "internal" angles θ_A, θ_B and ϕ_A and the distance R . It is of course not possible to present the complete hypersurface pictorially; in figs. 2 and 4 we have shown some typical cuts through the surface, fig. 3 displays the angular dependence of the different long range and short range contributions to the potential. Especially fig. 4 contains much information since the distance R has been varied to find the energy minimum $\Delta E_{\min.}$ of $(N_2)_2$ and the equilibrium distance $R_{\min.}$ for each orientation $(\theta_A, \theta_B, \phi_A)$. In fig. 3 we observe that, indeed, the T-shaped and the staggered parallel structure have maximum electrostatic attraction. The dispersion energy is most favourable, of course, for the linear structure ($\theta_A = \theta_B = \phi_A = 0^\circ$). For distances in the neighbourhood of the Van der Waals minimum the short range exchange repulsion is the dominant anisotropic term, however. Since it increases very steeply when the molecular charge clouds start to overlap (especially in the linear structure), it determines to a large extent the distance of closest approach of the molecules. If, for a given orientation, the long range interactions are not maximally attractive (when compared with other orientations, for equal distance R), but the molecules can approach each other closely, the Van der Waals well may still be relatively deep. This is, for instance, what happens for the crossed $(N_2)_2$ structure. In general, one can observe this role of the short range repulsion from fig. 4, where the well depth $\Delta E_{\min.}$ shows a strong correlation with the equilibrium distance $R_{\min.}$.

Only when the short range repulsion is not very sensitive to a change of orientation (for instance, the rotation over ϕ_A in the N_2 dimer with $\theta_A = \theta_B = 90^\circ$, see fig. 3) the long range interactions (in this case, the electrostatic ones, even though they are repulsive) can still be important in determining the equilibrium structure.

This crucial role of the short range interactions for the dimer structure (leading to closest packing) may suggest that the structure of nearest neighbour pairs in the molecular crystal forms a good indication for the equilibrium structure of the Van der Waals dimer. This has indeed been suggested [28]. Our results (see table 7) demonstrate, however, that maximum binding energy for the N_2 dimer does not occur for the nearest neighbour orientations from the crystal. And, in fact, it is not obvious, even if only packing considerations determine the structure, that the optimum packing in a crystal where each molecule is surrounded by several neighbours, must correspond with optimally packed dimers. The crystal neighbours should not have too unfavourable pair energies, though, but the results in table 7 show that this is not the case.

The absolute minimum in our N_2-N_2 potential surface (a complete search is made using the site-site potential, a cruder one on the spherically expanded potential), occurs for the crossed structure at $R = 0.35$ nm and $\Delta E = 1.5$ kJ/mol (see table 7). This minimum lies considerably closer and deeper than the minimum of the isotropic potential ($R_m = 0.417$ nm, $\Delta E = 0.75$ kJ/mol). The equilibrium distance is close to the value ($R = 0.37$ nm) inferred from the infrared spectrum [24], but the T-shaped structure proposed in this paper [24] has not been confirmed, due to the anisotropy of the short range repulsions. (Actually, our minimum for the T-shaped structure lies much further outwards, at $R = 0.42$ nm). The potential surface is rather flat around the minimum, however, the balance between the attractive and repulsive contributions is subtle and different possible structures are near in binding energy. In some directions the barriers for internal N_2 rotations are rather low; for instance, for a complete rotation over ϕ_A in the dimer with $\theta_A = \theta_B = 90^\circ$ it is about 0.2 kJ/mol (17 cm $^{-1}$) with practically no variation of the equilibrium distance (see fig. 4). This agrees nicely with the estimate of 15

Table 7. $(N_2)_2$ structure and binding energy

	R [nm]	θ_A	θ_B	ϕ_A	ΔE [kJ mol ⁻¹]
Most stable dimer structure ^{a)}	0.364 ^{a)} (0.346 ^{b)} , 0.350 ^{c)})	90°	90°	90°	1.35 ^{a)} (1.46 ^{b)} , 1.52 ^{c)})
α -N ₂ crystal ^{d)} neighbour pair	0.399 (0.404 ^{e)})	90°	35°	55°	1.05 (1.05 ^{e)})
γ -N ₂ crystal ^{d)} neighbour pair	0.379 (0.398 ^{e)})	90°	42°	90°	0.94 (1.09 ^{e)})

a) Neglecting the energy of the nuclear motions; complete search of the potential energy surface has been performed with the atom-atom potential I of table 3

b) From the spherical expansion, table 5

c) From the ab initio first order energy (table 1) and the second order energy from the dispersion multipole coefficients of ref. [3] (table 6), see table 5 and fig. 2

d) Experimental crystal structure, see ref. [1], nearest neighbour pair energy ΔE calculated with atom-atom potential I

e) $R_{\min.}$ and $\Delta E_{\min.}$ obtained with the atom-atom potential I (table 3) for fixed N₂ orientations from d)

to 30 cm^{-1} from the IR spectrum [24]. So we expect the N_2 molecules in the dimer to make rather wide angular oscillations (librations) or, maybe, hindered rotations (the rotational constant of free N_2 is 2.0 cm^{-1}). This is comparable to the situation in the plastic crystal phase, $\beta\text{-N}_2$. In other directions, rotations of the molecules are strongly quenched; the complex must almost dissociate before such a rotation becomes possible (for instance, rotations through the linear structure, see fig. 4). Before, we can make a conclusive comparison with the experimental spectrum, we have to solve the dynamical problem for the nuclear motions, which may be not an easy job in this case.

Note added

After completion of this manuscript we have received a preprint by Ree and Winter [29], also containing ab initio results for the $\text{N}_2\text{-N}_2$ potential. These authors have concentrated on the short range, strongly repulsive, region of the potential. The smaller basis set which they have used (overestimating, for instance, the N_2 quadrupole moment), in combination with the supermolecule SCF method (leading to some basis set superposition error), is less adequate for the long range and for the region of the Van der Waals minimum, which we have concentrated on. Moreover, they have not included the dispersion energy contribution.

Acknowledgement

We are most grateful to dr. Paul E.S. Wormer for his critical reading of the manuscript and for many very stimulating discussions. Also we acknowledge valuable discussions with drs. Fred Mulder and Tadeusz Luty.

The University Computing Center is thanked for a generous supply of facilities.

We thank drs. F.H. Ree and N.W. Winter for communicating their results prior to publication.

References

1. T.A. Scott, Phys. Repts. 27C, 89 (1976) and references therein.
2. J.C. Raich and N.S. Gillis, J. Chem. Phys. 66, 846 (1977) and references therein.
3. F. Mulder, G. van Dijk and A. van der Avoird, Mol. Phys. (in press).
4. P.E.S. Wormer, thesis, Nijmegen (1975).
5. P.E.S. Wormer, F. Mulder and A. van der Avoird, Intern. J. Quantum Chem., 11, 959 (1977).
6. G. Herzberg, Spectra of diatomic molecules, Van Nostrand, New York (1950).
7. B. Jeziorski and W. Kolos, Intern. J. Quantum Chem. 12S1, 91 (1977).
8. P.W. Langhoff, M. Karplus and R.P. Hurst, J. Chem. Phys. 44, 505 (1966).
9. F. Mulder, A. van der Avoird and P.E.S. Wormer, Mol. Phys. 37, 159 (1979).
10. K.C. Ng, W.J. Meath and A.R. Allnatt, Mol. Phys. 33, 699 (1977).
11. W.A. Steele, J. Chem. Phys. 39, 3197 (1963).
12. A.J. Stone, Mol. Phys. 36, 241 (1978).
13. A. van der Avoird, P.E.S. Wormer, F. Mulder and R.M. Berns, in: Van der Waals systems, ed. R. Zahradnik, Topics in Current Chemistry, Springer, Berlin (1980).
14. D.M. Brink and G.R. Satchler, Angular momentum, Clarendon Press, Oxford, 2nd edition (1975).
15. P.J.M. Geurts, P.E.S. Wormer and A. van der Avoird, Chem. Phys. Letters, 35, 444 (1975).
16. P.C. Hariharan and W. Kutzelnigg, Progress Rept. Lehrstuhl für Theoretische Chemie, Ruhr-Universität, Bochum (1977).
17. J. Schaefer and W. Meyer, J. Chem. Phys. 70, 344 (1979).
18. T. Wasilutynski, A. van der Avoird and R.M. Berns, J. Chem. Phys. 69, 5288 (1978).

19. T. Stoer, Einführung in die numerische Mathematik, I, Springer, Berlin (1972).
20. G.A. Parker and R.T. Pack, J. Chem. Phys. 69, 3268 (1978).
21. M. Abramowitz and I.A. Stegun, Handbook of Mathematical Functions, Dover, New York (1968).
22. J.O. Hirschfelder, C.F. Curtiss and R.B. Bird, Molecular Theory of Gases and Liquids, Wiley, New York; 2nd ed. (1964).
23. T. Luty, A. van der Avoird and R.M. Berns, to be published.
24. C.A. Long, G. Henderson and G.E. Ewing, Chem. Phys. 2, 485 (1973).
25. A. Koide and T. Kihara, Chem. Phys. 5, 34 (1974).
26. K. Sakai, A. Koide and T. Kihara, Chem. Phys. Letters, 47, 416 (1977).
27. S.E. Novick, P.B. Davies, T.R. Dyke and W. Klemperer, J. Am. Chem. Soc. 95, 8547 (1973).
28. J.M. Steed, T.A. Dixon and W. Klemperer, J. Chem. Phys. 70, 4940 (1979).
29. F.H. Ree and N.W. Winter, J. Chem. Phys., submitted.

Comparison of electron gas and ab initio potentials for the N_2-N_2 interactions. Application in the second virial coefficient.[†]

M.C. van Hemert

Gorlaeus Laboratories, Department of Physical Chemistry,
University of Leiden, P.O. Box 9502, 2300 RA Leiden, The Netherlands.

R.M. Berns

Institute of Theoretical Chemistry, University of Nijmegen,
Toernooiveld, Nijmegen, The Netherlands.

Abstract

A detailed potential for the interaction between two rigid N_2 molecules is given in the form of a spherical expansion. The interaction energy is found as the sum of the so-called Hartree-Fock part of the electron gas expression including the Rae correction and the "ab initio" dispersion energy in the multipole expansion. Potential surface cuts computed with this expansion agree to a large extent with a similar potential completely based on ab initio calculations. Comparison of the experimental second virial coefficient curve with the curves obtained from a four dimensional quadrature using both "ab initio" and electron gas potentials demonstrates the usefulness of these potentials, and underlines the importance of the anisotropic contributions.

[†] Supported in part by the Netherlands foundation for Chemical Research (SON) with financial aid from the Netherlands Organization for the Advancement of Pure Research (ZWO).

1. Introduction

It has recently been shown that it is possible to construct a detailed reliable anisotropic potential for the interactions between two N_2 molecules by means of ab initio calculations [1]. Crystal properties, such as structure, cohesion energy and lattice vibration frequencies, derived with this potential were found to be in close agreement with the experiment [1,2]. In order to construct this potential, perturbation theory was applied including exchange in first order. The first and second order long range parts were based on the multipole expansion, where orientation and distance dependence are uniquely defined in the form of a spherical expansion [3]. Also the short range part of the first order energy, containing the penetration and exchange contributions, was represented by a (distance dependent) spherical expansion. The individual coefficients in this expansion were determined by numerical integration of the interaction energy for a number of judiciously chosen orientations. The distance dependence was assumed to be equal for all short range terms and was adjusted so as to reproduce the potential curves for six typical orientations.

The procedure used is clear; the actual computation of accurate energies requires enormous amounts of computer time, however. The bottleneck is the computation of the $\sim 1/8 N^4$ (N equals the total number of basisfunctions used for the ab initio description of the two molecules) two electron integrals that are needed in the (short range) expressions for the first order energy for each configuration. When one also wants to determine the influence of internal degrees of freedom on this potential -as is needed for the description of many inelastic collision processes- computer time will be prohibitive. Also the ab initio calculation of detailed anisotropic potentials for polyatomics will be an enormous labour. Interest in cheaper, but still accurate methods, is therefore very vivid.

A promising method in this respect is the one based on the expressions in the electron gas theory of atoms and molecules. With the original formulation of the theory for the special case of the interaction between closed shell atoms and ions, as given by Gordon and Kim [4], in many cases very realistic potential curves could be obtained [5], in other cases the results were poor [6].

From the many critical comments that have been given, Rae's analysis of the consequences of the neglect of the so-called self

exchange terms [7] appears to have been the most valuable. In the accordingly corrected treatment all noble gas pairs could be described very accurately [8]. In the case of molecules there has been considerable discussion with respect to the applicability of this so-called Rae correction. On some occasions it was found that the potential surface cuts computed with ab initio techniques differed largely from the electron gas results [6] and that the inclusion of the Rae correction factor did not diminish the discrepancies [6,9].

It has to be noted, however, that also the ab initio results were not always completely reliable. Improper treatment of the basis set superposition error and neglect or severe underestimation of dispersion contributions are the most notorious. The accurate N_2-N_2 potential referred to the beginning forms a very attractive test for the electron gas approach and for the importance of the Rae correction.

In the following section we will describe the results of the computation of the interaction energy for two N_2 molecules at a large number of orientations and distances. Again the results are presented as a spherical expansion. The distance dependence of each term will be given. As we will see that also in the N_2 case the correlation energy part in the electron gas formulation gives rather unrealistic results, we just copy the second order energy from the ab initio calculations [10] in order to get a complete potential. The correctness of the expansion and fitting procedures will be shown by comparing the predicted results and the directly computed values for a few interesting potential surface cuts. During the preparation of this paper we became aware of the work of Ree and Winter [11], who also compared ab initio and electron gas results for the interaction between two nitrogen molecules. Their study was however meant for very short intermolecular distances only; long range dispersion terms were neglected.

We have not repeated the structure and lattice dynamics calculations that have been performed with the ab initio potential. Rather we have compared the ab initio and electron gas potentials with respect to their ability to predict the temperature dependence of the second virial coefficient over the 75-700 K range.

2. Theoretical and computational aspects

2.1. Monomer electron densities

Input to the computer program for the Gordon-Kim (GK), or when

the Rae correction is included (GKR), type energy terms (see below) is a Hartree-Fock type wavefunction for the monomer, where the molecular orbitals are given as a linear combination of Slater type atomic orbitals (STO's). In the ab initio calculations, we want to compare our results with, contracted cartesian gaussian type atomic orbitals (CGTO's) were used. We therefore preferred to compute a Hartree-Fock wavefunction starting from a basis set that did not differ too much from the one used in the ab initio calculations [1,10]. For the description of the core and valence shell we chose as many STO's as there were CGTO's in the ab initio calculations for the first order energy. The exponents were copied from ref. [12]. In order to get a proper description of the permanent multipole moments we added a 3d and a 4f STO with exponents 2.0 and 2.4 respectively. The total SCF energy, found at the experimental internuclear distance of 2.034 Bohr, was -108.9830 Hartree, compared to -108.9732 in ref. [10] and -108.9929 in the supposed Hartree-Fock limit [13]. The computer program used for the Hartree-Fock calculation was the Alchemy program [14]. Apart from the energy also the permanent multipole moments were computed with the help of this program. The results are included in Table I.

2.2. The interaction energy in the electron gas approach

In the electron gas approach the energy of a system is found as the sum of a potential (Coulomb), kinetic, exchange and correlation energy term. Each of these contributions is completely determined by the charge density distribution in the system. In the formalism of Gordon and Kim [4] the interaction energy between two systems A and B, E_{int} , defined by

$$E_{int} = E_{AB}(\rho_{AB}) - E_A(\rho_A) - E_B(\rho_B), \quad (1)$$

is obtained by using the electron gas formulae. The densities ρ_A and ρ_B of the two interacting molecules are taken from ab initio SCF or CI calculations and ρ_{AB} , the density in the interacting system, is taken as the sum of ρ_A and ρ_B . In this way also the interaction energy can be obtained as the sum of four terms. The expressions for the separate terms are given in many papers [4,15] and will not be repeated here. The electrostatic term is rigorously equal to the electrostatic part of the first order interaction energy according to perturbation theory.

TABLE I

Permanent multipole moments for N₂^a

	ab initio ^b	ab initio ^c	from approx.ρ ^d	from approx.ρ ^e	
Q ₂	-4.487	-4.952	-5.231	-5.199	10 ⁻⁴⁰ Cm ²
Q ₄	-9.233	-9.442	-9.843	-9.830	10 ⁻⁶⁰ Cm ⁴
Q ₆	-6.129	-5.228	-5.035	-5.026	10 ⁻⁸⁰ Cm ⁶

a. multipole moments are defined by: $Q_\ell = \langle 0 | \sum_i Z_i r_i^\ell P_\ell | 0 \rangle$.

b. obtained with CGTO wavefunction (ref. [10], table 1D).

c. obtained with STO wavefunction, this work.

d. computed analytically from expansion for charge density used in electron gas energy expressions.

e. computed by numerical integration using expansion for charge density.

It has often been stated [16], that the kinetic energy part should equal the difference between the expectation value of the kinetic energy operator using the first order (anti-symmetrized product) wavefunction and the sum of the monomer kinetic energies. In the few cases, where a numerical comparison has been made, great differences are observed [16,17]. Also the exchange part in first order perturbation theory -that should be defined as the difference between the complete first order energy and the sum of Coulomb and kinetic energy-[†] appears to differ from the exchange contribution in the electron gas approach. We therefore adhere to a more pragmatic point of view and only require the sum of Coulomb, kinetic and exchange terms, also often referred to as the Hartree-Fock part of the electron gas binding energy, to be equal to the first order perturbation theory results. In order to correct the exchange term for spurious self exchange contributions, it is sufficient -as shown by Rae [7]- to multiply the original exchange term in the Gordon-Kim formulation by a factor that depends only on the total number of electrons in the system. The factor approaches zero for two electrons and becomes unity only in the limit of a very large number of electrons. Although in a later paper [8] Rae has suggested that it would be better to set the number of electrons in this factor equal to the number of valence shell electrons in the isolated molecule, we have nevertheless in our calculations based the factor on 28 electrons. We found that with this factor the best agreement with the ab initio results was obtained.

The expression for the correlation energy contribution in the original Gordon and Kim (GK) formulation [4] is somewhat questionable and produces unrealistic results. In the complete potential we have therefore, as others [18], replaced the correlation contribution by the second order dispersion energy from perturbation theory. In the case of N_2 it was shown that all relevant distances the use of the multipole expansion for this term was justified [1]. However, since the individual molecules are described with the help of accurate, but uncorrelated, LCAO SCF wavefunctions, a scaling in the second order energy is necessary, as is demonstrated in [10], where also the values of the scaling factors are derived.

[†] This definition of the exchange theory is not the one usually encountered in the first order in exchange perturbation theory.

The program used for the computation of the GK (or GKR) interaction energies has been written by Parker and Pack and was obtained from QCPE [19]. Details of the program can be found in [15]. In the first part of the program the monomer charge distribution, as determined from the Hartree-Fock wavefunctions for the monomers, is approximated by a sum of STO's. The coefficients of this expansion are found from a weighted linear least squares procedure. In total 43 expansion functions were used, of which 7 were located on the centre of mass and the remainder on the two nuclei. The exponents were chosen as the sums of the exponents of those pairs of basisfunctions in the Hartree-Fock calculation that correspond to the largest elements in the density matrix. For the least squares fit 50 radial and 40 angular points were considered. The largest distance (with the centre of mass as the origin) was 12 Bohr. The standard deviation was .019 (the relative standard deviation was .0069). With the help of this approximate charge density we also (analytically) computed the multipole moments (see Table I). The difference with the values obtained from the original Hartree-Fock density is rather large and indicates that the approximate charge density is not completely correct. We were not able to obtain significant improvement with other expansion sets. Probably the restriction to a maximum l value of 2 for the expansion functions is responsible.

In the second part of the program, which calculates E_{int} , the numerical integration -a 3 dimensional Gauss-Legendre quadrature- over the charge density functionals is executed. Here we used 48 integration points for each of the two angle variables and 45 integration points for the radial variable. Using the same integration grid also the permanent multipole moments are determined numerically. The results (see Table I) differ only slightly from the ones computed analytically from the same approximate charge distribution. This difference must be attributed to the numerical integration procedure. In order to give an accurate analytical representation of the anisotropic potential we have used a spherical expansion technique (see next section). For this purpose we computed the intermolecular potential for 105 orientations at 6 intermolecular distances. The computation of the energy at the 630 points required three hours of cpu time on a Cyber 175/100 (actually the GK and GKR approach costs around one hundredth of the computer time needed in the ab initio approach for the same number of points).

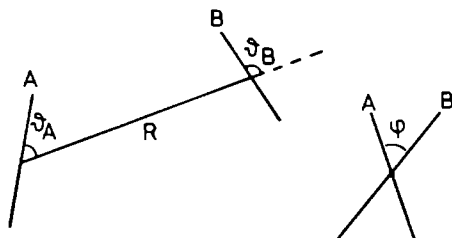


Fig. 1. Definition of internal coordinates.

2.3. Representation in terms of a spherical expansion

Since the spherical expansion technique has been formulated in great detail in refs. [1,10,20], we only summarize the main aspects for clarification of our computational procedure.

For two linear molecules in Σ states the distance and orientation dependence of the interaction energy can be written as

$$E_{\text{int}}(\hat{f}_A, \hat{f}_B, \underline{R}) = (4\pi)^{3/2} \sum_{L_A} \sum_{L_B} \sum_L V_{L_A L_B L}(R) A_{L_A L_B L}(\hat{f}_A, \hat{f}_B, \hat{R}) \quad (2)$$

Here $\hat{f}_A = (\theta_A, \phi_A)$ and $\hat{f}_B = (\theta_B, \phi_B)$ define the orientations of the molecular axes and $\underline{R} = (R, \theta, \phi)$ is the vector which connects the molecular centres of mass (pointing from A to B). All variables are measured relative to the same arbitrary coordinate system. The expansion coefficients $V_{L_A L_B L}$, that are functions of distance only, completely determine the orientational dependence of the potential.

Because the interaction energy is invariant under rotation of the arbitrary coordinate system, we may choose a special coordinate system where we need only consider the three internal angles $\theta_A, \theta_B, \phi_A$ ($\theta = \phi = \phi_B = 0$) (see fig. 1). The angular functions then can be expressed as:

$$A_{L_A L_B L} = \sum_{M=0}^{\min(L_A, L_B)} X_{L_A L_B L M} P_{L_A}^M(\cos\theta_A) P_{L_B}^M(\cos\theta_B) \cos M\phi \quad (3)$$

The P_L^M are associated Legendre functions according to the definition in [21]. The numerical factor $X_{L_A L_B L M}$ is given by[†]

[†] In ref. [1] the factor $(-1)^M$ has been accidentally omitted.

$$X_{L_A L_B L}^M = \left[\frac{(2L_A+1)(2L_B+1)(2L+1)}{64\pi^3} \right]^{\frac{1}{2}} \left[\frac{(L_A-M)!(L_B-M)!}{(L_A+M)!(L_B+M)!} \right]^{\frac{1}{2}} \begin{pmatrix} L_A L_B L \\ M -M 0 \end{pmatrix} (2-\delta_{M,0}) (-1)^M \quad (4)$$

The symbol $\begin{pmatrix} \\ \end{pmatrix}$ stands for a 3-j coefficient.

Once the interaction potential is known, the expansion coefficients can be found from

$$V_{L_A L_B L}(\mathbf{R}) = \pi^{\frac{1}{2}} \int_{-1}^1 d \cos \theta_A \int_{-1}^1 d \cos \theta_B \int_0^{2\pi} d\phi A_{L_A L_B L}(\theta_A, \theta_B, \phi) E_{\text{int}}(\theta_A, \theta_B, \phi, \mathbf{R}) \quad (5)$$

For the interaction between two identical homonuclear molecules the lower integration limits for $\cos \theta_A$ and $\cos \theta_B$ can be replaced by 0 and the upper limit of the ϕ integration can be lowered to π (the final result then has to be multiplied by 8 of course). In that case also only even values of L_A, L_B and L have to be taken into account, furthermore $V_{L_A L_B L}$ is symmetric in the first two indices.

As the interaction energy can be decomposed in short range and first and second order long range contributions, the $V_{L_A L_B L}$ can be analyzed in the same terms:

$$V_{L_A L_B L}(\mathbf{R}) = V_{L_A L_B L}^{\text{SR}}(\mathbf{R}) + V_{L_A L_B L}^{\text{1 mult.}}(\mathbf{R}) + V_{L_A L_B L}^{\text{2 disp.}}(\mathbf{R}) \quad (6)$$

For the long range first and second order contributions both the orientation and distance dependence can be calculated directly:

$$V_{L_A L_B L}^{\text{1 mult.}}(\mathbf{R}) = C_{L_A+L_B+1}^{L_A L_B L} R^{-(L_A+L_B+1)} \quad \text{and} \quad (7a)$$

$$V_{L_A L_B L}^{\text{2 disp.}}(\mathbf{R}) = \sum_{n=6,8,10} C_n^{L_A L_B L} R^{-n} \quad (7b)$$

The relation between the multipole moments and the coefficients $C_{L_A+L_B+1}^{L_A L_B L}$ is given in ref. [22]. In ref. [10] it is shown how the dispersion coefficients $C_n^{L_A L_B L}$ can be found. The short range coefficients $V_{L_A L_B L}^{\text{SR}}$ are thus obtained by subtracting the long range contributions from $V_{L_A L_B L}$. For the description of the distance dependence of the short range coefficients a relation of the form:

$$V_{L_A L_B L}^{SR} = a_{L_A L_B L} e^{bR+cR^2} \quad (8)$$

was used in ref. [1], with necessarily the same b and c for each L_A , L_B and L. Others have used interpolation methods in stead of a fit in comparable cases [21]. In this paper each short range component is fitted separately to a relation of the form of eq. (8).

The numerical integration of eqn. (5) was, as in [1], performed with a Gauss-Legendre quadrature of the potential computed at six θ_A and six θ_B angles and with a Gauss-Chebyshev quadrature for the five θ angles. Because of symmetry only $21\theta_A, \theta_B$ pairs have to be considered. The standard deviation of the spherical expansion (using the first 18 terms and derived from the recalculated potential at the integration grid) was less than 0,5% at the shortest R value and increasing to about 10% at the largest R value. At this largest R value the short range contribution is already small when compared with the long range contributions.

2.4. The second virial coefficient

For a system consisting of general molecules the second virial coefficient B_2 is given by:

$$B_2(T) = N_A \int \dots \int [1 - \exp(-E_{int}(R_A, R_B, \omega_A, \omega_B)/kT)] dR_A dR_B d\omega_A d\omega_B \quad (9)$$

Here R_A stands for the position vector of the centre of mass of molecule A in a space fixed coordinate system, ω_A determines the orientation of the molecule by the three eulerian angles.

For identical homonuclear diatomic molecules this expression can be simplified considerably by the removal of redundant coordinates and by the use of symmetry. When we introduce the spherical expansion (2) for the intermolecular potential we obtain:

$$B_2(T) = 2N_A \int_0^1 \int_0^1 \int_0^\pi \int_0^\infty [1 - \exp\{- (4\pi)^{3/2} \sum_{L_A > L_B} \sum_L \text{(even)} V_{L_A L_B L}(R) \frac{1}{2} [A_{L_A L_B L}(\theta_A, \theta_B, \phi) + A_{L_A L_B L}(\theta_B, \theta_A, \phi)] (2 - \delta_{L_A, L_B}) / kT\}] d\cos\theta_A d\cos\theta_B d\phi R^2 dR \quad (10)$$

In the case of an isotropic potential (all $V_{L_A L_B L}$ are zero but V_{000}) expression (10) becomes identical to the formula for B_2 for the monoatomic gas ($A_{000}(\theta_A, \theta_B, \phi) = (4\pi)^{-3/2}$)

$$B_2(T) = 2\pi N_A \int_0^{\infty} [1 - \exp\{-V_{000}(R)/kT\}] R^2 dR \quad (11)$$

In the numerical evaluation of eq. (10) the integral was replaced by a four dimensional Gauss-Legendre quadrature. Since the behaviour of the interaction energy, when expressed as in (6), is incorrect at very short distances (the potential becomes negative again) we had to set a lower limit of 2.3 Å for the R integration (within this distance the molecules were considered as hard spheres, small variations of this limit showed little influence on the final results). At the long distance end above 25 Å no more significant contribution was found. In this interval only 60 radial integration points were needed. The angular integration was already stable at 6 θ_A , 6 θ_B and 6 ϕ angles. Since at all distances the same set of angular functions $A_{L_A L_B L}(\theta_A, \theta_B, \phi)$ is needed, much computer time can be saved when both the radial functions $V_{L_A L_B L}(R)$ and the angular functions $A_{L_A L_B L}(\theta_A, \theta_B, \phi)$ are computed before the actual integration is performed. Although the potential is rather complicated the integration of eq. (10) with 12960 points for 20 temperatures in the 75 to 700 K interval required only 4 seconds on the Cyber 175/100.

3. Discussion

In Table II we have summarized the results of the spherical expansion for the short range part of the electron gas interaction energies. The spherical expansion coefficients based directly on the ab initio calculations [1], are only available for one distance (0.3 nm). At that distance we see that the leading term, the isotropic one, is nearly equal in the ab initio and the electron gas approach, if the Rae correction is included in the latter (GKR). The anisotropic components are somewhat smaller, in general, in the GKR than in the ab initio calculations. At this stage we are not able to decide whether the difference in the anisotropy is caused by the difference in the monomer wavefunctions used in the ab initio and electron gas expressions, or by the electron gas model itself, or by the numerical procedures used in this method. It is clearly seen that omission of the Rae factor causes -because of a much too large negative exchange contribution-a far too weak repulsion.

The results of the fit of the exponential distance dependence of the short range expansion coefficients according to eq. (8), are

TABLE II

Spherical expansion coefficients $V_{L_A L_B L}^{SR}(R)$ of the short range interaction energy^{a)}

R(nm)	ab	GK ^{c)}	GKR ^{d)}					
	initio ^{b)}		0.300	0.331	0.357	0.384	0.410	0.437
$L_A L_B L$								
0,0,0	44.258	22.048	41.156	14.618	5.813	2.145	0.747	0.248
2,0,2	23.871	13.270	20.606	7.908	3.416	1.376	0.549	0.229
2,2,0	2.947	1.259	1.636	0.830	0.434	0.185	0.076	0.030
2,2,2	-4.734	-2.243	-3.013	-1.384	-0.678	-0.284	-0.114	-0.044
2,2,4	13.154	6.769	9.855	3.836	1.681	0.674	0.262	0.099
4,0,4	4.309	2.068	2.851	1.242	0.604	0.277	0.137	0.077
4,2,2	0.314	-0.053	-0.059	0.026	0.021	0.002	-0.004	-0.006
4,2,4	-0.732	-0.109	-0.153	-0.112	-0.059	-0.017	-0.001	0.005
4,2,6	3.151	1.163	1.636	0.666	0.301	0.120	0.046	0.017
4,4,0	0.005	-0.072	-0.075	-0.025	-0.014	-0.009	-0.006	-0.004
4,4,2	-0.006	0.083	0.087	0.030	0.017	0.011	0.007	0.005
4,4,4	0.026	-0.091	-0.095	-0.033	-0.019	0.013	-0.008	-0.006
4,4,6	-0.131	0.083	0.083	0.023	0.013	0.011	0.008	0.006
4,4,8	1.035	0.148	0.252	0.107	0.047	0.014	0.003	-0.001
6,0,6	0.389	0.252	0.302	0.189	0.107	0.070	0.051	0.038
6,2,4	0.011	-0.033	-0.034	-0.011	-0.013	-0.012	-0.009	-0.008
6,2,6	-0.057	0.033	0.032	0.015	0.017	0.017	0.015	0.013
6,2,8	0.399	0.150	0.186	0.092	0.040	0.019	0.010	0.006

a. Units are kJ/mol.

b. Copied from ref. [1].

c. Hartree-Fock part of the electron gas expression for the interaction energy minus first order long range contributions.

d. As c, but with Rae correction included in the exchange contribution.

given in Table III. Both the linear and the quadratic term in R are rather different for the various coefficients. We have also tried to fit the short range components without the quadratic term. This fit was in most cases much worse. Although the leading components have an about equal linear term, the use of only one equal linear term in formula (5) for all components produces an incorrect potential. In ref. [1] it was found, however, that when besides an equal linear term, also an equal quadratic term for all components was included, rather accurate potential curves for six specific orientations could be obtained (see below).

The first order long range coefficients, based on the multipole moments given in the 4th column of Table I, are included in Table III. For completeness we also copied in this table the second order long range terms from the ab initio calculations [10].

In order to compare the ab initio and GKR results somewhat more in detail, we have reconstructed from the spherical expansion and distance dependence fit of the coefficients, potential surface cuts at six different orientations (see Fig. 2). At the same time we have directly computed the (GKR) first order energy at six distance points and added the second order energy from the multipole expansion. We see that generally a good agreement is found between ab initio and GKR curves. Also the agreement between the points that have been computed directly and the curves that are based on the spherical expansion and distance fit are good, except for the T configuration (90, 0, 0 in Fig. 2). For this T configuration the differences occur principally at the larger distance. We believe that this is caused by strongly orientation dependent errors introduced during the numerical integration used for the GK or GKR energies. From the observed increase with R of the standard deviation for the spherical expansion (see part IIIc), we conclude that the errors in the GK or GKR energies become more important at large R . Since we expect the orientation dependent errors to average out to a large extent by the use of eq. (5), the results predicted by the analytical representation should be the more accurate. Indeed for the T configuration, the curve based on expansion and fit for GKR lies closer to the ab initio curve than the points that are calculated directly in GKR.

In Fig. 3 we compare the coulombic part of the first order energy obtained from the ab initio calculation (ref. [1]) on the

TABLE III

Spherical expansion of interaction energy^{a,b,c}

$$V_{L_A L_B L_C}^{(R)} = a_{L_A L_B L_C} e^{b_{L_A L_B L_C} R + c_{L_A L_B L_C} R^2} + C_{L_A L_B L_C}^{L_A + L_B + 1} R^{-(L_A + L_B + 1)} \\ + C_6^{L_A L_B L_C} R^{-6} + C_8^{L_A L_B L_C} R^{-8} + C_{10}^{L_A L_B L_C} R^{-10}$$

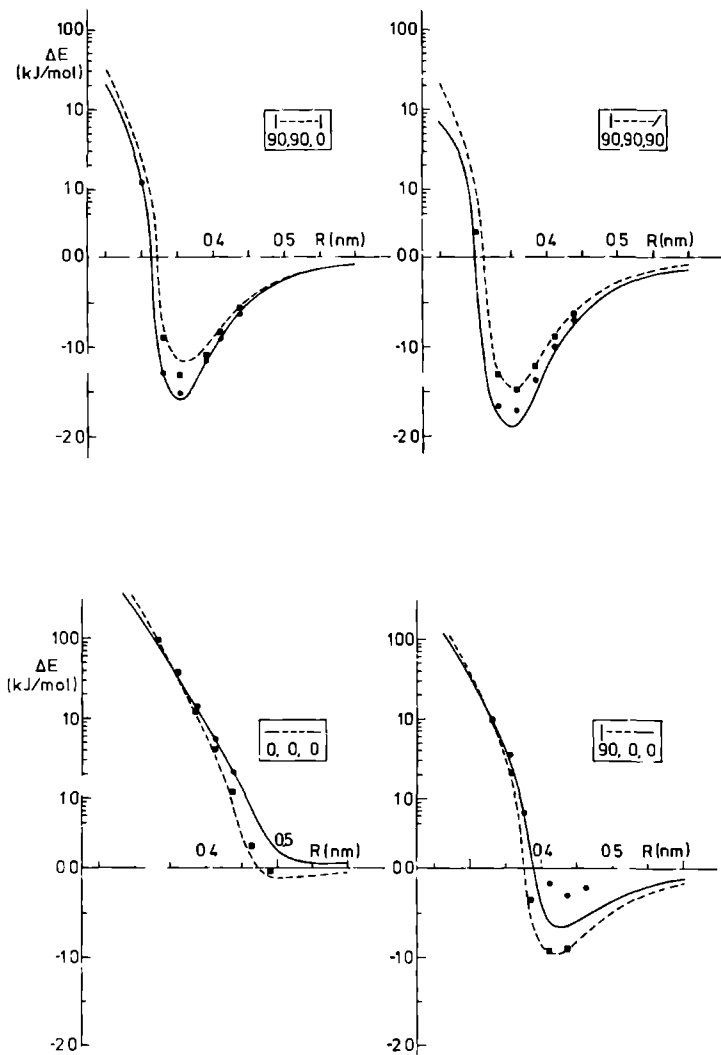
$L_A L_B L_C$	a	b	c	$C_{L_A + L_B + 1}^{L_A L_B L_C}$	C_6	C_8	C_{10}
0,0,0	$1.742 \cdot 10^4$	- 8.32	- 39.50	-	$-4.231 \cdot 10^{-3}$	$-2.946 \cdot 10^{-4}$	$-2.239 \cdot 10^{-5}$
2,0,2	$1.802 \cdot 10^4$	-15.01	- 25.25	-	$-1.815 \cdot 10^{-4}$	$-5.277 \cdot 10^{-5}$	$-5.974 \cdot 10^{-6}$
2,2,0	1.611	20.39	- 67.71	-	$-3.764 \cdot 10^{-6}$	$-6.098 \cdot 10^{-6}$	$-2.256 \cdot 10^{-7}$
2,2,2	$-2.262 \cdot 10^1$	10.05	- 55.85	-	$-4.505 \cdot 10^{-6}$	$1.026 \cdot 10^{-6}$	$-3.692 \cdot 10^{-7}$
2,2,4	$4.009 \cdot 10^3$	-10.64	- 31.32	$2.449 \cdot 10^{-3}$	$-3.638 \cdot 10^{-6}$	$-3.638 \cdot 10^{-6}$	$-1.219 \cdot 10^{-7}$
4,0,4	$9.159 \cdot 10^4$	-39.67	17.50				
4,2,2	-	-	-				
4,2,4	$-2.729 \cdot 10^2$	-17.24	- 22.00				
4,2,6	$8.071 \cdot 10^1$	1.19	- 47.32	$9.177 \cdot 10^{-5}$			
4,4,0	$-2.322 \cdot 10^1$	-16.74	- 9.39				
4,4,2	$1.373 \cdot 10^1$	-13.23	- 13.57				
4,4,4	-8.066	-10.20	- 16.89				
4,4,6	5.754	- 9.99	- 16.14				
4,4,8	$3.744 \cdot 10^{-4}$	73.41	-147.10				
6,0,6	$3.558 \cdot 10^3$	-41.75	35.43	$6.594 \cdot 10^{-6}$			
6,2,4	$-2.853 \cdot 10^{-1}$	- 8.42	-				
6,2,6	$1.063 \cdot 10^{-1}$	- 4.94	-				
6,2,8	$3.583 \cdot 10^3$	36.99	14.28	$7.486 \cdot 10^{-7}$			

a. derived from short range GKR coefficients (Table II), multipole moments (Table I, column 4) and dispersion coefficients from ref. [10].

b. short range coefficients valid for $0.23 \leq R \leq 1.2$ nm

c. $V_{L_A L_B L_C}$ in KJ/mol, R in nm.

Fig. 2



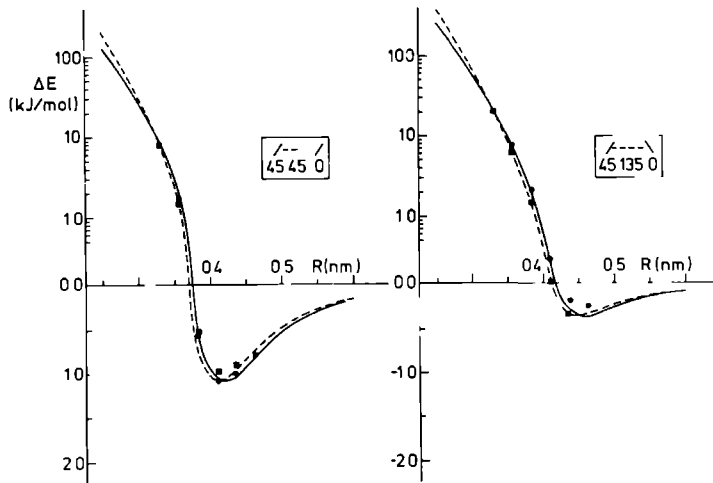
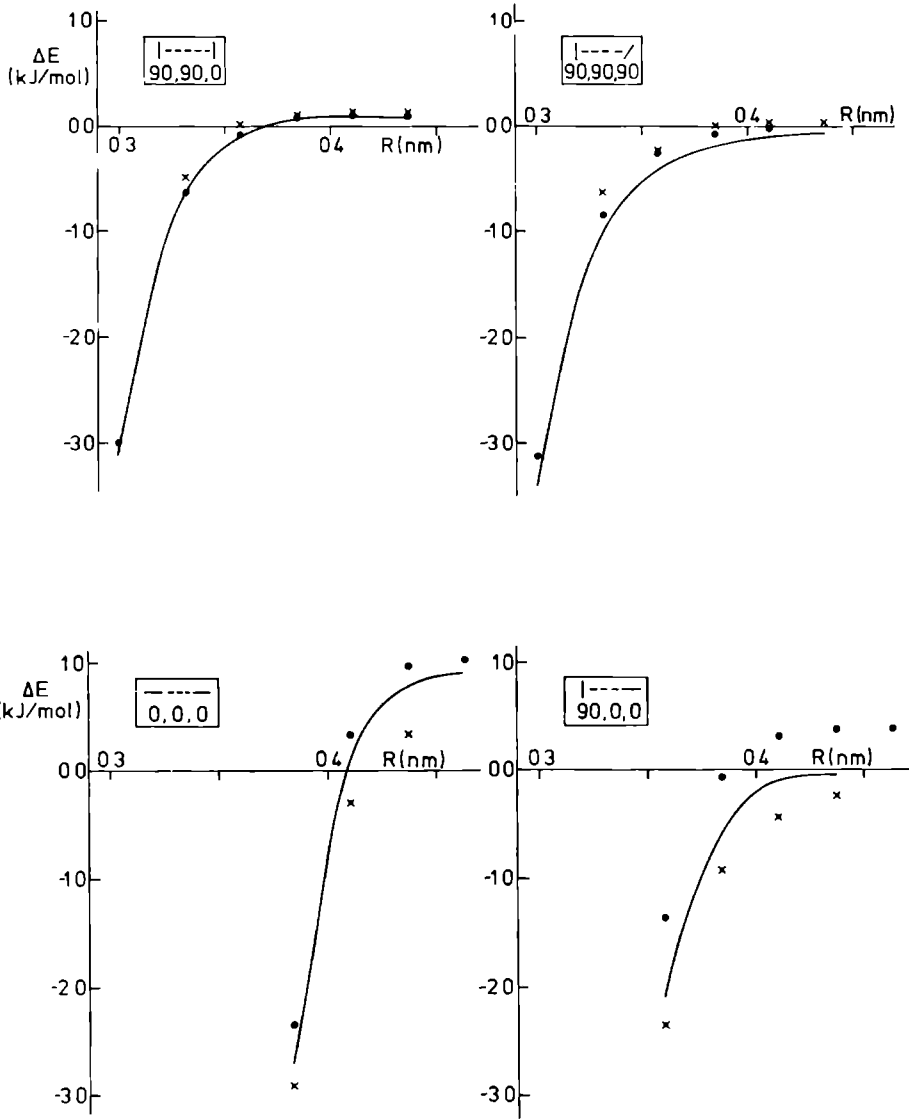


Fig. 2. Potential surface cuts for six different orientations. Solid lines based on spherical expansion of GKR results; dashed lines based on spherical expansion of ab initio calculations (ref. [1]); ● computed directly with GKR method; ■ computed directly with ab initio method (ref. [1]).

Fig. 3



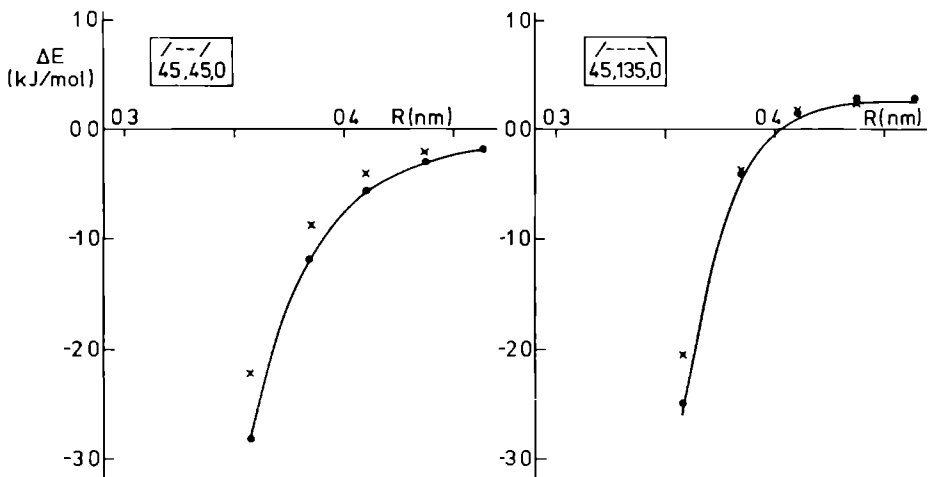


Fig. 3. Coulomb part of the interaction energy for six different orientations. Solid lines based on spherical expansion of the Coulomb contribution in the electron gas expression for the interaction energy; ● computed directly in electron gas program; x computed directly with ab initio program (ref. [1]).

one hand and from the GKR approach on the other. We look for the latter both at the results of direct calculations and at the results predicted by the spherical expansion made at the various distances (no fit of the distance dependence of the expansion coefficients for the coulombic energy was made). We see that the disagreement between ab initio points and GKR points is again largest for the T configuration. As before, use of the spherical expansion reduces the difference between GKR and ab initio values.

From the spherical expansion analysis of the electron gas correlation energy we found that at all distances the value for the isotropic component was about three times smaller than the value obtained from the ab initio dispersion coefficients ($C_6^{000}/R^6 + C_8^{000}/R^8 + C_{10}^{000}/R^{10}$). Also the anisotropic terms in the electron gas correlation energy differ from the ab initio dispersion energy terms. Furthermore they do not have the correct distance dependence.

Although the second virial coefficient certainly does not form the most stringent test of the anisotropy of a potential, we believe that it does give an additional indication of the correctness or shortcomings of a potential. In Fig. 4 we compare the predictions

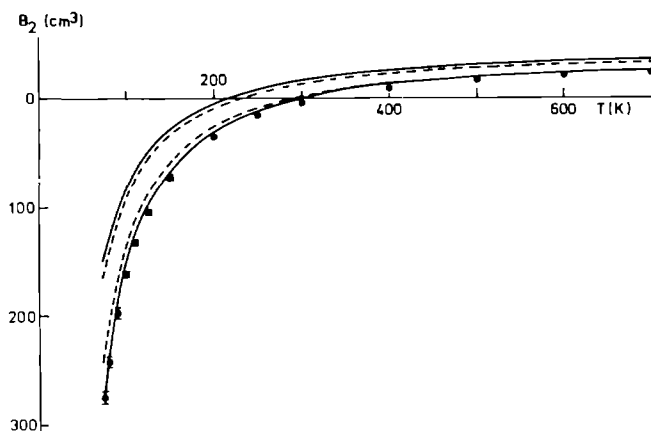


Fig. 4. Temperature dependence of the second virial coefficient. \blacksquare experimental points with spread taken from Ref. [23]. Solid line obtained with formula (10) and data from Table III. Dashed line obtained with the ab initio expansion (ref. [1]). Curves marked iso obtained with isotropic (V_{000}) potential. (formula (11)).

based on the ab initio and on the GKR potential with the experimental results [24]. Since the GKR and the ab initio potential are not very different, it is not surprising that they predict similar curves. It is, however, very encouraging that both curves are so close the experimental one, taking into account that no adjustable parameters appear. The GKR potential does slightly better over the whole range, this may be caused by the more detailed description of the distance dependence of the short range spherical expansion coefficients. We have tried to trace the origin of the remaining discrepancies -the too low Boyle temperature and the too large slope at low temperature- by scaling the short range isotropic component and all dispersion terms by small amounts. This leads only to minor improvements, however, and it is contrary to the philosophy of a non-empirical potential. Since the ab initio and the GKR potentials are so similar we tend to the conclusion that neglect of intramolecular correlation in the determination of the monomer electron densities and possibly still some minor inaccuracy in the dispersion terms are responsible for the small differences.

Finally we want to comment on the isotropic potentials frequently used to generate second virial coefficients. From Fig. 4 we see that the isotropic part of the ab initio or GKR potential produces B_2 curves rather far away from the experimental one. In ref. [25], the same conclusion was reached in an analysis of model potentials for the construction of B_2 curves for N_2 . Also the neglect of some first and second order long range coefficients in the expansion leads to incorrect B_2 curves. We do not share the conclusion of ref. [25], that "quadrupole-quadrupole interaction makes a negligible contribution to $B_2(T)$ for N_2 ". In ref. [25] temperatures below 273K were not considered. It is exactly in the low temperature range that the effect of a nonzero quadrupole moment shows up. At 75K the B_2 value found with the GKR + dispersion potential is $-273.2 \text{ cm}^3 \text{ mol}^{-1}$ (experimental value $-274 \text{ cm}^3 \text{ mol}^{-1}$). Neglect of the contribution due to quadrupole-quadrupole interaction (the C_5^{224} coefficient from Table III is chosen to be zero) gives $-287.9 \text{ cm}^3 \text{ mol}^{-1}$.

For diatomic and larger molecules, the so-called inversion, i.e. obtaining the intermolecular potential from experimental B_2 curves, seems to us impossible. For instance the minimum of the isotropic part of the GKR + dispersion potential is found at 0.422 nm (ab initio, ref. [1], 0.417 nm). This value is larger than the value used

in model potentials that have been adjusted especially to reproduce the B_2 curves (0.388-0.404 nm in ref. [26]). Also the isotropic well depth of the GKR + dispersion potential of $0.709 \text{ kJ mol}^{-1}$ ($\sim 85.3 \text{ K}$, the ab initio value in ref. [1] was $0.748 \text{ kJ mol}^{-1} \sim 90.2 \text{ K}$) is smaller than in these model potentials (95.175 K) in refs. [26,27]). It is clear that if, moreover, these model potentials are assumed to be isotropic, the resulting parameters are void of any physical meaning.

Acknowledgement

We are most grateful to Professor Van der Avoird for his critical reading of the manuscript and for many stimulating discussions.

References

1. R.M. Berns and A. van der Avoird, J. Chem. Phys. 72, 6107 (1980)
2. T. Luty, A. van der Avoird and R.M. Berns, J. Chem. Phys. 73, 5305 (1980).
3. F. Mulder, A. van der Avoird and P.E.S. Wormer, Mol. Phys. 37, 159 (1979).
4. R.G. Gordon and Y.S. Kim, J. Chem. Phys. 56, 3122 (1972).
5. Y.S. Kim, Thesis, Harvard University (1975); S. Green J. Chem. Phys. 60, 2654 (1974).
6. S. Green, B.J. Garrison, W.A. Lester, J. Chem. Phys. 63, 1154 (1975); B.J. Garrison, W.A. Lester, H.F. Schaefer III, J. Chem. Phys. 64, 1449 (1975).
7. A.I.M. Rae, Chem. Phys. Lett. 18, 574 (1973).
8. A.I.M. Rae, Mol. Phys. 29, 467 (1975).
9. J. Detrich and R.W. Conn, J. Chem. Phys. 64, 3091 (1976).
10. F. Mulder, G. van Dijk and A. van der Avoird, Mol. Phys. 39, 407 (1980).
11. F.H. Ree and N.W. Winter, J. Chem. Phys. 73, 322 (1980).
12. E. Clementi, J. Chem. Phys. 40, 1944 (1964).
13. P.A. Christiansen and E.A. McCullough Jr., J. Chem. Phys. 67, 1877 (1977).
14. P.S. Bagus, in: Selected topics in molecular physics (Chemie, Weinheim, 1972) p. 187.
15. G.A. Parker, R.L. Snow and R.T. Pack, Chem. Phys. Lett. 33, 399 (1975).
16. W. Kolos and E. Radzio, Int. J. Quantum Chem. XIII, 627 (1978).
17. M. Waldman and R.G. Gordon, J. Chem. Phys. 71, 1325 (1979).

18. J.S. Cohen and R.T. Pack, *J. Chem. Phys.* 61, 2372 (1974).
19. G.A. Parker and R.T. Pack, Program 305, Quantum Chemistry Program Exchange, Indiana University, Bloomington, IN 47401.
20. A. van der Avoird, P.E.S. Wormer, F. Mulder and R.M. Berns in: *Van der Waals Systems*, R. Zahradnik ed., *Topics in Current Chemistry*, 93, 1-51, Springer, Berlin (1980).
21. D.M. Brink and G.R. Satchler, *Angular Momentum*, Clarendon Press, Oxford, 2nd edition (1975).
22. P.E.S. Wormer, F. Mulder and A. van der Avoird, *Intern. J. Quantum Chem.* 11, 959 (1977).
23. S. Green, *J. Chem. Phys.* 67, 715 (1977).
24. J.H. Dymond and E.B. Smith, *The Virial Coefficient of Gases*, Clarendon Press, (1969).
25. M.D. Whitmore and D.A. Goodings, *Can. J. Phys.* 58, 820 (1980).
26. T.B. MacRury, W.A. Steele and B.J. Berne, *J. Chem. Phys.* 64, 1288 (1976).
27. D.J. Evans, *Mol. Phys.* 33, 979 (1977).

Lattice dynamics of solid N₂
with an "ab initio" intermolecular potential[†]

T. Luty^{*}, A. van der Avoird and R.M. Berns

Institute of Theoretical Chemistry

University of Nijmegen

Toernooiveld, Nijmegen

The Netherlands

Abstract

We have performed harmonic and self-consistent phonon lattice dynamics calculations for α and γ N₂ crystals using an intermolecular potential from ab initio calculations. This potential contains electrostatic (multipole) interactions, up to all R⁻⁹ terms inclusive, anisotropic dispersion interactions, up to all R⁻¹⁰ terms inclusive, and anisotropic overlap interactions caused by charge penetration and exchange between the molecules. The lattice constants, cohesion energy, the frequencies of the translational phonon modes and the Grüneisen parameters for the librational modes are in good agreement with experimental values, confirming the quality of the potential. The frequencies of the librational modes and those of the mixed modes are less well reproduced, especially at temperatures near the α - β phase transition. Probably, the self-consistent phonon method used does not fully account for the anharmonicity in the librations.

[†] Supported in part by the Netherlands Foundation for Chemical Research (SON) with financial aid from the Netherlands Organization for the Advancement of Pure Research (ZWO).

^{*} Present address: Institute of Organic and Physical Chemistry, Technical University, Wrocław, Poland.

1. Introduction

During the past several years, a considerable number of experimental and theoretical investigations (see [1] and references therein) have been made of the molecular motions and intermolecular potentials in solid nitrogen as one of the simplest molecular crystals. Lattice dynamics studies have been performed, mostly because they are considered to be very critical tests of model potentials, since the phonon excitations in solids are much more sensitive for the details of the intermolecular potential than gas phase properties. All the potentials have been semi-empirical, i.e. they have been based on simplified models, especially for the short range forces but also for the anisotropic long range interactions, and the parameters have been fitted to the experimental data. Here, we present, for the first time, lattice dynamics calculations for the ordered low temperature α and γ phases of solid N_2 , starting from an anisotropic intermolecular potential from ab initio calculations [2,3].

One has to remember that the accuracy by which the experimental lattice mode frequencies can be reproduced depends not only on the quality of the potential used, but also (sometimes critically) on the method (approximations) employed to solve the dynamics of the crystal. Therefore, we have applied the harmonic model [4], as well as the self-consistent phonon procedure [5] which corrects for the effects of anharmonicity in the potential. So, this work can be regarded both as a check on the calculated N_2 - N_2 potential and as a test of the approximations commonly used in lattice dynamics studies of molecular crystals.

2. Methods and potential

The harmonic [4] and self-consistent phonon [5] treatments of the lattice vibrations in molecular crystals have been described in detail elsewhere. Before solving the harmonic dynamical equations, we have minimized the lattice energy for the given potential as a function of the lattice constants, as required theoretically [4]. The self-consistent phonon (SCP) method is one way to correct for the effects of the anharmonicity in the potential. This method uses a harmonic model with effective force constants that are derived by minimizing the first or-

der expression of the free energy for the actual potential employed. These force constants are calculated as the second derivatives of the potential averaged over the molecular displacements; the latter are described by the displacement-displacement correlation function. Since this function depends on the lattice mode frequencies and eigenvectors, which are related to the force constants via the dynamical equations, the calculations have to be carried out self-consistently. The free energy is minimized also with respect to the lattice constants (and the molecular orientations in the unit cell if these are not fixed by symmetry, as in nitrogen).

The SCP method has been applied earlier to α -N₂ with a Lennard-Jones 12-6 atom-atom potential [6]. Since this method has been formulated for (rare gas) atomic crystals [5], which have no librational degrees of freedom, the authors [6] have actually solved the dynamical equations for the individual N atoms after introducing an intramolecular N-N force constant. They found some deviations of the librational frequencies from experiment, however, which they ascribed to deficiencies in the intermolecular potential (in particular, the lack of quadrupole-quadrupole interactions). The SCP method which we have applied is a generalization [7] of the original formalism [5], which does explicitly include the librational motions of the molecules, but assumes (in the kinetic energy expression and in the displacement-displacement correlation function) that the amplitudes of the librations are relatively small.

The angle dependent N₂-N₂ potential on which our lattice dynamics calculations are based, has been obtained from ab initio calculations [2,3]. It includes the long range electrostatic (multipole-multipole) interactions (all R⁻⁵, R⁻⁷ and R⁻⁹ terms), the dispersion interactions (all R⁻⁶, R⁻⁸ and R⁻¹⁰ terms) and the short range (overlap) forces arising from charge penetration (electrostatic effects) and exchange (Pauli repulsion). The induction (multipole-induced multipole) interactions, which would lead to the largest deviations from a pairwise additive intermolecular potential [8-10], are negligibly small for N₂ [2,3]. The remaining three-molecule interactions, in which the long range triple-dipole dispersion energy and the short range exchange contributions are the dominant terms, are estimated to be only a few percent of the pair energies in the range of the Van der Waals mini-

mum [10,11].

If one expands the angular dependence of our N_2-N_2 potential in spherical harmonics describing the rotations of the individual molecules (A and B), one finds that the anisotropic dispersion interactions are important up to $L_A = L_B = 2$ inclusive, while the electrostatic and overlap contributions have to be taken up to $L_A = L_B = 4$ inclusive [2,3]. For comparison, the most extensive and probably the best empirical potential [1] used in N_2 crystal studies only contains isotropic ($L_A = L_B = 0$) dispersion interactions and quadrupole-quadrupole ($L_A = L_B = 2$) electrostatic contributions. We have not used the spherical expansion of the potential in the present lattice dynamics calculations, however, but instead we have applied an atom-atom exp-6-1 potential with the parameters fitted to the ab initio results. It has been shown [2] that, in the case of N_2 , the atom-atom (or rather site-site) model yields a fairly good representation of the intermolecular potential, even in describing its angular dependence. It is necessary to use two positive and two negative charges (symmetrically) placed on the N-N axis for representing the electrostatic multipole interactions and, preferably, slightly shifted force centers for the dispersion interactions, too. The site-site potentials with the dispersion centers on the nuclei and with shifted centers, have been named potentials A and B, respectively; the parameters are listed in table 1 (cf. table 3 of [2]).

The lattice dynamics calculations have been made for α - N_2 assuming the space group $Pa3(T_h^6)$ [12], including 54 neighbouring molecules in the lattice sums for the (free) energy and the force constants. Only a single lattice constant (a) had to be optimized for this cubic phase. For the γ -phase, which is stable under pressures above 3.5 kbar, the space group is $P4_2/mnm(D_{4h}^{14})$ [13] and we have taken 42 neighbouring molecules into account; two lattice parameters (a and c) had to be optimized due to the tetragonal symmetry. The SCP program developed by Wasilutynski [7] has been adapted to these α and γ lattice symmetries; there are 4 and 2 molecules per unit cell, respectively. For the calculations under pressure we have used the procedure prescribed by Pawley et al. [14] for the harmonic model and we have minimized the Gibbs free energy instead of the Helmholtz quantity in the SCP method [7].

Table 1

Atom-atom potential fitted to ab initio results [2]

Force centers i have positions $+z_i$ and $-z_i$ on the N-N axes
(different for each contribution, in principle).

Contributions	Parameters	Potential A	Potential B
Electrostatic $q_i q_j r_{ij}^{-1}$	charges ^{a)} $q_+ = -q_-$ positions ^{b)} $z_+, z_- [\text{Å}]$	0.373 0.847, 1.044	0.373 0.847, 1.044
Overlap $A \exp(-B r_{ij})$	A [kJ/mol] B [Å^{-1}] positions ^{b)} $z_O [\text{Å}]$	770 000 4.037 0.547	770 000 4.037 0.547
Dispersion $C r_{ij}^{-6}$	C [kJ $\text{Å}^6/\text{mol}$] positions ^{b)} $z_D [\text{Å}]$	1407 0.547	1511 0.471

a) in unit charges $e = 1.602 \cdot 10^{19} \text{C}$

b) nuclear positions are $z_N = \pm 0.547 \text{Å}$

3. Results

The results calculated for the lattice constant, the cohesion energy and the frequencies of various phonon modes are listed in tables 2 and 3 for the α and γ phases, respectively, at zero pressure and 4 kbars. They can be compared with the experimental data [13,15-17] included in these tables. Phonon frequencies have been measured by inelastic neutron scattering in α -N₂ at 15K [16] and by Raman spectroscopy in γ -N₂ at 4.2K [17]; the SCP calculations have been performed at the same temperatures. We have also included the results obtained by Raich and Gillis [1] with their recommended empirical potential (1), but not the earlier semi-empirical calculations as these were extensively discussed by the latter authors.

Our calculated lattice constants and cohesion energy are in good agreement with the experimental data. Raich and Gillis [1] have used these quantities, for the α phase, as fitting data for their potential, but the present calculations do not contain such fitting procedures, since the potential is entirely determined a priori. The lattice mode frequencies from the harmonic calculations are always higher than the experimental values, except for the librational B_{1g} mode in the γ phase. Potential B which has a somewhat smaller anisotropy in the dispersion interactions (the force centers are closer) than potential A, yields slightly higher frequencies in particular for the librational (the g modes at the Γ point in the Brillouin zone and the R⁺ modes at the R points) and mixed (M point) modes. This seems contradictory, but it must be remembered that the anisotropy in the dispersion interactions in fact reduces the larger anisotropy in the electrostatic quadrupole interactions [3].

The SCP formalism, which we have only applied with potential A since it is very (computer) time consuming, consistently lowers the frequencies. This can be understood, since the effective potential, averaged over the molecular displacements, is softer than the bare potential at the Van der Waals minimum [7]. This lowering brings the frequencies of the translational modes (u modes at Γ and R⁻ modes at R) into excellent agreement with experiment. The librational and mixed mode frequencies remain substantially too high, however, although the anharmonic SCP corrections are always in the right direction (except for the γ phase B_{1g} frequency which is somewhat too low already). In principle, this might be due to the potential still not

Table 2

 α -N₂ crystal data, at zero pressure and T = 15K

	Experiment ^{a)}	Semi-empirical calculations [1] Harmonic, potential 1	Present calculations		
			Harmonic		SCP
			potential A	potential B	potential A
Lattice constant a [Å]	5.644	5.644 ^{c)}	5.644	5.611	5.796
Lattice energy ^{b)} [kJ/mol]	6.92	6.92 ^{c)}	6.00	6.43	6.05
Phonon frequencies ω [cm ⁻¹]					
$\Gamma(0,0,0)$					
E _g	32.3	37.5	40.8	42.4	39.5
T _g	36.3	47.7	50.7	52.9	48.5
T _g	59.7	75.2	74.3	77.7	70.3
A _u	46.8	45.9	52.4	52.8	48.8
T _u	48.4	47.7	52.0	52.6	48.4
E _u	54.0	54.0	57.6	58.9	53.5
T _u	69.4	69.5	77.5	78.8	72.0
M($\pi/a, \pi/a, 0$)					
M ₁₂	27.8	29.6	34.7	34.9	32.5
M ₁₂	37.9	40.6	45.9	46.4	43.3
M ₁₂	46.8	51.8	57.3	59.1	54.0
M ₁₂	54.9	59.0	62.5	64.4	58.5
M ₁₂	62.5	66.4	69.6	72.3	64.9
R($\pi/a, \pi/a, \pi/a$)					
R ₁ ⁻	33.9	34.4	36.6	37.1	34.2
R ₂₃ ⁻	34.7	35.7	38.6	39.2	35.9
R ₂₃	68.6	68.3	76.3	77.6	71.0
R ₁ ⁺	43.6	50.7	55.6	58.1	52.7
R ₂₃ ⁺	47.2	57.8	58.3	61.0	55.7

a) from [16], lattice energy from [15]

b) experimental: heat of sublimation at 0K [15]

calculated: lattice energy at 0K including zero-point motions

c) fitted to experiment in optimization of the potential parameters

Table 3

 γ -N₂ crystal data, at 4 kbars and T = 4K

Experiment ^{a)}	Semi-empirical calculations [1],		Present calculations		
	Harmonic, Potential 1		Harmonic		SCP
			potential A	potential B	potential A
Lattice constants					
a [Å]	3.957	3.940	4.052	4.032	4.100
c [Å]	5.103	5.086	5.029	5.000	5.188
Phonon frequencies ω [cm ⁻¹]					
$\Gamma(0,0,0)$					
E _g	55.0	50.5	57.9	60.1	56.5
B _{1g}	98.1	74.8	86.5	89.2	85.2
A _{2g}	-	105.1	109.7	111.2	107.1
E _u	-	58.3	72.0	71.4	69.3
B _{1u}	-	103.1	110.3	113.8	107.4

a) lattice constants from [13], phonon frequencies from [17]

having the correct anisotropy, but it has been argued before [1] that, irrespective of the precise potential used, the librational modes require larger anharmonic corrections than the translational ones (this is related to their larger relative amplitudes). The SCP method, especially the version that we have used which assumes relatively small librational amplitudes (see section 2), might be less effective in correcting for the anharmonic effects in the librations.

The best potential of Raich and Gillis [1] with parameters fitted to the experimental data for solid N_2 , yields somewhat lower frequencies already in the harmonic approximation and slightly better overall agreement with the experimental data than the harmonic model applied with the ab initio potential. Still, some of their librational frequencies are considerably too high also, while other values are lower than the experimental ones (especially the γ phase B_{1g} frequency, which we find too low, is even much lower in their case). It is uncertain whether the anharmonic corrections would systematically improve the quality of their results, as they do in our case.

The remaining discrepancy between the SCP results and the experimental librational frequencies is clearly illustrated in fig. 1. Here, we have displayed the temperature dependence in the frequency of the lowest librational E_g mode in the α phase [18]. When the α - β transition temperature (35.6K) is approached, the amplitudes of libration increase and mode-mode coupling may occur. Apparently, the (present) SCP model cannot completely follow this trend.

In fig. 2 we have shown the pressure dependence of the $\underline{g} = \underline{0}$ mode frequencies (ω_1) at 12K, calculated by the SCP method. This dependence is related to the molar volume (v) dependence of these modes measured by the Grüneisen parameters:

$$\gamma_1 = - \left(\frac{\partial \ln \omega_1}{\partial \ln v} \right)_T$$

So, the results presented in fig. 2 can be indirectly compared with experiment by looking at the Grüneisen parameters that have been measured for the librational frequencies in both the α [18] and the γ [17] phase. If the quadrupole-quadrupole interaction would be the only anisotropic contribution to the potential these parameters would be equal to 5/6. Table 4 shows good agreement between the SCP and the measured results at 8K; this confirms the quality of the anisotropic

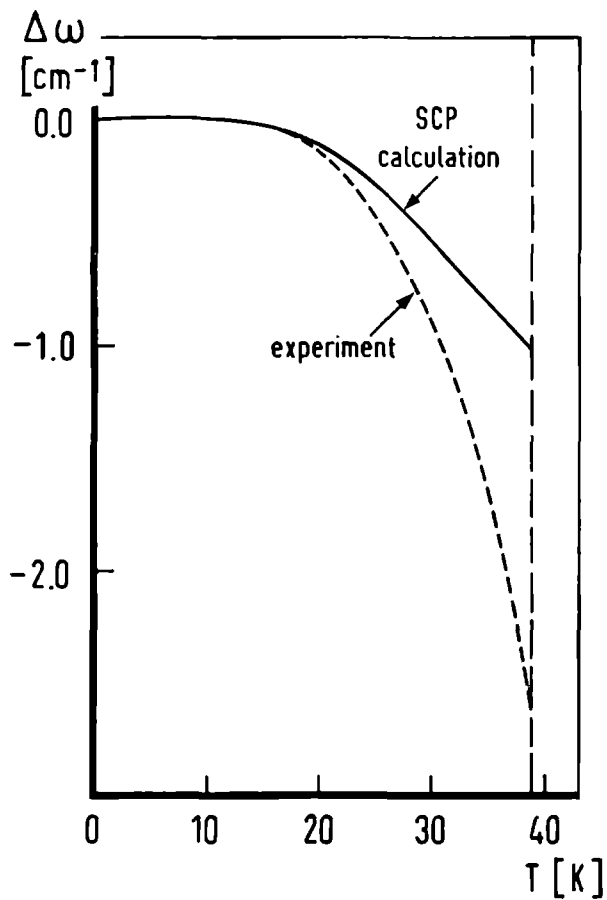


Fig. 1. Temperature dependence of the E_g librational frequency in the α phase. The difference $\Delta\omega$ is defined as $\omega(T) - \omega(T=0)$; experimental data from [18].

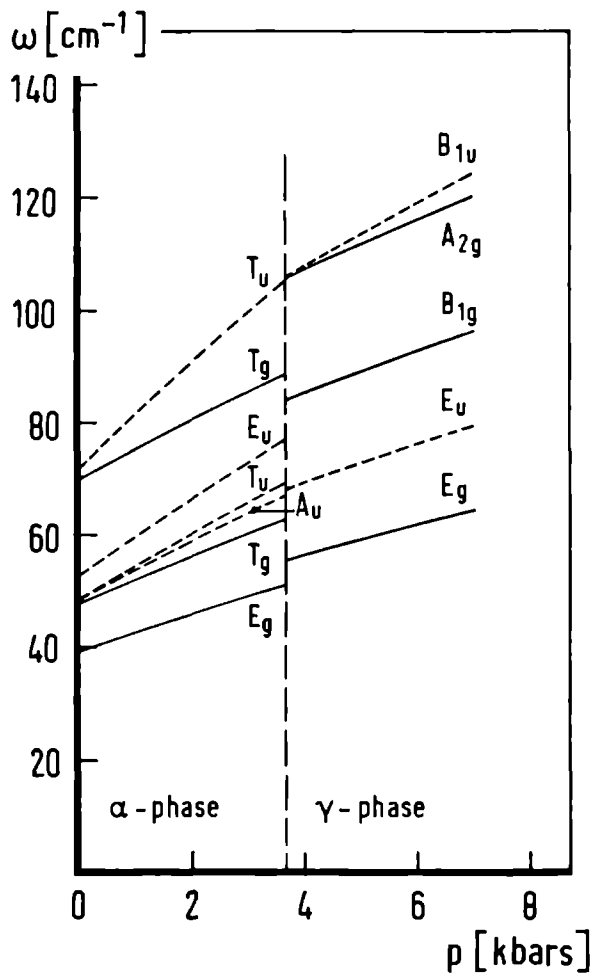


Fig. 2. Pressure dependence of the lattice mode frequencies in the α and γ phases, calculated by the SCP method at 12K. Closed lines represent the librational modes, dashed lines the translational ones.

Table 4

Grüneisen parameters at 8K for the librational modes in
the α and γ phases of solid nitrogen

Mode		Grüneisen parameters	
		Experiment ^{a)}	SCP calculations, potential A
α -N ₂	E _g	1.95	2.00
	T _g	1.63	1.90
	T _g	1.68	1.68
γ -N ₂	E _g	2.3	2.28
	B _{1g}	2.3	2.02

a) for α -N₂ from [18], for γ -N₂ from [17]

ab initio potential as the Grüneisen parameters are critically dependent on the shape of the potential. The experiment [18] finds the parameters of the α -phase to be practically temperature independent, however, whereas the SCP calculations predict a rather strong dependence, see fig. 3. This discrepancy indicates again that the (our) SCP method is not fully capable of reproducing the anharmonic effects occurring in the (α -phase) librations especially at higher temperatures.

4. Conclusions

Our lattice structure and dynamics calculations with the ab initio N_2-N_2 potential [2] yield good agreement with experiment for the lattice constants and the translational mode frequencies of α and γ N_2 crystals. The anharmonic corrections by the self-consistent phonon method essentially improve the latter. The SCP method also yields good Grüneisen parameters for the librational modes in α and γ nitrogen at low temperature. Furthermore, the cohesion energy of α - N_2 is rather accurately calculated, especially with the best atom-atom representation of the ab initio potential, potential B. So, we may conclude that the ab initio potential [2] is quite realistic, both in its radial and angular dependence.

In the librational frequencies some discrepancies with the experimental data remain even in the SCP values, although the anharmonic corrections generally point to the right direction. Apparently, the librational modes have relatively large amplitudes especially in the (low pressure) α phase near the α - β transition temperature, and the SCP method used [7] cannot completely deal with this case. One should improve on the small amplitude expansion for the librational motions or, possibly, use a quantum mechanical libron treatment [19] in terms of free rotor basis functions instead of the harmonic oscillator basis. In that case, the spherical expansion [2] of the ab initio potential is very useful. Also classical molecular dynamics (computer simulation) studies of the librational motions in solid N_2 [20] may be worth trying with the ab initio potential [2] instead of the approximate Lennard-Jones 12-6 atom-atom potential.

Acknowledgement

We thank dr. Tadeusz Wasilutynski for making available his harmonic and self-consistent phonon lattice dynamics programs.

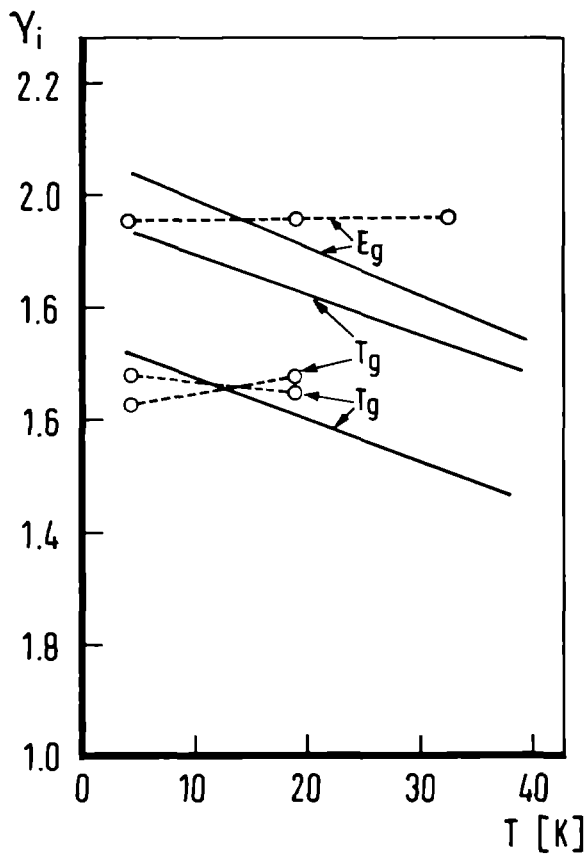


Fig. 3. Temperature dependence of the Grüneisen parameters for the librational modes in the α phase, calculated by the SCP method at zero pressure (closed lines). Experimental values (---o---) from [18].

References:

1. J.C. Raich and N.S. Gillis, *J. Chem. Phys.* 66, 846 (1977).
2. R.M. Berns and A. van der Avoird, *J. Chem. Phys.* (1 June 1980).
3. F. Mulder, G. van Dijk and A. van der Avoird, *Mol. Phys.* 39, 407 (1980).
4. G. Venkataraman and V.S. Sahnı, *Rev. Mod. Phys.* 42, 409 (1970).
5. N.R. Werthamer in: *Rare Gas Solids Vol. I*, M.L. Klein and J.A. Venables eds., Academic Press, London (1976), p.265.
6. J.C. Raich, N.S. Gillis and A.B. Anderson, *J. Chem. Phys.* 61, 1399 (1974).
7. T. Wasıutyński, *Phys. Stat. Sol. (b)* 76, 175 (1976).
8. A. Beyer, A. Karpfen and P. Schuster, *Chem. Phys. Letters* 67, 369 (1979).
9. E. Clementı, W. Kolos, G.C. Lie and G. Ranghino, *Int. J. Quantum Chem.* 17, 377 (1980)
10. A. van der Avoird, P.E.S. Wormer, F. Mulder and R.M. Berns in: *Van der Waals Systems*, R. Zahradnik ed., Topics in Current Chemistry, Springer, Berlin (1980).
11. P. Claverie in: *Intermolecular Interactions: From Diatomics to Biopolymers*, B. Pullman ed., Wiley, New York (1978), p. 69.
12. J.A. Venables and C.A. English, *Acta Cryst.* B30, 929 (1974).
13. R.L. Mills and A.F. Schuch, *Phys. Rev. Letters* 23, 1154 (1969), A.F. Schuch and R.L. Mills, *J. Chem. Phys.* 52, 6000 (1970).
14. G.S. Pawley and K. Mıka, *Phys. Stat. Sol. (b)* 66, 679 (1974).
15. B.C. Kohın, *J. Chem. Phys.* 33, 882 (1960).
16. I.K. Kjems and G. Dolling, *Phys. Rev.* B11, 1639 (1975).
17. M.M. Thiéry and D. Fabre, *Mol. Phys.* 32, 257 (1976).
18. F.D. Medina and W.B. Daniels, *J. Chem. Phys.* 64, 150 (1976).
19. M.J. Mandell, *J. Low Temp. Phys.* 17, 169 (1974); 18, 273 (1975).
20. J.J. Weis and M.L. Klein, *J. Chem. Phys.* 63, 2869 (1975).

Lattice dynamics of the ethylene crystal
with interaction potentials from ab initio calculations.

T. Wasiutynski^{*}, A. van der Avoird and R.M. Berns

Institute of Theoretical Chemistry

University of Nijmegen

Toernooiveld, Nijmegen

The Netherlands

Abstract

The long range (electrostatic, dispersion, induction) and short range (exchange and penetration) interaction energy between ethylene molecules has been calculated by ab initio methods as a function of the molecular orientations and distances. The results, when fitted with an exp-6-1 atom-atom potential and used in a harmonic lattice dynamics calculation on the ethylene crystal, yield fair agreement with the experimental structure data, IR and Raman phonon frequencies. Although the fit with the atom-atom potential is reasonably good, some specific deviations from the ab initio results indicate the importance of the effects of chemical bonding on the intermolecular potential (leading to non-central and non-pairwise additive atom-atom forces). The usual empirical atom-atom potentials are grossly corroborated, their main defect being the neglect or underestimate of electrostatic (quadrupole-quadrupole) interactions.

* Present address: Institute of Nuclear Physics, Krakow, Poland.

1. Introduction

Practically all calculations to date on the lattice stability and dynamics of molecular crystals have used simple empirical expressions for the interaction potential between the molecules. Very popular, for instance, is the use of so-called atom-atom potentials [1] of the Lennard-Jones (12-6) or Buckingham (exp-6) type. The parameters occurring in these potentials are derived from experimentally known crystal data, such as the structure, the cohesion energy, the elastic constants [2-4], or sometimes they are obtained by fitting the calculated lattice frequencies to measured IR and Raman spectra [5] or to phonon dispersion curves from inelastic neutron scattering [6].

It is not certain that these empirical potentials correspond with the "real" interaction potential between the molecules, first of all, because the atom-atom potential model still lacks a sound physical basis and has never been thoroughly tested [7] and, secondly, because the crystal properties may not be equally sensitive to all aspects of the interaction potential. Some interactions, the electrostatic forces for example, may to some extent average out in the crystal [8] and it is typical that in many of the empirical potentials [1,2] these forces are left out completely, while the potentials still yield a reasonable description of several crystal properties.

For small, mostly diatomic molecules more detailed information about the interaction potential is becoming available, from beam scattering experiments [9,10], relaxation measurements [11] and spectroscopic studies [12,13]. Only for the simplest case of the H₂ molecule, however, one has now rather good knowledge of the shape and the

anisotropy of the interaction potential, mainly as a result of ab initio calculations on the H_2-H_2 [14-20] and H_2-He [19-25] interactions. Some of this information has already been used in lattice dynamics calculations on solid H_2 [26, 27].

It is important to obtain similar information about the intermolecular interaction in the hydrocarbon crystals, in view of the various physically interesting effects displayed by these crystals. They have been subject of extensive semi-empirical studies [1-3,28-37], especially by Williams [2,3,28-30] who has been using atom-atom potentials with carefully optimized empirical parameters. Although Williams' calculated results show a nice quantitative agreement with the experimental properties considered (which have been used, for the main part, in the parameter fit), the remaining discrepancies [30] indicate already that the empirical atom-atom potentials must still be deficient in some respects.

Therefore, we thought it useful to perform an ab initio study of the interaction between ethylene molecules and to apply the results to a calculation of the structure and the dynamics of the ethylene crystal. This study is a continuation of earlier ab initio work on the ethylene dimer [38-40,8] and the crystal [8]. Thus, we can find out in how far the atom-atom potential model can be theoretically justified, how the empirical parameters compare with the theoretical results and which are the deficiencies of the model that must be corrected. On the other hand, since several experimental properties have been measured on solid ethylene, the crystal results provide a check on the accuracy of our ab initio calculations.

A similar study, concerning the static crystal properties, has recently been carried out for some hydrogen bonded systems [41,42].

2. Ab initio calculations of the ethylene-ethylene interaction

A Procedure and results

Although our first calculation of the ethylene-ethylene interaction potential [38] was actually the most elegant one, since it yielded all short range (exchange and penetration) and long range (electrostatic, induction and dispersion) interactions in the single consistent formalism of the Multistructure Valence Bond method, further ab initio calculations [39,40] and some preliminary lattice dynamics studies have shown that the basis set employed originally was too small. As a result we had underestimated both the (first order) exchange repulsion and the (second order) induction and dispersion attractive interactions. Therefore, we have extended the basis and we have performed the calculation of the first order and second order interaction energy separately, for several intermolecular distances R and for several orientations, $\underline{\Omega}_A$ and $\underline{\Omega}_B$, of the ethylene molecules in the dimer.

The first order energy, defined as:

$$\Delta E^{(1)}(R, \underline{\Omega}_A, \underline{\Omega}_B) = \langle A \psi_0^A \psi_0^B | H^{AB} | A \psi_0^A \psi_0^B \rangle - \langle \psi_0^A | H^A | \psi_0^A \rangle - \langle \psi_0^B | H^B | \psi_0^B \rangle, \quad (1)$$

was calculated "exactly", [43] which means that all occurring one- and two-electron integrals were accurately evaluated and that the result is valid at all distances. The ethylene monomer wave functions, ψ_0^A and ψ_0^B , were taken as ground state Hartree-Fock MO-LCAO wave functions (Slater determinants), the operators H^{AB} , H^A and H^B are the dimer and monomer hamiltonians, respectively, and A is the antisymmetrizer over the dimer (including normalisation). For the expansion of the

MO's a double-zeta basis of Gaussian type atomic orbitals (basis B of ref. 39) was used and sometimes [44], for comparison, also a still more extended basis containing 3d orbitals on C and 2p on H (basis C of ref. 39).

This first order energy comprises an electrostatic component, $\Delta E_{\text{elec.}}^{(1)}$, which is obtained from expression (1) by substituting the identity operator for A , and a short-range exchange contribution, $\Delta E_{\text{exch.}}^{(1)} \equiv \Delta E^{(1)} - \Delta E_{\text{elec.}}^{(1)}$, arising from the antisymmetrization. For large distance the electrostatic energy can be approximated by the multipole expansion:

$$\Delta E_{\text{mult.}}^{(1)} = C_5(\underline{\Omega}_A, \underline{\Omega}_B)R^{-5} + C_7(\underline{\Omega}_A, \underline{\Omega}_B)R^{-7} + \dots \quad (2)$$

and the deviation, $\Delta E_{\text{elec.}}^{(1)} - \Delta E_{\text{mult.}}^{(1)} = \Delta E_{\text{pen.}}^{(1)}$, is due to the penetration between the charge clouds A and B, at short distance. The two leading terms in the multipole interaction energy, $\Delta E_{\text{mult.}}^{(1)}$, have been calculated in refs. 8 and 39 for the same basis sets. All the first order results have been collected in tables 1 and 2.

The second order energy was calculated in the multipole expansion, truncated after the two principal terms:

$$\Delta E^{(2)}(R, \underline{\Omega}_A, \underline{\Omega}_B) = -C_6(\underline{\Omega}_A, \underline{\Omega}_B)R^{-6} - C_8(\underline{\Omega}_A, \underline{\Omega}_B)R^{-8} \quad (3)$$

and the second order Rayleigh-Schrödinger perturbation expressions for the orientation dependent coefficients C_6 and C_8 were also evaluated by ab initio calculations. To this end, Mulder et al. [39,45] have

TABLE 1

Electrostatic energy

dimer geometry a)		$\Delta E_{elec.}^{(1) b)}$	$\Delta E_{mult.}^{(1) b)}$	$\Delta E_{fit}^{c)}$ ①	$\Delta E_{fit}^{d,e)}$ ②
Ω_A, Ω_B	R(bohr)	[kcal/mole]	[kcal/mole]	[kcal/mole]	[kcal/mole]
I	7	0.5226	0.4959	0.9799	0.8990
	8	0.5008	0.3953	0.5534	0.5221
	10	0.2085	0.1882	0.2049	0.2009
	12	-	0.0857	0.0884	0.0888
	15	-	0.0312	0.0308	0.0316
20	-	0.0080	0.0077	0.0080	
II f)	7	0.2434	0.4729	0.5119	0.4791
	8	0.2963	0.2932	0.3224	0.3060
	10	0.1439	0.1324	0.1394	0.1358
	12	-	0.0657	0.0665	0.0661
	15	-	0.0259	0.0254	0.0258
20	-	0.0072	0.0068	0.0071	
III	7	-3.1958	-0.1552	-0.3067	-0.4402
	8	-0.6170	-0.1639	-0.2074	-0.2934
	9	-0.1851 (-0.1907)	-0.1230	-0.1364	-0.1920
	10	-0.0964 (-0.0997)	-0.0861	-0.0902	-0.1268
	12	-	-0.0417	-0.0417	-0.0585
	15	-	-0.0156	-0.0152	-0.0214
20	-	-0.0040	-0.0039	-0.0055	
IV	7	-3.7029	-0.2056	-0.3865	-0.4887
	8	-0.6986	-0.1829	-0.2335	-0.2918
	10	-0.1033	-0.0898	-0.0938	-0.1182
	12	-	-0.0426	-0.0422	-0.0538
	15	-	-0.0157	-0.0152	-0.0196
	20	-	-0.0041	-0.0039	-0.0051
V	7	-3.4614	0.5866	1.0211	1.3843
	8	-0.2050	0.3056	0.4241	0.5392
	10	0.1176	0.1019	0.1119	0.1266
	12	-	0.0414	0.0413	0.0437
	15	-	0.0137	0.0130	0.0131
	20	-	0.0033	0.0030	0.0030
VI	7	-3.2847	-0.6615	-0.6123	-0.8981
	8	-0.6359	-0.2347	-0.2266	-0.3653
	10	-0.0461	-0.0366	-0.0367	-0.0711
	12	-	-0.0059	-0.0062	-0.0166
	15	-	0.0004	0.0003	-0.0021
	20	-	0.0006	0.0005	0.0001
VII	7	-	0.7039	1.3373	2.6724
	8	-2.7724	0.3535	0.5116	0.9006
	9	-0.1688	0.1933	0.2370	0.3842
	12	-	0.0447	0.0452	0.0668
	15	-	0.0145	0.0140	0.0204
	20	-	0.0034	0.0032	0.0047
XII	7	-	-0.0231	-0.3060	-0.0553
	8	-	-0.1067	-0.1898	-0.0520
	10	-	-0.0715	-0.0789	-0.0318
	12	-	-0.0367	-0.0363	-0.0175
	15	-	-0.0142	-0.0133	-0.0073
20	-	-0.0038	-0.0035	-0.0021	
g)		-	0.0	0.036	0.23

a) The orientations $(\underline{\Omega}_A, \underline{\Omega}_B)$ of the molecules numbered by the Roman figures are indicated schematically in fig. 2.

b) From ab initio calculations; definitions, see the text. The GTO basis used is: C(9,5/4,2), H(4/2) (ref. 39, basis B), for the results in parentheses: C(9,5,1/4,2,1), H(4,1/2,1) (ref. 39, basis C).

c) Atom-atom fit with the point charges shifted from the nuclei, see fig. 1. This fit was made for the distances $R = 12, 13, 14, 15, 16, 18, 20, 22$ bohr.

d) Atom-atom fit with the point charges on the nuclei. The same distances were used in the fit as in c).

e) The empirical atom-atom potential (2) from ref. 29 yields an electrostatic energy which differs from this fit by exactly a factor of 0.37. This leads to a root mean square deviation $\sigma = 0.62$ with respect to $\Delta E_{\text{mult}}^{(1)}$.

f) For this orientation R is the distance between the two molecular planes.

g) The root mean square relative deviation is defined as:

$$\sigma = \left[\frac{1}{N_R} \sum_{\substack{\Omega_A, \Omega_B \\ \Omega_A, \Omega_B}} \frac{\sum (\Delta E_{\text{fit}} - \Delta E_{\text{mult}}^{(1)})^2}{\sum \Delta E_{\text{mult}}^{(1)2}} \right]^{1/2}$$

where the summations run over all the orientations $(\underline{\Omega}_A, \underline{\Omega}_B)$ in this table and the distances $R = 12 - 22$ bohr ($N_R = 8$). The summation over the orientations was carried out before taking the ratios, since for some orientations the electrostatic energy is very close to zero.

TABLE 2 Short range energy

dimer geometry a)	$\Delta E^{(1)}$ b)	$\Delta E^{(1)}$ c)	d)	e)	f)	g)	
Ω_A, Ω_B	R(bohr)	$\Delta E_{\text{short range}}$	$\Delta E_{\text{fit}} \textcircled{3}$	$\Delta E_{\text{fit}} \textcircled{1}$	$\Delta E_{\text{empirical}} \textcircled{1}$	$\Delta E_{\text{empirical}} \textcircled{2}$	
	[kcal/mole]	[kcal/mole]	[kcal/mole]	[kcal/mole]	[kcal/mole]	[kcal/mole]	
I	7	2.4498	1.4699	1.4198	0.7830	0.4604	0.4435
	8	0.8685	0.3151	0.2742	0.1495	0.0709	0.0685
	10	0.2182	0.0133	0.0101	0.0054	0.0017	0.0016
II ^{h)}	7	1.4151	0.9032	0.9704	0.5552	0.3185	0.3148
	8	0.5199	0.1975	0.1919	0.1078	0.0501	0.0496
	10	0.1498	0.0104	0.0074	0.0040	0.0012	0.0012
III	7	7.1000	7.4066	6.6205	5.6981	4.4580	5.2510
	8	1.2387	1.4461	1.2806	1.0863	0.7173	0.8543
	9	0.1098(0.1021)	0.2462	0.2454	0.2026	0.1126	0.1349
	10	-0.0555(-0.0588)	0.0347	0.0468	0.0373	0.0174	0.0209
IV	7	7.6388	8.0251	6.7170	6.6206	5.2915	6.5263
	8	1.2821	1.5155	1.2934	1.2059	0.8153	1.0032
	10	-0.0605	0.0333	0.0470	0.0394	0.0188	0.0230
V	7	17.3186	16.2972	15.4433	18.1144	21.9214	25.7024
	8	2.9360	2.5118	2.5771	3.0438	3.2852	3.8871
	10	0.1705	0.0586	0.0745	0.0858	0.0719	0.0861
VI	7	7.1250	7.7372	8.2481	10.0932	9.2440	11.6088
	8	0.6744	1.2963	1.6617	2.0217	1.7096	2.1391
	10	-0.0142	0.0225	0.0604	0.0699	0.0487	0.0605
VII	8	12.4209	11.9094	10.8979	12.2708	13.6009	16.0984
	9	1.9890	1.7521	1.8549	2.0806	2.0207	2.4152
	10.5	0.1902	0.0956	0.1340	0.1452	0.1145	0.1381
	11.5	0.0734	0.0164	0.0236	0.0247	0.0168	0.0203
VIII	8	7.8373	8.1044	8.0638	9.4368	8.8979	11.0085
	9	1.1378	1.2354	1.5248	1.7505	1.4834	1.8337
	10.5	0.0321	0.0548	0.1208	0.1320	0.0937	0.1155
	11.5	-0.0053	0.0028	0.0221	0.0231	0.0144	0.0177
σ^1)	-	0.0	0.13	0.33	0.45	0.53	

- a) The orientations ($\underline{\Omega}_A, \underline{\Omega}_B$) of the molecules are indicated schematically in fig. 3.
- b) From ab initio calculations, basis B; results in parentheses with basis C (see table 1).
- c) Defined as: $\Delta E_{\text{short range}}^{(1)} = \Delta E^{(1)} - \Delta E_{\text{point charge}}^{(1)}$, where $\Delta E_{\text{point charge}}^{(1)}$ is the electrostatic energy from the best long range fit to the ab initio results in table 1, fit ①.
- d) Atom-atom fit to $\Delta E_{\text{short range}}^{(1)}$ (for the shortest two distances, R) as described in the text, but without averaging constraints for the C-H parameters.
- e) Same as d) with averaging constraints for the C-H parameters.
- f) From Williams [28].
- g) From Williams [29].
- h) For this orientation R is the distance between the two molecular planes.

- i) The root mean square relative deviation:

$$\sigma = \left[\frac{1}{N} \sum_R \sum_{\underline{\Omega}_A, \underline{\Omega}_B} \frac{(\Delta E_{\text{fit}} - \Delta E_{\text{short range}}^{(1)})^2}{(\Delta E_{\text{short range}}^{(1)})^2} \right]^{\frac{1}{2}}$$

for the smallest two distances (N = 16).

used another basis set (D of ref. 39), which is also an extension of basis B with 3d orbitals on C and 2p's on H with the purpose of providing a nearly complete set of virtual states in the second order expression [39]. As a check on this basis several completeness tests have been performed and the calculated molecular dipole polarizability of ethylene ($\alpha_{xx} = 26.5$ a.u., $\alpha_{yy} = 41.1$ a.u., $\alpha_{zz} = 23.2$ a.u.) agrees rather well with experiment [46,47] ($\alpha_{xx} = 26.1$ a.u., $\alpha_{yy} = 36.4$ a.u., $\alpha_{zz} = 23.0$ a.u.). Also the orientationally averaged C_6 plus C_8 contribution [40] is in good agreement with the experimental result from viscosity data [48]. The calculation of the separate contributions to $\Delta E^{(2)}$, i.e. the induction and the dispersion energy, for several conformations of the ethylene dimer is described in refs. 8 and 39 and some results are listed in table 3.

B Conclusions

Although we cannot be certain about the accuracy of the ab initio interaction energies listed in tables 1,2 and 3, we have tried to make some estimates of this accuracy.

The calculated molecular quadrupole moment, $Q_{2,0}$, agrees fairly well with the experimental value [49] and hardly changes when the AO basis set in the calculations is further extended. Also the different first order energy contributions $\Delta E_{\text{exch.}}^{(1)}$, $\Delta E_{\text{elec.}}^{(1)}$, $\Delta E_{\text{mult.}}^{(1)}$, $\Delta E_{\text{pen.}}^{(1)}$ are practically insensitive to basis set extension and so we expect both the long range interaction, $\Delta E_{\text{mult.}}^{(1)}$, which is nearly equal to $\Delta E_{\text{elec.}}^{(1)}$ for large R, and the "overlap" contributions $\Delta E_{\text{exch.}}^{(1)}$ and $\Delta E_{\text{pen.}}^{(1)}$ to be rather accurate. The main error in

these first order results is caused by the neglect of the intramolecular electron correlation and, on the basis of experience with smaller molecules, we estimate this error to be not larger than 10% of the interaction energy in the whole region of interest.

The same agreement with the scarce experimental quantities available is found for the second order properties: the dipole polarizability [39] and the isotropic C_6 value [40]. Also it was checked that the second order results are practically "saturated" with respect to basis set extension. In contrast with the first order energy, however, which was evaluated "exactly", the second order energy was calculated in the multipole expansion only. This implies the neglect of charge overlap effects so that, formally, the results are just valid for large distances. Moreover, the multipole expansion was truncated after the first two terms, while we found [39] that this expansion converges rather slowly for short distances. The resulting errors must cancel to some extent, though, and we estimate on the basis of previous studies [8,39,40] that the maximum error in the second energy, which occurs for the nearest neighbour contacts in the ethylene crystal, is still not larger than about 20%.

As we have indicated in table 3, the induction energy is only a very small fraction of the total second order interaction, so that it can be neglected with respect to the dispersion energy.

TABLE 3

Dispersion energy

dimer geometry a)		$\Delta E^{(2)}$ b)	ΔE_{fit} c) ①	$\Delta E_{\text{empirical}}$ d) ①	$\Delta E_{\text{empirical}}$ e) ②
Ω_A, Ω_B	R(bohr)	[kcal/mole]	[kcal/mole]	[kcal/mole]	[kcal/mole]
I	12	0.0782	0.0804	0.0626	0.0600
	15	0.0203	0.0219	0.0172	0.0166
	19	0.0049	0.0055	0.0043	0.0041
IX	12	0.1487	0.1457	0.1207	0.1226
	15	0.0348	0.0323	0.0264	0.0264
	19	0.0077	0.0070	0.0056	0.0056
III	12	0.1163	0.1160	0.0936	0.0926
	15	0.0280	0.0280	0.0225	0.0222
	19	0.0063	0.0064	0.0051	0.0050
X	12	0.1646	0.1686	0.1460	0.1542
	15	0.0378	0.0346	0.0289	0.0296
	19	0.0083	0.0072	0.0059	0.0059
V	12	0.1323	0.1332	0.1124	0.1162
	15	0.0314	0.0304	0.0252	0.0254
	19	0.0070	0.0067	0.0055	0.0055
XI	12	0.0826	0.0845	0.0669	0.0650
	15	0.0213	0.0227	0.0179	0.0175
	19	0.0051	0.0056	0.0045	0.0043
VII	12	0.1806	0.1857	0.1586	0.1656
	15	0.0415	0.0375	0.0311	0.0317
	19	0.0091	0.0076	0.0062	0.0062
XII	12	0.0888	0.0895	0.0720	0.0711
	15	0.0225	0.0235	0.0188	0.0185
	19	0.0053	0.0057	0.0046	0.0045
$\sigma^f)$		0.0	0.071	0.20	0.21

- a) The orientations $\underline{\Omega}_A, \underline{\Omega}_B$ of the molecules are indicated schematically in fig. 4.
- b) From ab initio calculations in the multipole expansion (see text) using the non-empirical mean energy approximation with basis set D (see ref. 39, formulas 4 and 5).
The induction energy is not tabulated since it is always smaller than the dispersion energy by a factor of 35 or more.
- c) Atom-atom fit for $R = 12, 13, \dots, 19$ bohr as described in the text.
- d) From Williams [28].
- e) From Williams [29].
- f) The root mean square relative deviation σ is defined as in table 2, for $R = 12, 13, \dots, 19$ bohr ($N = 64$).

3. Analytic fit by atom-atom potentials

A Fitting procedure and results

Since the atom-atom potential model has been extensively applied (with empirical parameters) and since it is rather convenient for lattice dynamics calculations, we have chosen this model to fit our ab initio calculated interaction potential between two ethylene molecules. The interaction energy between two molecules, A and B, is written as:

$$\Delta E_{AB} = \sum_i^A \sum_j^B V_{ij} \quad (4)$$

with

$$V_{ij}(r_{ij}) = q_i q_j r_{ij}^{-1} - A_{ij} r_{ij}^{-6} + B_{ij} \exp(-C_{ij} r_{ij}) \quad (5)$$

where the first term in V_{ij} should account for the electrostatic energy between two atoms with net charges q_i and q_j at a distance r_{ij} , the second term for the long range attractive interactions and the last term for the short range repulsions. At first, we have tried to fit the total first plus second order interaction energy by adapting all parameters at once, but as there is a high degree of correlation between the fit parameters we have used the following procedure.

- (i) The first order electrostatic energy as calculated in the multipole expansion, $\Delta E_{\text{mult.}}^{(1)}$, for several conformations for $R = 12.0$ to 22.0 a.u. (see table 1) is fitted by the term:

$$v_{ij}^{el.} = q_i q_j r_{ij}^{-1} \quad (5a)$$

which contains the following fit parameters for every atom i :

- the charge q_i
- the coordinates (x_i, y_i) that fix the position of the charge i , which is displaced in the molecular plane with respect to the corresponding nucleus. (see fig. 1)

Altogether, because of symmetry and charge neutrality, this yields 4 independent fit parameters for the ethylene molecule.

A model with the charges centered on the nuclei contains only one independent parameter, which could be fitted to the main component $Q_{2,0}$ of the molecular quadrupole moment, for instance. Such a model could not correctly represent the electrostatic interaction as a function of the molecular orientations, however [8]. The fit to the electrostatic interaction is much improved by the present 4-parameter model with the shifted charges (Table 1, fig. 2). A model with the charge centers displaced from the nuclei is also physically reasonable, since it reflects the effects of the chemical bonding.

We have chosen to fit only the long range part of the electrostatic energy, $\Delta E_{mult.}^{(1)}$, which is nearly equal to $\Delta E_{elec.}^{(1)}$ for large R , because for shorter distance the "exactly" calculated behaviour of $\Delta E_{elec.}^{(1)}$ could not be correctly represented by the point charge model. This is due to the penetration between the charge clouds: the deviation of $\Delta E_{point\ charge}^{(1)}$ from $\Delta E_{elec.}^{(1)}$ begins to occur at the same distance as the deviation between $\Delta E_{elec.}^{(1)}$ and $\Delta E_{mult.}^{(1)}$. This penetration interaction is a short range effect, it has about the same distance dependence

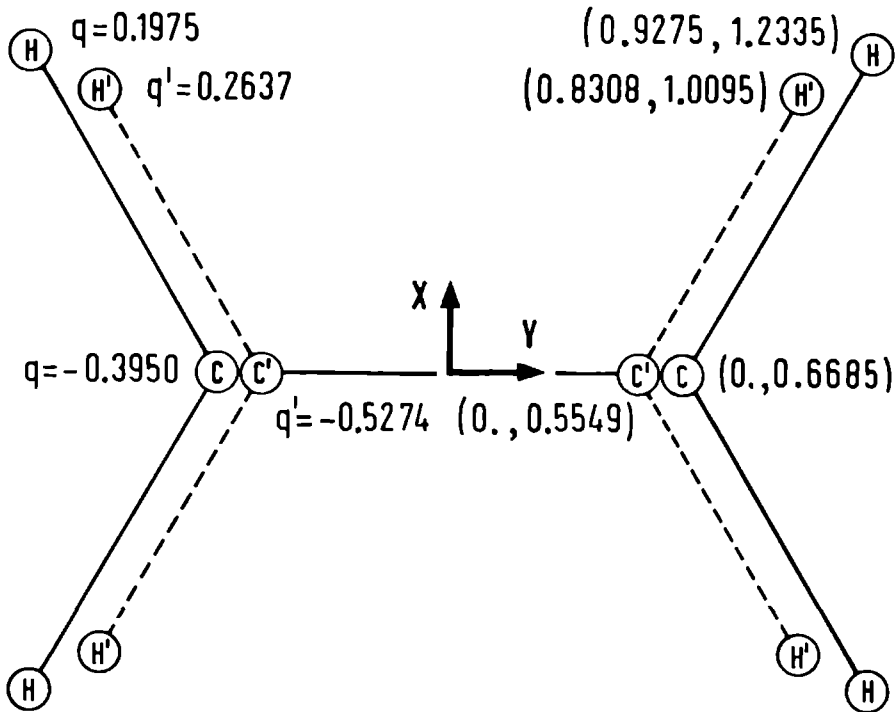


Fig. 1. Point charges (in unit charges) and coordinates (in Å) in the ethylene molecule. The charges q' with positions C' and H' , which are shifted with respect to the nuclei C and H , are obtained from the best fit of the long range electrostatic interaction in the dimer (see table 1, fig. 2). The charges q on the nuclei fix the main component of the molecular quadrupole moment, $Q_{2,0}$.

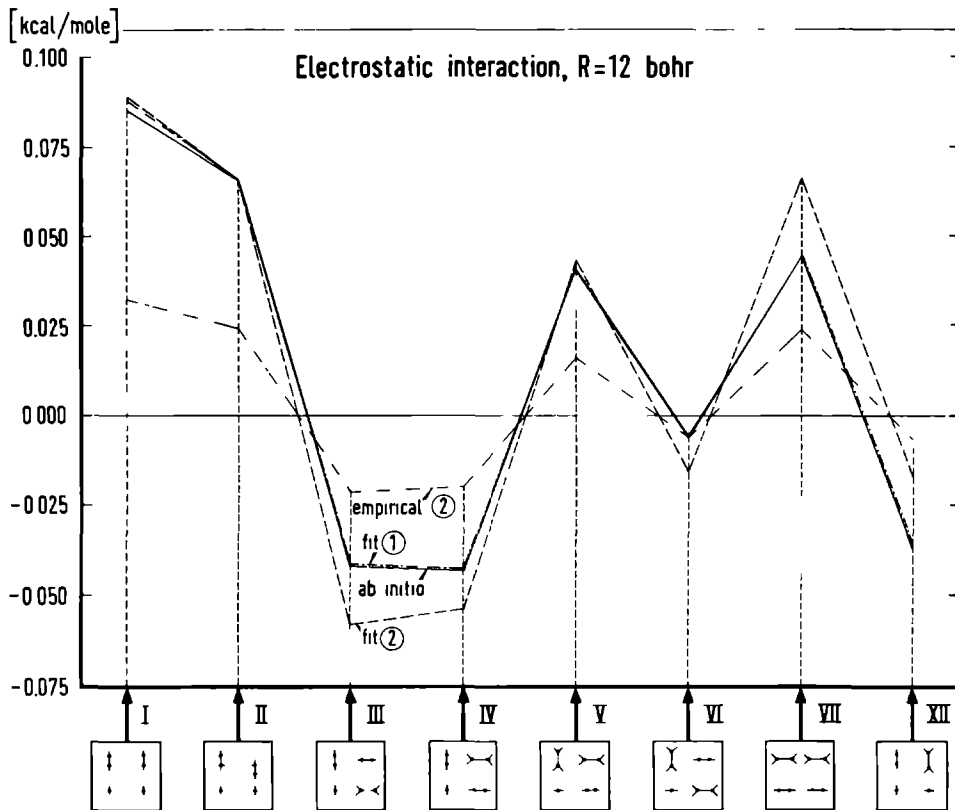


Fig. 2. Orientation dependence of the electrostatic interaction in the ethylene dimer (see also table 1);

ab initio: calculated in the multipole expansion,
 $\Delta E_{\text{mult.}}^{(1)}$

fit (1) : point charges shifted from the nuclei
 (see fig. 1)

fit (2) : point charges on the nuclei

empirical (2) : point charges from Williams [29]

The molecular orientations are indicated by giving two views of the dimer. For orientation II R is the distance between the molecular planes.

as $\Delta E_{\text{exch.}}^{(1)}$, and so we have added the difference ($\Delta E_{\text{elec.}}^{(1)} - \Delta E_{\text{point charge}}^{(1)}$) to the short range exchange repulsion, $\Delta E_{\text{exch.}}^{(1)}$ [50]. The sum of these two "overlap" contributions has been fitted with an exponential function (ii).

- (ii) The short range interactions arising from penetration, $\Delta E_{\text{elec.}}^{(1)} - \Delta E_{\text{point charge}}^{(1)}$, and from exchange, $\Delta E_{\text{exch.}}^{(1)}$, have been fitted by:

$$v_{ij}^{\text{overlap}} = B_{ij} \exp(-C_{ij} r_{ij}) \quad (5b)$$

The present results and, even more so, our previous ab initio results for smaller systems [24,51,52] which have been calculated for a wider range of distances, show that the short range interactions indeed display a nearly exponential distance dependence.

In fitting the orientational dependence of the short range interactions we have met the following problem, however. If all the parameters $B_{\text{CC}}, C_{\text{CC}}, B_{\text{CH}}, C_{\text{CH}}, B_{\text{HH}}, C_{\text{HH}}$ in the atom-atom potential of type (5b) were freely varied to obtain the best fit to the ab initio short range repulsion calculated for 8 different orientations and 2 or 3 distances of the molecules in the ethylene dimer, we obtained several results with small numerical deviations but with quite unphysical interaction parameters. An example is shown by the fit (3) in fig. 3 which has a much smaller mean square deviation (see table 2) from the ab initio results than the final fit described below. The carbon-hydrogen repulsion is absent in this fit ($B_{\text{CH}} = 0$), however, and its

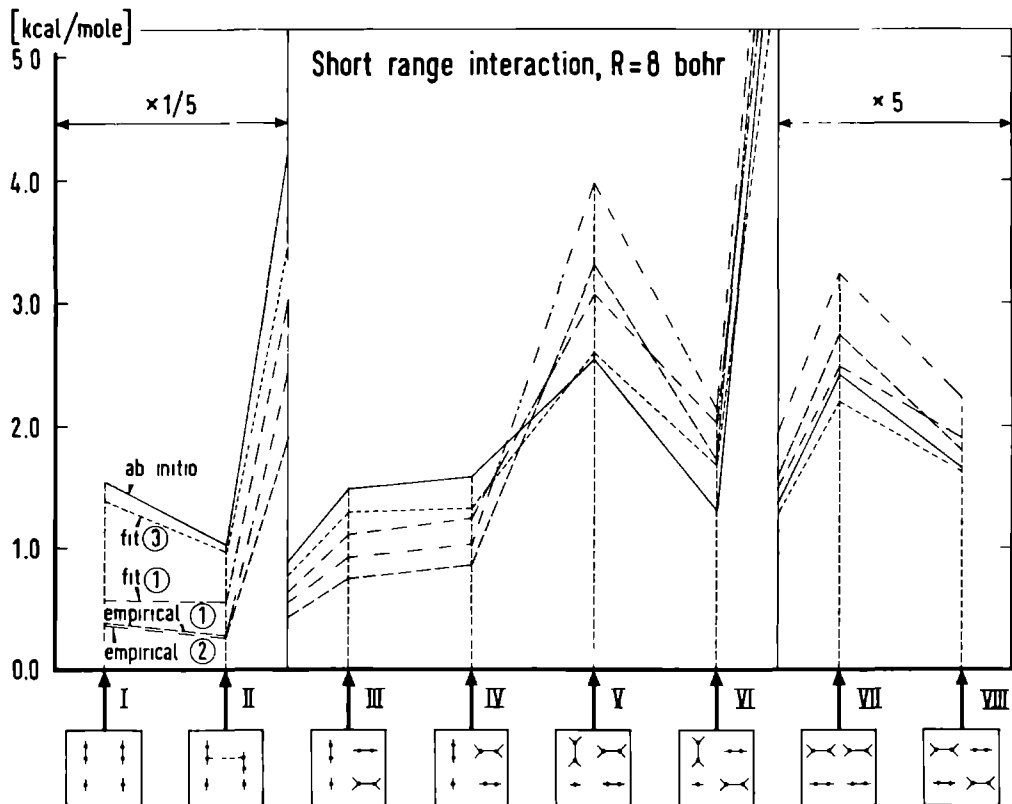


Fig. 3. Orientation dependence of the short range repulsion in the ethylene dimer. (see also table 2);
 ab initio: calculated "exactly", $\Delta E^{(1)} - \Delta E_{p.c.}^{(1)}$ (see text)
 fit (1) : atom-atom potential with averaging constraints for the C-H parameters
 fit (3) : atom-atom potential without averaging constraints
 empirical (1) : atom-atom potential from Williams [28]
 empirical (2) : atom-atom potential from Williams [29]
 The molecular orientations are indicated as in fig. 2.

application to the lattice structure optimization and the phonon calculations yielded quite unrealistic results. We have tried, without success, to avoid this problem by taking a different form of the atom-atom repulsion, e.g. r^{-n} , or by shifting the atomic force centers away from the nuclei to the charge centers from fit (i).

We explain this problem as follows. The true interaction potential between the molecules does not have the atom-atom model potential form; it will include non-central forces between the atoms as well as non-additive three-atom and higher interactions. This is illustrated by the results in table 2 where we see, for instance, that the carbon-carbon repulsions, which are the ones with the longest range, actually have a smaller exponential decay for the geometries I and II than for other geometries. The exponent C_{CC} , if it were only fitted to the results of geometries I and II, would have a value 2.95\AA^{-1} . This particular effect is caused, we think, by the relatively diffuse carbon π -electron clouds. As a result of such effects there is probably a sizable deviation between any atom-atom model potential and the true potential. Fitting the potential parameters for a limited set of dimer geometries it may be possible to obtain smaller deviations but this will not give a better atom-atom potential (for arbitrary other geometries). Therefore, in using a restricted set of ab initio results, as we have done, one must be very careful in fitting .

We have used the following procedure: the hydrogen-hydrogen repulsion parameters, B_{HH} and C_{HH} , were obtained from the

the difference in interaction energy between geometries V and VI and from the difference between VII and VIII, which are both caused mainly by the hydrogen contacts. The agreement between these two results is good. Then we have fitted the carbon-carbon repulsion parameters (B_{CC} and C_{CC}) to the ab initio results for all orientations while the carbon-hydrogen parameters were constrained to be averages:

$$B_{CH} = (B_{CC} \cdot B_{HH})^{\frac{1}{2}}$$

$$C_{CH} = (C_{CC} + C_{HH})/2$$

and the hydrogen-hydrogen parameters were kept fixed. For this fit we have used the results at the shortest two distances where the ab initio results for the exchange and penetration interactions are expected to have the highest relative accuracy. Although the mean square deviation is considerably larger than the value for the best unrestricted parameter fit, we think that the present fit gives a better representation of the real interaction potential and that the resulting errors are mainly inherent to the atom-atom potential model. Trying to improve on this model would augment the number of parameters considerably and would require a much larger set of ab initio results to make a reliable fit of these parameters.

(iii) The second order dispersion attraction was fitted by an atom-atom potential:

$$V_{ij}^{disp.} = - A_{ij} r_{ij}^{-6} \quad (5c)$$

It has appeared already in ref [8] that the first two multipole terms $-C_6R^{-6}$ $-C_8R^{-8}$ in the dispersion energy between two ethylene molecules could be rather well represented, for several molecular orientations, by an atom-atom potential of the r^{-6} type. This is confirmed by the present results shown in table 3 and fig. 4. If we choose the three parameters A_{CC} , A_{CH} and A_{HH} independently they show a rather high correlation, i.e. almost equally good fits can be obtained for quite different combinations of the parameters. Therefore, we have applied the constraint $A_{CH} = (A_{CC} \cdot A_{HH})^{\frac{1}{2}}$ which can be justified by theoretical arguments and which has also been used in deriving most of the empirical parameter sets. This constraint hardly affects the quality of the fit and it gave much better defined values of the two independent parameters.

From the results in table 3 it is evident that the fit between the atom-atom potential and the ab initio dispersion energy becomes worse for very large distances: the atom-atom interaction energy between the molecules is not sufficiently anisotropic for large R. This defect of the r^{-6} atom-atom potential is easily explained by making an expansion of the r^{-6} atom-atom interaction energy around the molecular centers of mass. The leading term in this expansion is an isotropic R^{-6} interaction between the molecules, while the exact coefficient C_6 for the interacting molecules depends on the molecular orientations.

The second order induction interactions have been neglected in the fit for reasons explained in section 4.

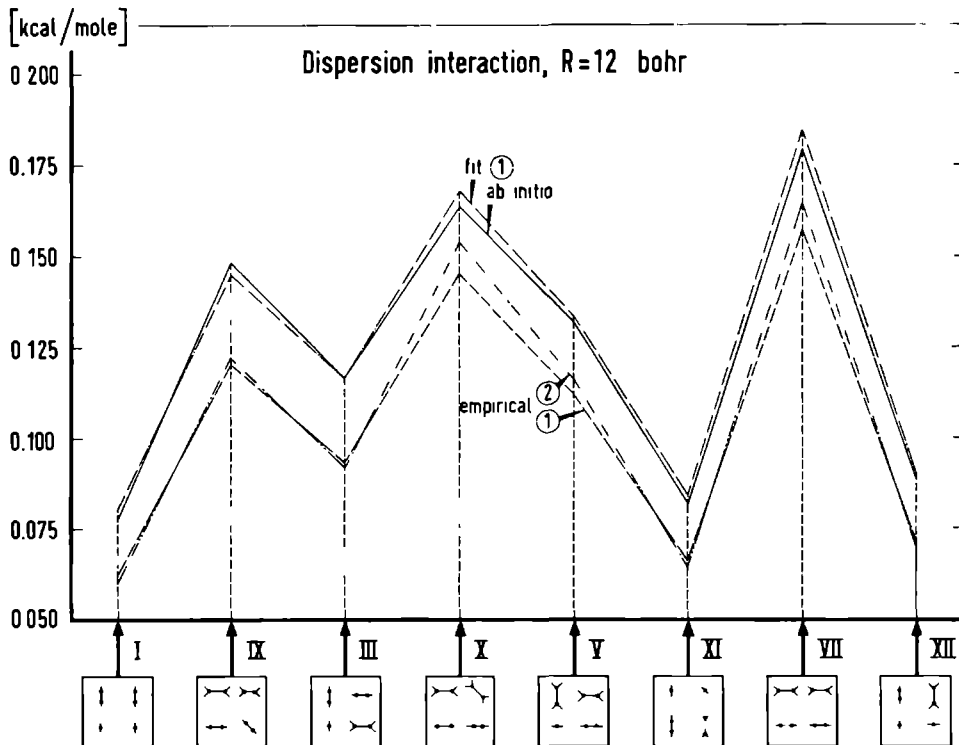


Fig. 4. Orientation dependence of the long range dispersion interactions in the ethylene dimer (see also table 3);

ab initio : calculated in the multipole expansion,
 $\Delta E_{\text{mult}}^{(2)}$.

fit (1) : atom-atom potential (with averaging constraint for the C-H parameter).

empirical (1) : atom-atom potential from Williams [28]

empirical (2) : atom-atom potential from Williams [29]

The molecular orientations are indicated as in fig. 2.

The set of parameters in the atom-atom potential (1) which have been obtained from the fits (i), (ii) and (iii) are collected in table 4. For comparison we have also listed two of the most frequently used empirical parameter sets for hydrocarbons, one without electrostatic interactions and one including these, which were both proposed by Williams [28,29]. The overall quality of the fit appears from tables 1, 2 and 3, whereas the ability of the fitted and empirical atom-atom potentials to represent the orientational dependence of the interaction energy is illustrated by figs. 2, 3 and 4.

B Conclusions

We conclude that the long range electrostatic and dispersion interactions (i) and (iii), are very accurately fitted by the atom-atom potentials. The quality of fit (i) is definitely lower for some orientations if the point charges were constrained to be at the nuclear positions. The fit (iii) becomes slightly worse for very large R due to the incorrect asymptotic behaviour of the r^{-6} atom-atom potential. The fit of the short range overlap repulsion (ii) shows a significantly larger mean square deviation than the long range fits. This must probably be assigned to the deviations of the exact intermolecular potential from a central atom-atom potential due to the effects of chemical bonding. Considering the large overlap between chemically bonding atoms the importance of such effects on the intermolecular overlap repulsion is not surprising [53].

For some orientations (with relatively small repulsion) the atom-atom potential deviates by a factor of 2 from the ab initio

TABLE 4

Potential parameters

Parameters	ab initio fit	① empirical	① empirical	②
	C-C	27116	83630	71461
B	C-H	6378	8770	14316
[kcal/mole]	H-H	1500	2650	2868
	C-C	3.16	3.60	3.60
C	C-H	3.43	3.67	3.67
[Å ⁻¹]	H-H	3.70	3.74	3.74
	C-C	876	568	449.3
A	C-H	132	125	134.3
[$\frac{\text{kcal}}{\text{mole}} \text{Å}^6$]	H-H	20	27.3	40.15
q	C	-0.5274 *)	-	-0.24
[unit charges]	H	+0.2637 *)	-	+0.12

*) With the charges shifted from the nuclei (see fig. 1); from the fit ② with the charges on the nuclei we find

$$q_C = -0.3950, q_H = +0.1975.$$

result. If we consider the very pronounced anisotropic character of the short range repulsions, however, (a factor of 50 difference in ΔE^{AB} for different orientations at the same R), as well as their strong distance dependence (a large deviation in ΔE^{AB} corresponds with a small shift in R), we may still say that the atom-atom potential gives a reasonable description of the short range repulsion.

About the empirical atom-atom potentials we can make the following observations. Although the individual parameters A_{CC} and A_{HH} are different [54], the total atom-atom interaction for the dispersion energy is in remarkably good agreement with the ab initio result, yielding a nearly constant fraction of 80% of this result for different orientations. The remaining difference of 20% can have several reasons, but it may be due also to the inaccuracy of the ab initio result for the dispersion energy, which has been computed in the multipole expansion only (see section 2). For the short range repulsions the most striking difference is the longer range (smaller exponent) of the C-C interactions in the ab initio calculations ($C_{CC} = 3.16\text{\AA}^{-1}$). The empirical exponent of 3.60\AA^{-1} was found from the layer spacing and compressibility of graphite [55] and was fixed while the other parameters, A and B, were empirically optimized [2]. In relation to this ab initio result, it is interesting that Williams has observed [2] that the substitution of optimized A and B parameters into the graphite calculation [55] would have yielded an exponent of 3.20\AA^{-1} or 2.94\AA^{-1} . He ascribes this to the "softness" of the π -electron clouds, which is confirmed by our ab initio calculations (the fit of C_{CC} on the π -stacked geometries I and II yields a value of 2.95\AA^{-1}). The exponent for the H-H repulsion is in very good agree-

ment. Although the deviation between the theoretical and the empirical atom-atom repulsions is definitely larger than for the dispersion attraction, the strong anisotropy in the short range repulsion is still rather well represented by the empirical potential. The electrostatic interactions are not well represented by the empirical atom-atom potentials. In most empirical parametrizations, e.g. in the first Williams' potential in table 4, they are simply omitted. In some other parametrizations (the second Williams' potential in our table 4) they are included, and it has recently been argued [20] that this considerably improves the calculated results for the lattice structure and the phonon frequencies. Still, the charges in the empirical models are much smaller than the values from our theoretical atom-atom potential and this will lead to an underestimate of the electrostatic (mainly quadrupole-quadrupole) interaction. Probably, this lack of electrostatic interactions between the molecules is implicitly corrected for by the adjustment of the other empirical parameters.

4. Lattice dynamics calculations on the ethylene crystal

A Procedure and results:

Before using the intermolecular potential derived from dimer calculations in the crystal we must consider the problem of additivity of the interactions between molecules (which may still hold even if the additivity assumption does not hold for the atom-atom potentials). The electrostatic interactions are exactly pairwise additive. For the exchange interactions between molecules the many-body components are expected to be small [56] because the intermolecular overlap is quite small. For the dispersion forces the most important many-body component is the Axilrod-Teller or triple-dipole energy which is also small compared with the pair energy [57]. The only component in the first and second order interaction energy for which pairwise additivity does not even hold approximately is the induction energy. This energy is already very small in the ethylene dimer, however, relative to the other terms and we can expect it to be even smaller in the crystal, because there each molecule is surrounded by a more symmetric environment. Therefore, we can safely neglect the induction energy in our calculations for the ethylene crystal and assume pairwise additivity for all other interactions.

The precise structure of the ethylene crystal is known only recently from X-ray [58] and neutron [59] diffraction. Both for normal ethylene and for the completely deuterated substance the symmetry group is the monoclinic space-group $P2_1/n$ (C_{2h}^5), with two centrosymmetric molecules in the unit cell (fig. 5). For a long

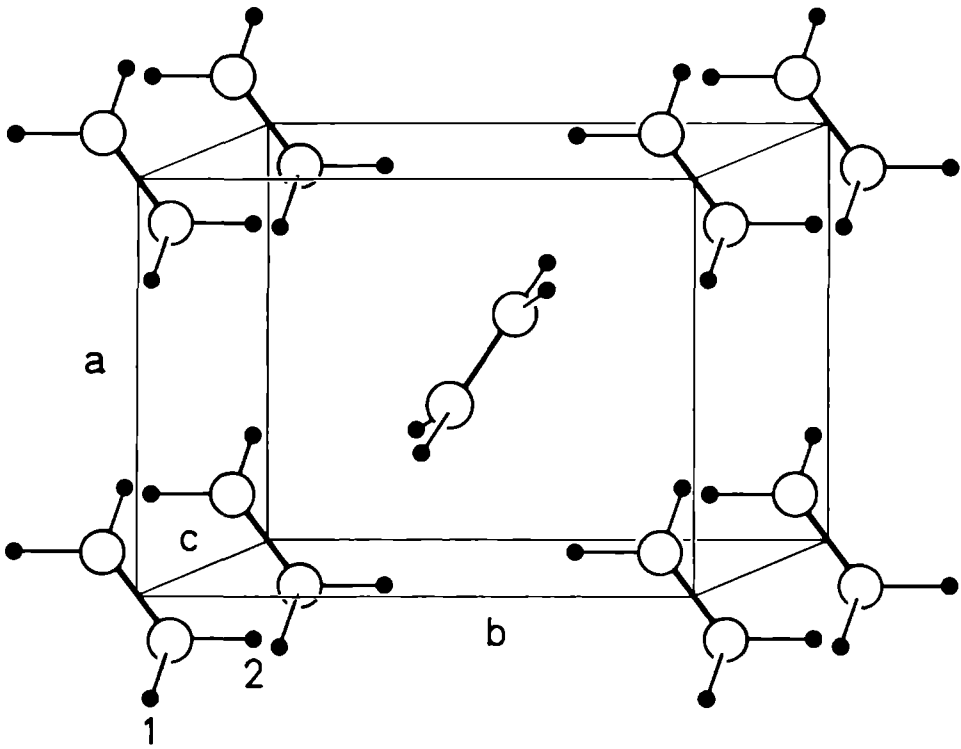


Fig. 5. Structure of the ethylene crystal, symmetry $P2_1/n$ ($Z = 2$)

time, there has been some uncertainty regarding the positions of the hydrogen atoms, i.e. about the rotation of the molecular plane around the C-C axis. From the older X-ray data [60] and simple packing considerations two crystal structures appeared possible, which are both in agreement with the measured IR spectra [61] and which differ only in that the two molecules in the unit cell are tilted in the same or in opposite sense around their C-C axes, thus leading to a screw-axis in the a or b direction, respectively. Actually, several lattice dynamics calculations [33-36] with empirical atom-atom potentials were performed in an attempt to settle this problem.

In our lattice dynamics calculations we have assumed the b-structure, which proved to be the correct one [58,59]. As a first step, which is theoretically required [62] but which is often not made in practice, we have optimized the 7 structural parameters (the unit cell dimensions a , b , c and the angle β and the angles ξ , η , ζ describing the molecular orientation) for the given potential. This optimization was carried out by minimizing the lattice energy with respect to all 7 parameters simultaneously, using the procedures contained in the MINUIT program package [63] (with repeated checks that the minimum obtained was really the absolute one). The lattice sum was taken over 42 neighbouring molecules [64], after checking that the inclusion of further shells did not influence the results anymore (except, slightly, the total cohesion energy). The structural data are listed in table 5. Then, the force constants were evaluated and the dynamical problem was solved in the harmonic approximation:

$$\sum_{\sigma'=1}^2 \sum_{\beta=1}^6 \left[D_{\alpha\beta}^{\sigma\sigma'}(\vec{q}) - \omega^2(\vec{q},j) M_{\alpha\beta} \delta_{\sigma\sigma'} \right] e_{\beta}^{\sigma'}(\vec{q},j) = 0 \quad (6)$$

The tensor \underline{M} contains the molecular mass ($M_{\alpha\beta} = M \delta_{\alpha\beta}$ for $\alpha, \beta = 1, 2, 3$) and the moments of inertia ($M_{\alpha\beta} = I_{\alpha-3, \beta-3}$ for $\alpha, \beta = 4, 5, 6$). The dynamical matrix is given by:

$$D_{\alpha\beta}^{\sigma\sigma'}(\vec{q}) = \sum_{\ell, \ell'} \phi_{\alpha\beta} \begin{pmatrix} 0 & \ell' \\ \sigma & \sigma' \end{pmatrix} e^{-i\vec{q} \cdot (\vec{R}^0 - \vec{R}^{\ell'})}$$

and the force constants:

$$\phi_{\alpha\beta} \begin{pmatrix} \ell & \ell' \\ \sigma & \sigma' \end{pmatrix} = \left[\frac{\partial^2 V \begin{pmatrix} \ell & \ell' \\ \sigma & \sigma' \end{pmatrix}}{\partial u_{\alpha}^{\sigma}(\ell) \partial u_{\beta}^{\sigma'}(\ell')} \right]_0$$

have been evaluated at the equilibrium positions of the molecules found from the energy minimization. The indices

σ, σ' label different sublattices,

ℓ, ℓ' label different unit cells,

$\alpha, \beta = 1, 2, 3$ denote translational coordinates (x, y, z),

$\alpha, \beta = 4, 5, 6$ denote rotational coordinates ($\theta_x, \theta_y, \theta_z$).

The quantities $\omega(\vec{q}, j)$ are the phonon frequencies for the given wave vector \vec{q} and branch j . All calculations were carried out in an orthogonal fixed frame a, b, c^* . For details of the formalism we refer to the review paper by Venkataraman [62].

We expect that the effect of anharmonic corrections is not very large for ethylene since the temperature effect on the IR spectra [66] is small (for $10^{\circ}\text{K} < T < 65^{\circ}\text{K}$). Actually, we have studied this effect in a self-consistent phonon calculation [67], using an empirical potential. Also the other approximation which is inherent

TABLE 5

Lattice dynamics of the C_2H_4 crystal

potential:		experiment	ab initio fit (1) ^{a)}	empirical (1) ^{b)}	empirical (2) ^{c)}	fit (1) with $q=0$ ^{d)}	fit (2) ^{e)}					
unit cell ^{f)}	a [Å]	4.626	4.730	4.856	4.726	4.844	4.763					
	b [Å]	6.620	6.205	6.342	6.435	6.516	5.990					
	c [Å]	4.067	4.005	3.832	4.135	3.886	4.138					
molecular orientation ^{f)}	β [degrees]	94.4	88.5	96.8	94.0	99.0	88.1					
	ξ [degrees]	-27.0	-31.7	-36.2	-27.0	-34.4	-26.3					
	η [degrees]	-14.6	-9.3	-5.0	-11.7	-7.4	-8.4					
	ζ [degrees]	-34.3	-31.3	-27.8	-31.8	-28.7	-31.8					
cohesion energy ^{g)} [kcal/mole]	short range	-	-4.84	-3.42	-3.08	-3.88	-4.93					
	dispersion	-	8.89	7.46	6.58	8.16	8.87					
	electrostatic	-	1.41	0	0.42	0	1.69					
	total	4.7	5.46	4.04	3.92	4.28	5.63					
IR ^{h)} ω [cm ⁻¹]	-	57 ^(1.07)	75 ^(1.07)	50 ^(1.07)	60 ^(1.07)	61 ^(1.07)	63 ^(1.07)	59 ^(1.07)	52 ^(1.07)	55 ^(1.07)	78 ^(1.07)	Au
	73 ^(1.05)	73 ^(1.07)	94 ^(1.07)	60 ^(1.07)	67 ^(1.07)	75 ^(1.07)	75 ^(1.07)	96 ^(1.07)	66 ^(1.07)	75 ^(1.07)	105 ^(1.07)	Au
	110 ^(1.06)	94 ^(1.07)	126 ^(1.07)	90 ^(1.07)	115 ^(1.07)	108 ^(1.07)	113 ^(1.07)	132 ^(1.07)	111 ^(1.07)	93 ^(1.07)	132 ^(1.07)	Bu
Raman ⁱ⁾ ω [cm ⁻¹]	73 ^(1.22)	51 ^(1.22)	50 ^(1.21)	51 ^(1.21)	55 ^(1.20)	59 ^(1.22)	38 ^(1.22)	46 ^(1.21)	56 ^(1.20)	26 ^(1.24)	imag ⁻	Bg
	90 ^(1.20)	84 ^(1.22)	80 ^(1.19)	74 ^(1.18)	87 ^(1.17)	89 ^(1.19)	79 ^(1.21)	23 ^(1.24)	76 ^(1.18)	72 ^(1.22)	85 ^(1.18)	Ag
	97 ^(1.24)	87 ^(1.17)	105 ^(1.20)	83 ^(1.21)	100 ^(1.21)	94 ^(1.20)	90 ^(1.18)	89 ^(1.20)	82 ^(1.21)	88 ^(1.18)	93 ^(1.20)	Ag
	114 ^(1.20)	131 ^(1.18)	157 ^(1.17)	102 ^(1.17)	114 ^(1.18)	128 ^(1.18)	131 ^(1.18)	99 ^(1.33)	103 ^(1.18)	128 ^(1.21)	168 ^(1.19)	Bg
	167 ^(1.36)	181 ^(1.41)	196 ^(1.41)	156 ^(1.40)	183 ^(1.41)	1.75 ^(1.40)	163 ^(1.40)	139 ^(1.35)	140 ^(1.41)	178 ^(1.40)	164 ^(1.19)	Ag
	177 ^(1.31)	211 ^(1.40)	249 ^(1.41)	139 ^(1.41)	193 ^(1.41)	1.71 ^(1.40)	170 ^(1.41)	144 ^(1.25)	142 ^(1.41)	200 ^(1.36)	220 ^(1.39)	Bg

- a) Best atom-atom fit to the ab initio potential.
- b) From Williams [28].
- c) From Williams [29].
- d) Potential from ab initio fit (1) with the electrostatic (point charge) term omitted.
- e) Atom-atom fit with the point charges on the nuclei.
- f) Experimental results from ref. 58 at $T = 85^{\circ}\text{K}$.
The angles ξ , η , ζ describing the molecular orientation are defined as follows: Start with the molecule lying in the ac^* plane, the C-C axis along the a-axis, and rotate by ξ , η , ζ about the a, b and c^* axes, respectively.
- g) Experimental result from ref. 69, corrected for the zero point vibrational energy (0.5 kcal/mole, from ref. 67).
- h) Experimental frequencies from ref. 66 at $T = 20^{\circ}\text{K}$.
- i) Experimental frequencies from ref. 35 at $T = 30^{\circ}\text{K}$.
The number in parentheses denotes the isotope ratio $\omega_{\text{C}_2\text{H}_4}/\omega_{\text{C}_2\text{D}_4}$.
The calculated frequencies in the first column have been obtained from the dynamical matrix at the experimental geometry, those in the second column at the equilibrium geometry for the given potential (Except for the fit (1) with $q = 0$, where the first column was calculated at the equilibrium geometry for the full fit (1) potential.).

in the present formalism, the rigid molecule approximation, is expected to hold rather well for ethylene since the lowest internal vibration mode lies at a frequency of 810 cm^{-1} [35], far above the lattice modes.

We have performed the calculation of the IR and Raman frequencies $\omega(\vec{q}=0)$ both for normal C_2H_4 and for C_2D_4 in order to look at the isotopic shifts in the Raman spectrum; the phonon dispersion curves have been calculated for C_2D_4 (fig. 6) since inelastic neutron scattering experiments can be expected in the near future [68]. For comparison with other lattice dynamics calculations on ethylene which have not optimized the structure parameters for the atom-atom potential used, we have also performed some calculations of the phonon frequencies in the experimental [58] structure.

The results for the theoretical atom-atom potential are listed in table 5, together with the results for the two empirical Williams potentials from table 4. Since these empirical potentials neglect or undervalue the effect of the electrostatic forces, we have studied the effect of these forces by performing a calculation with the theoretical atom-atom potential without the electrostatic (point charge) interactions (with or without reoptimizing the crystal structure). Also we have carried out phonon calculations using the theoretical potential with the atomic charges centered on the nuclei .

B Conclusions

The structure of the ethylene crystal calculated with the interaction potential from ab initio calculations is in rather good agreement with the experimental structure [58]. The lattice cohesion

energy is just slightly too high [69]. The frequencies of the lattice modes agree reasonably well with the IR and Raman data [66,35]. Particularly we find, in accordance with the experimentally observed isotope shifts in the Raman frequencies that the two highest frequency modes correspond with librations of the molecules around their C-C axes.

The theoretical model potential with the atomic charges centered on the nuclei, besides making a less good fit to the ab initio electrostatic interaction, also behaves considerably worse in the lattice calculations.

When comparing with the results for the empirical potentials we observe that the latter are still giving better crystal properties, especially the second Williams potential which comprises an electrostatic term. We must keep in mind, however, that part of these properties (the structure and the cohesion energy for a series of related hydrocarbons), have actually been used for parametrizing these potentials, whereas the other properties, the phonon frequencies, are strongly related with the criterion used for optimizing the empirical parameters [30] (the minimization of the forces on the molecules for the experimental crystal structure). The latter relation is confirmed by Williams' recent conclusion [30] that the inclusion of the phonon frequencies in the parametrization of the empirical atom-atom potentials hardly changes the potential obtained from the static crystal properties. The ab initio potential has not been adapted to any empirical data and, therefore, we can consider the agreement with the experimental crystal properties as very satisfactory.

The omission of the electrostatic (point charge) interactions

Fig. 6a

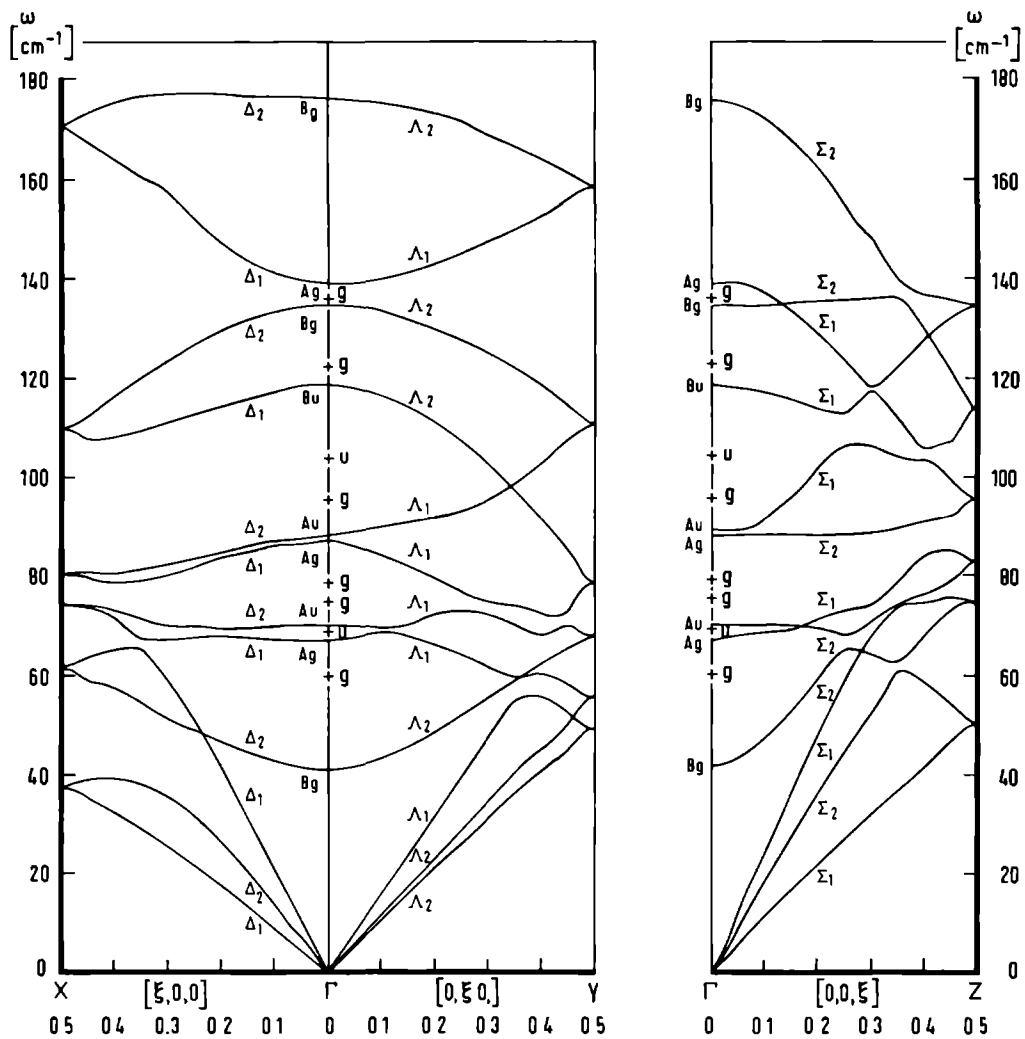


Fig. 6b

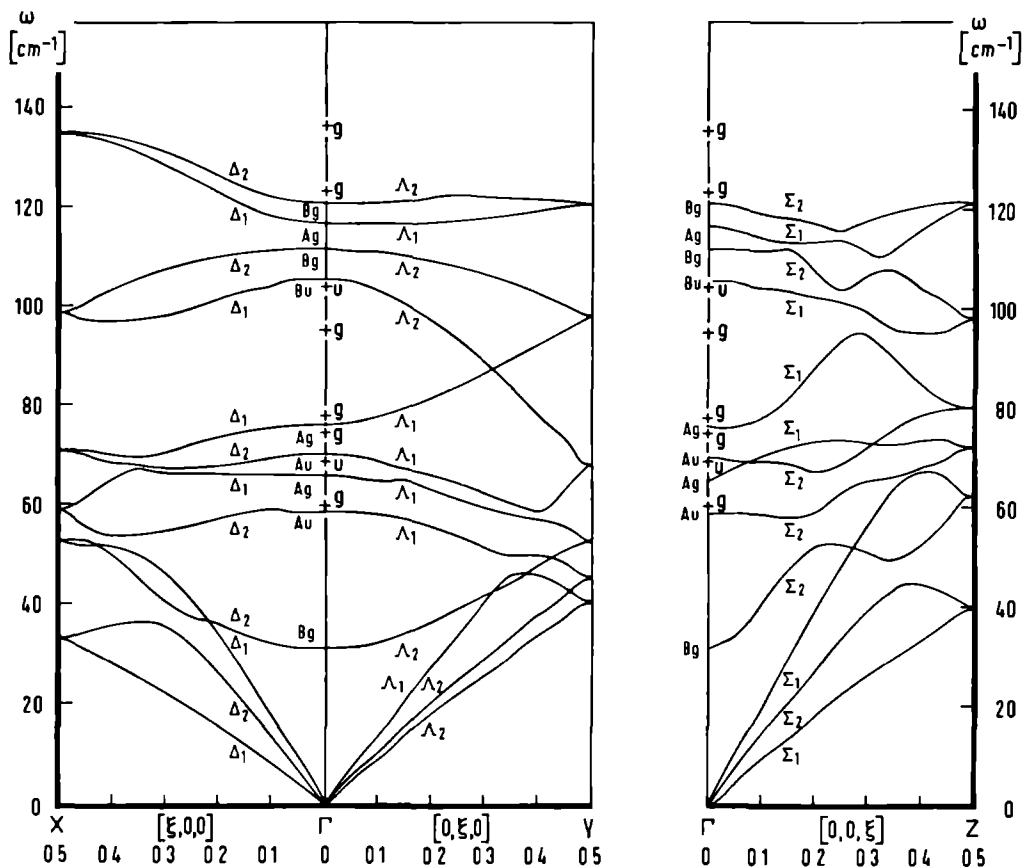


Fig. 6. Phonon dispersion curves in C_2D_4 for \vec{q} along the X ($= a^*$), Y ($= b^* = b$) and Z ($= c^*$) directions in the ethylene crystal.

- a. Calculated with the ab initio atom-atom potential, fit (1).
- b. Calculated with the atom-atom potential, empirical (2), from Williams [29].

For each potential the crystal structure is relaxed to equilibrium (within the given symmetry) before calculating the dynamical matrix. The crosses at the Γ -point ($\vec{q} = \vec{0}$) indicate the experimental results from IR (u) and Raman (g) spectroscopy.

from the ab initio potential has a distinct (lowering) effect on the phonon frequencies, in particular for the higher librational modes. This is quite understandable in view of the strong orientational dependence of these interactions. It is typical that the empirical potentials which underestimate or even neglect these (mainly molecular quadrupole-quadrupole) interactions still yield the correct magnitude for the phonon frequencies. This could be caused by a slight adaptation of the empirical parameters in the short range repulsions. If such potentials are used for the calculation of (macroscopic) properties which are dependent on the long range anisotropy of the interactions between the molecules this could lead to serious errors.

While we have found that the empirical potentials are in reasonable agreement with the ab initio calculations, except for the electrostatic contribution, we can also conclude that further parameter optimization of the (empirical) atom-atom potentials for the hydrocarbons, taking into account even more experimental solid state data, is probably not meaningful. We think on the basis of our ab initio results that remaining discrepancies between calculated and experimental crystal properties are due to the deficiencies of the atom-atom model. Possibly the use of other data, from beam scattering, relaxation measurements or Van der Waals molecules, could support our conclusions about the importance of electrostatic interactions.

Acknowledgement

The authors are very much indebted to Drs. Paul Wormer and Fred Mulder for providing several of the ab initio results presented in this paper. Moreover, Paul Wormer has made available the program COULEX for the ab initio calculation of the first order interactions. Thanks are due also to Drs. Wormer, Mulder and to Dr. Tadeusz Luty for many stimulating discussions.

References

- [1] A.I. Kitaigorodski, *Molecular Crystals and Molecules*, Academic Press, New York (1973)
- [2] D.E. Williams, *J. Chem. Phys.* 45, 3770 (1966)
- [3] D.E. Williams, *Acta Cryst. A* 30, 71 (1974)
- [4] A.T. Hagler and S. Lifson, *Acta Cryst. B* 30, 1336 (1974)
- [5] T. Luty and G.S. Pawley, *Chem. Phys. Letters*, 28, 593 (1974)
- [6] R.P. Rinaldi and G.S. Pawley, *J. Phys. C* 8, 599 (1975)
- [7] A first test for the long range interactions has been made in ref. [8]. The results have been included in the discussion in this paper
- [8] F. Mulder and C. Huiszoon, *Mol. Phys.* 34, 1215 (1977)
- [9] M. Faubel and J.P. Toennies, *Advan. At. Mol. Phys.* 13, 0000 (1978)
- [10] J. Reuss, *Advan. Chem. Phys.* 30, 389 (1975)
- [11] R. Schafer and R.G. Gordon, *J. Chem. Phys.* 58, 5422 (1973)
- [12] R.J. LeRoy and J. van Kranendonk, *J. Chem. Phys.* 61, 4750 (1974)
- [13] S.E. Novick, S.S. Harris, K.C. Janda and W. Klemperer, *Can. J. Phys.* 53, 2007 (1975)
- [14] V. Magnasco and G.F. Musso, *J. Chem. Phys.* 48, 2657 (1968)
- [15] G. Tapia, G. Bessis and S. Bratoz, *Int. J. Quantum Chem.* S4, 289 (1971)
- [16] C.F. Bender and H.F. Schaefer, *J. Chem. Phys.* 57, 217 (1972)
- [17] M. Jazunski, E. Kochanski and P. Siegbahn, *Mol. Phys.* 33, 139 (1977)

- [18] G.A. Gallup, *Mol. Phys.* 33, 943 (1977)
- [19] W. Meyer, *Chem. Phys.* 17, 27 (1976)
- [20] F. Mulder, A. van der Avoird and P.E.S. Wormer, *Mol. Phys.*,
submitted
- [21] M. Kraus and F.M. Mies, *J. Chem. Phys.* 42, 2703 (1965)
- [22] M.D. Gordon and D. Secrest, *J. Chem. Phys.* 52, 120 (1970)
- [23] B. Tsapline and W. Kutzelnigg, *Chem. Phys. Letters* 23,
173 (1973)
- [24] P.J.M. Geurts, P.E.S. Wormer and A. van der Avoird,
Chem. Phys. Letters 35, 444 (1975)
- [25] P.C. Hariharan and W. Kutzelnigg, Progress Report Lehrstuhl
für Theoretische Chemie, Ruhr Universität Bochum, Fed. Repu-
blic of Germany
- [26] R.D. Ethers, R. Danilowicz and W. England, *Phys. Rev.* A12,
2199 (1975)
- [27] J.F. Silvera and V.V. Goldman, to be published
- [28] D.E. Williams, *J. Chem. Phys.* 47, 4680 (1967)
- [29] D. Hall and D.E. Williams, *Acta Cryst.*, A31, 56 (1975)
- [30] T.L. Starr and D.E. Williams, *Acta Cryst.* A33, 771 (1977)
- [31] A. Warshell and S. Lifson, *J. Chem. Phys.* 53, 582 (1970)
- [32] G. Fillipini, C.M. Gramaccioli, M. Simonetta, G.B. Suffritti,
J. Chem. Phys. 59, 5088 (1973)
- [33] D.A. Dows, *J. Chem. Phys.* 36, 2836 (1967)
- [34] G. Taddei and E. Giglio, *J. Chem. Phys.* 53, 2768 (1970)
- [35] G.R. Elliot and G.E. Leroy, *J. Chem. Phys.* 59, 1217 (1973)
- [36] F. Vovelle and G.G. Dumas, *C.R. Acad. Sc. Paris*, 281,
B239 (1975)

- [37] M. Hashimoto, M. Hashimoto and T. Isobe, Bull. Chem. Soc. Japan, 44, 3230 (1971)
- [38] P.E.S. Wormer and A. van der Avoird, J. Chem. Phys. 62, 3326 (1975)
- [39] F. Mulder, M. van Hemert, P.E.S. Wormer and A. van der Avoird, Theoret. Chim. Acta, 46, 39 (1977)
- [40] P.E.S. Wormer, F. Mulder and A. van der Avoird, Int. J. Quantum Chem. 11, 959 (1977)
- [41] P.H. Smit, J.L. Derissen and F.B. van Duijneveldt, Mol. Phys., submitted
- [42] P.H. Smit, Thesis, Utrecht (1978)
- [43] Using the program COULEX written by P.E.S. Wormer, Nijmegen, 1976
- [44] P.E.S. Wormer, unpublished results
- [45] F. Mulder, unpublished results
- [46] N.J. Bridge and A.D. Buckingham, Proc. Roy. Soc. A295, 334 (1966)
- [47] G.W. Hills and W.J. Jones, J. Chem. Soc. Faraday Trans. II 71, 812 (1975)
- [48] L.W. Flynn and G. Todos, Am. Inst. Chem. Eng. 8, 362 (1962)
- [49] A.D. King, J. Chem. Phys. 51, 1262 (1969)
- [50] It should be noted here that we have also considered other solutions for correcting $\Delta E_{\text{point charge}}^{(1)}$ for penetration effects, such as the use of screened point charge interactions. This model fails in representing the "exact" penetration interactions, however, which are attractive for all molecular orientations due to the incomplete screening of

the nuclei with respect to the electrons (except for very small R , where the nuclear repulsions dominate)

- [51] F. Mulder, P.J.M. Geurts and A. van der Avoird, Chem. Phys. Letters, 33, 215 (1975)
- [52] A. van der Avoird and P.E.S. Wormer, Mol. Phys. 33, 1367 (1977)
- [53] L. Salem, Proc. Royal Soc. A 264, 379 (1961)
- [54] This difference would have been reduced if we had used fore-shortened C-H bond lengths [30] in fitting the ab initio results
- [55] A.D. Crowell, J. Chem. Phys. 29, 446 (1958)
- [56] R.F.W. Bader, O.A. Novaro and V. Beltran-Lopez, Chem. Phys. Letters, 8, 568 (1971)
- [57] H. Margenau and N.R. Kestner, The Theory of Intermolecular Forces, Pergamon, Oxford (1969), p. 151
- [58] G.J.H. van Nes and A. Vos, Acta Cryst. B33, 1653 (1977)
- [59] W. Press and J.J. Eckert, J. Chem. Phys. 65, 4362 (1976)
- [60] C.W. Bunn, Trans. Faraday Soc. 40, 23 (1944)
- [61] C. Brecher and R.S. Halford, J. Chem. Phys. 35, 1109 (1961)
- [62] G. Venkataraman and V.S. Sahni, Rev. Mod. Phys. 42, 409 (1970)
- [63] CERN Computer Centre Program Library, D 506, D 516, F. James and M. Roos, authors.
- [64] The separation of molecules into parts, when truncating the lattice sum of the atom-atom interactions [65] should be avoided since this makes the electrostatic interactions fall off with R^{-1} , whereas the leading term is R^{-5} (quadrupole-quadrupole) when whole molecules are considered.

- [65] D.E. Williams and T.L. Starr, *Computers & Chemistry*,
1, 173 (1977)
- [66] M. Brith and A. Ron, *J. Chem. Phys.* 50, 3053 (1969)
- [67] T. Wasiutynski, in: *Proc. Lattice Dynamics Conf.*,
ed. Balkanski, Flammarion, Paris, 1977
- [68] U. Buchenau, Jülich, private communication.
- [69] C.J. Egan and J.D. Kemp, *J. Am. Chem. Soc.* 59, 1264 (1937)

Dynamical and optical properties of the ethylene crystal;
self-consistent phonon calculations using an "ab initio"
intermolecular potential[†]

T. Luty*, A. van der Avoird, R.M. Berns and T. Wasitowski**
Institute of Theoretical Chemistry
University of Nijmegen
Toernooiveld, Nijmegen
The Netherlands

Abstract

Using an intermolecular potential from ab initio calculations, we have calculated the structure and solved the lattice dynamics problem of the ethylene crystal in the self-consistent phonon formalism. The anharmonic effects, as included by this formalism, systematically improve the optical mode frequencies, in comparison with experiment, but the corrections to the harmonic frequencies are still substantially too small. The crystal structure and its pressure dependence are well represented. From the phonon polarization vectors we have also evaluated the Raman scattering and infrared absorption intensities of the optical modes, applying a scheme which takes into account the mutual polarization of the molecules (the "local field corrections"). The Raman intensities agree quite well with experiment, the infrared intensities are less realistic, probably due to the neglect of intermolecular overlap effects in the intensity calculations. Using an empirical atom-atom potential for hydrocarbons instead of the ab initio potential, the assignment of the optical lattice modes by their calculated frequencies was not fully consistent with the Raman intensity ratios obtained from their polarization vectors.

* Present address: Institute of Organic and Physical Chemistry,
Technical University,
Wybrzeze Wyspianskiego 27, 50-370 Wroclaw.
Poland.

**Present address: Institute of Nuclear Physics,
Radzikowskiego 152, 31-342 Krakow.
Poland.

[†] Supported in part by the Netherlands Foundation for Chemical Research (SON) with financial aid from the Netherlands Organization for the Advancement of Pure Research (ZWO).

1. Introduction

As a first step in any lattice dynamical study which is not purely phenomenological the potential of the solid must be defined. To date, practically all calculations on molecular crystals have used simple empirical intermolecular potentials, mostly of the atom-atom type [1-3] (pairwise additive isotropic interactions between the atoms in different molecules), with parameters fitted to the experimental data. The lattice dynamics is usually treated in the harmonic approximation; sometimes [3-5], the calculated phonon frequencies are included in the optimization of the (atom-atom) potential parameters. The danger of such treatments is that possible deficiencies in the model potential and in the dynamical model are blurred: the fit of the parameters to the experimental data may (partly) compensate these deficiencies.

In the present study of the ethylene crystal we have tried to improve on the usual treatments in three ways. In the first place, we have used an intermolecular potential derived from ab initio calculations [6-9], with no empirical fit parameters. The crystal lattice structure calculated with this potential agrees well with experiment. When used in a harmonic lattice dynamics calculation the potential has yielded fairly good phonon frequencies also [6], although the best empirically fitted potentials match the experimental data still somewhat better. Part of the remaining discrepancies may originate from the harmonic model, however, and the second characteristic of the present study is that we have used the self-consistent phonon method [10] in order to correct for the effects of anharmonicity. Thus, the importance of these effects can be assessed and the temperature and pressure dependence of the crystal properties can be calculated and compared with experiment. The third point concerns the assignment of the phonon modes. The optical modes (wave vector $\underline{q} = 0$) can be observed by IR and Raman spectroscopy. The (symmetry) character of these modes is not usually measured, however, except for the distinction between g and u modes in centrosymmetric crystals, which modes are Raman and IR active, respectively. So, if only the frequencies of these modes are obtained from lattice dynamics calculations and compared with optical spectra, the agreement may seem reasonable but some of the modes may be interchanged. More-

over, the frequencies, i.e. the eigenvalues of the dynamical problem, may depend less sensitively on the potential than the corresponding eigenvectors. Therefore, we have provided additional information by calculating also the intensities of the optical modes, which depend on the phonon eigenvectors. For this purpose, we have applied a formalism for the Raman and IR intensities in molecular crystals [11,12] which explicitly includes the (electrostatic) long range interactions between the molecules.

2. Methods and potential

2.1. Intermolecular potential

The ab initio calculations leading to the ethylene-ethylene potential used in the present studies have been reported in a previous paper [6], as well as the fitting procedure which yields the parameters in the analytical representation of the results. This analytical representation has the form of a pairwise additive isotropic atom-atom potential with distance dependent functions of the exp-6-1 type, just as some of the empirical hydrocarbon potentials [2,3] (a Buckingham exp-6 potential, supplemented with Coulombic interactions between atomic point charges). The "atomic" point charges have been shifted away from the nuclei, however, since this yields a much better representation of the ab initio calculated (long range) electrostatic interaction between the molecules. The coefficients of the r^{-6} attractive terms have been obtained by fitting r^{-6} attractions between the carbon and hydrogen atoms (C-C, C-H and H-H) to the (long range) anisotropic dispersion interactions between the molecules (from ab initio calculated multipole expansion coefficients [8]). The repulsive exponential terms represent the overlap interactions obtained from an ab initio calculation of the (first order) interaction energy between two ethylene molecules which includes these overlap (charge penetration and exchange) effects by retaining the exact intermolecular interaction operator, instead of its multipole expansion, and using wave functions antisymmetrized over the dimer. The resulting repulsive interactions indeed fall off exponentially with the intermolecular distance. The induction (multipole-induced multipole) interactions are very small [8,9] and, since these would yield the dominant three-body contributions [13,14], we

can expect the ethylene crystal potential to have small deviations from pairwise (molecule-molecule) additivity [15,16] (a few percent of the binding energy, at the Van der Waals minimum).

The ab initio data [6] have been calculated for eight different orientations of the ethylene molecules and several intermolecular distances. For the long range r^{-n} interactions the atom-atom model works very well (if the "atomic" charges are shifted); the fit of the overlap (exponential) terms is somewhat less good, but the orientational and distance dependence of the ab initio potential is reasonably well represented. The parameters determining the analytical "ab initio" potential are collected in table 1, together with the parameters in a recent hydrocarbon atom-atom potential [2] fitted to the experimental data. In ref. [6] we have seen that the most striking difference between the ab initio potential and various empirical hydrocarbon potentials [2,3] is that the latter substantially underestimate the electrostatic multipole-multipole interactions between the C_2H_4 molecules.

2.2. Self-consistent phonon method; implementation for molecular crystals

The self-consistent phonon (SCP) formalism for lattice dynamics calculations has been developed for applications to the light rare gas crystals (helium, in particular) which have anharmonic interaction potentials in combination with relatively high zero-point vibrational energies [10]. The formalism starts from the following dynamical eigenvalue equations, just as the harmonic model:

$$\underline{D}(\underline{q}) \underline{e}(\underline{q}) = \omega^2(\underline{q}) \underline{M} \underline{e}(\underline{q}) \quad (1)$$

where the tensor \underline{M} contains the masses M^σ of the atoms in each sublattice σ :

$$M_{\alpha\beta}^{\sigma\sigma'} = M^\sigma \delta_{\sigma\sigma'} \delta_{\alpha\beta} \quad (\alpha, \beta = x, y \text{ or } z) \quad (2)$$

The eigenvalues $\omega_j(\underline{q})$ and eigenvectors $\underline{e}_j(\underline{q})$ are the frequencies and polarization vectors of the phonon modes with wave vector \underline{q} . In the harmonic approximation \underline{D} is the Fourier transform of the

Table 1

Parameters of the atom-atom potentials used for ethylene (C₂H₄)^{a)}

$$V(r_{1j}) = -A_{1j}r_{1j}^{-6} + B_{1j} \exp(-C_{1j}r_{1j}) + q_1q_jr_{1j}^{-1}$$

Parameters		Ab initio potential [6]	Empirical potential [2]
A [kcal Å ⁶ mole ⁻¹]	C-C	876	449.3
	C-H	132	134.3
	H-H	20	40.15
B [kcal mole ⁻¹]	C-C	27116	71461
	C-H	6368	14316
	H-H	1500	2868
C [Å ⁻¹]	C-C	3.16	3.60
	C-H	3.43	3.67
	H-H	3.70	3.74
q [unit charges]	C	-0.5274 ^{b)}	-0.24
	H	+0.2637 ^{b)}	+0.12

a) atomic coordinates C: (±0.6685, 0.0 , 0.0)Å
 (in molecular frame) H: (±1.2335, ±0.9275, 0.0)Å

b) "atomic" charges shifted
 to positions: C': (±0.5549, 0.0 , 0.0)Å
 H': (±1.0095, ±0.8308, 0.0)Å

force constant matrix ϕ :

$$D_{\alpha\beta}^{\sigma\sigma'}(\underline{q}) = \sum_{\ell} \phi_{\alpha\beta}^{\sigma\sigma'}(\ell) \exp[i \underline{q} \cdot \underline{R}(\ell)] \quad (3)$$

where the force constants are the second derivatives of the potential for the equilibrium structure of the crystal; $\underline{R}(\ell)$ is the direct lattice vector of the unit cell ℓ . In the SCP method the force constants are replaced by effective force constants which are derived [10] by minimizing the quantum statistical expectation value of the free energy, F , of the system, i.e. the canonical ensemble average of the "exact" anharmonic potential V over the harmonic oscillator states:

$$F = \sum_{\underline{q}, j} [\beta^{-1} \ln \{ 2 \sinh \frac{1}{2} \beta \omega_j(\underline{q}) \} - \frac{1}{2} \omega_j(\underline{q}) \coth \frac{1}{2} \beta \omega(\underline{q})] + \frac{1}{2} N \sum_{\underline{R}_{\sigma\sigma'}(\ell)} \langle V(\underline{R}_{\sigma\sigma'}(\ell) + \underline{u}_{\sigma\sigma'}(\ell)) \rangle \quad (4)$$

The vector $\underline{R}_{\sigma\sigma'}(\ell)$ is defined as $\underline{R}_{\sigma\sigma'}(\ell) = \underline{R}(\ell) + \underline{R}_{\sigma} - \underline{R}_{\sigma'}$ where \underline{R}_{σ} is the vector joining the origin of the unit cell with the σ sublattice. The relative atomic displacements are $\underline{u}_{\sigma\sigma'}(\ell) = \underline{u}_{\sigma}(\ell) - \underline{u}_{\sigma'}(0)$ and the vectors $\underline{u}_{\sigma}(\ell)$ denote the displacements of the σ atoms in unit cell ℓ , relative to their equilibrium positions, $\underline{R}(\ell) + \underline{R}_{\sigma}$. The temperature enters into the formalism via the quantity $\beta = \hbar/kT$. The minimization of expression (4) with respect to the effective force constants ϕ leads to the following expression for these force constants:

$$\phi_{\alpha\beta}^{\sigma\sigma'}(\ell) = \langle \nabla_{\alpha}^{\sigma} \nabla_{\beta}^{\sigma'} V(\underline{R}_{\sigma\sigma'}(\ell) + \underline{u}_{\sigma\sigma'}(\ell)) \rangle \quad (5)$$

This means that the second derivatives of the potential V have now to be averaged over the relative atomic displacements $\underline{u}_{\sigma\sigma'}(\ell)$. The averaging of any quantity Q , whether it is the potential in equation (4) or its second derivatives in equation (5), can be expressed by means of the displacement-displacement correlation function $\underline{\lambda}$:

$$\langle Q(\underline{R}_{\sigma\sigma'}(\ell) + \underline{u}_{\sigma\sigma'}(\ell)) \rangle = (2\pi)^{-3/2} [\det(\underline{\lambda})]^{-1/2} \times \int d\underline{u} Q(\underline{R}_{\sigma\sigma'}(\ell) + \underline{u}) \exp(-\frac{1}{2} \underline{u} \underline{\lambda}^{-1} \underline{u}) \quad (6)$$

These functions $\underline{\lambda}$ are given by:

$$\lambda_{\alpha\beta}(\sigma, \sigma', \ell) = \langle [\underline{u}_\sigma(\ell) - \underline{u}_\sigma(0)]_\alpha [\underline{u}_{\sigma'}(\ell) - \underline{u}_{\sigma'}(0)]_\beta \rangle \quad (7)$$

and they can be calculated from the following expression:

$$\lambda_{\alpha\beta}(\sigma, \sigma', \ell) = \frac{\hbar}{cN} \sum_{\underline{q}, j} [1 - \cos \underline{q} \cdot \underline{R}(\ell)] \omega_j(\underline{q})^{-1} \coth \frac{1}{2} \beta \hbar \omega_j(\underline{q}) \times e_j(\underline{q})_\alpha^\sigma e_j(\underline{q})_\beta^{\sigma'} \quad (8)$$

where c is the light velocity, if $\underline{e}_j(\underline{q})$ is normalized as $\underline{e}_j(\underline{q}) \cdot \underline{M} \cdot \underline{e}_j(\underline{q}) = 1$. Since the expression (8) contains the eigenvalues and eigenvectors of the dynamical equation (1), the equations (1) to (8) have to be solved self-consistently.

The first application of this formalism to molecular crystals was made by Raich et al. [17] for the α phase of solid N_2 . Actually, these authors treated the motions of the individual N atoms, which interact via an intermolecular atom-atom potential and an intramolecular harmonic or Morse type potential describing the N_2 stretch. Wasiutynski [18] has extended the formalism by considering explicitly the librational motions that occur in molecular crystals. In that case, one has translational displacements $\underline{u}^t = (x, y, z)$ and rotational displacements $\underline{u}^r = (\theta_x, \theta_y, \theta_z)$ of the (rigid) molecules; together these are grouped in a six-dimensional displacement vector $\underline{u} = (\underline{u}^t, \underline{u}^r) = \{u_\alpha; \alpha=1, \dots, 6\}$. Wasiutynski starts from the same dynamical equations (1), but the dimension of the problem is doubled, since the eigenvectors $\underline{e}_j(\underline{q})$ have librational components, $e_j(\underline{q})_\alpha$ for $\alpha = 4, 5, 6$. The mass tensor (2) must be extended as follows:

$$M_{\alpha\beta}^\sigma = 0 \text{ for } \alpha = 4, 5, 6 \text{ and } \beta = 1, 2, 3 \\ \text{and for } \alpha = 1, 2, 3 \text{ and } \beta = 4, 5, 6 \quad (9)$$

$$M_{\alpha\beta}^\sigma = I_{\alpha-3, \beta-3}^\sigma \text{ for } \alpha = 4, 5, 6 \text{ and } \beta = 4, 5, 6$$

where \underline{I}^σ is the moment of inertia tensor of the molecules in the σ sublattice (in the crystal system of axes). The effective force constant matrix $\underline{\phi}$, and its Fourier transform \underline{D} , have mixed translational-rotational (tr and rt) and pure rotational (rr) elements, in addition to the pure translational (tt) elements given by eq. (5). Also the displacement-displacement correlation functions (7), (8), have such components $\underline{\lambda}^{tt}, \underline{\lambda}^{tr}, \underline{\lambda}^{rt}$ and $\underline{\lambda}^{rr}$.

For intermolecular potentials which consist of additive atom-atom contributions (or interactions between generalized force centers on the molecules, such as the potential described in section 2.1), Wasitynski has worked out the calculation of the effective force constants (5) in terms of the atomic displacement-displacement correlation functions. These can be related to the molecular functions $\underline{\lambda}^{tt}, \underline{\lambda}^{tr}, \underline{\lambda}^{rt}$ and $\underline{\lambda}^{rr}$ by substituting into eq. (7) the following relation between atomic displacements $\underline{u}(m)$ and the rigid molecule translations \underline{u}^t and rotations \underline{u}^r :

$$\underline{u}(m) = \underline{u}^t + \underline{u}^r \times \underline{R}(m) \quad (10)$$

where $\underline{R}(m)$ is the position vector of atom m relative to the molecular center of mass. It must be realized, however, that eq. (10) and also the harmonic oscillator kinetic energy expression in terms of $\underline{u}^r = (\theta_x, \theta_y, \theta_z)$ are exact only for infinitesimal rotations \underline{u}^r . So the SCP method, as generalized to molecular crystals by Wasitynski [18] may be less effective in correcting the harmonic model for larger amplitude anharmonic librations. Numerical calculations which have been carried out [19] on the ordered (α and γ) phases of solid N_2 (using an ab initio interaction potential [20] similar to the present one) confirm this observation. The SCP corrections for the translational mode frequencies lead to almost perfect agreement with experiment; the librational frequencies, especially at temperatures near the α - β phase transition, remain somewhat in error.

Wasitynski has applied this generalized SCP method to the cubic hexamethylene tetramine crystal with one molecule in the primitive unit cell [18]. The application of the formalism to the monoclinic ethylene crystal, space group $P2_1/n$, with two molecules in the primitive cell, is rather straightforward. The integrations over the atomic displacements (6) which have to be made for the potential, in the free energy expression (4), and for its second derivatives, in the effective force constant matrix (5), have been carried out numerically by Gauss-Hermite quadrature [21], using 3^3 and 5^3 points, respectively. Non-diagonal terms in the displacement-displacement correlation functions $\underline{\lambda}$ appear to be very small [18]; when evaluating expression (6), the off-diagonal terms in $\underline{\lambda}^{-1}$ have been neglected. The Helmholtz free energy (4), or the Gibbs free energy $G = F + pv$ for crystals under constant pressure, has been minimized, not only with respect to the effective force constants as implied by the SCP method, but also with respect to the lattice structure: the unit

cell parameters and the positions and orientations of the molecules in the primitive cell (if not determined by the crystal symmetry). This structure optimization is repeated in each SCP iteration. As a starting point for the SCP iterations we have used the eigenvalues and eigenvectors from a harmonic calculation.

The summations over \underline{q} in equations (4) and (8) replace exact integrations over the first Brillouin zone, and so it is important to choose a set of wave vectors \underline{q} which correctly represent these integrals. In principle, we have chosen a uniform mesh in reciprocal space. The set of \underline{q} must reflect the complete symmetry of the crystal, however, including the point group operations. Since the tensor $\underline{\lambda}$ given by equation (8) transforms under symmetry operations in the same way as the force constant tensor $\underline{\phi}$, eq. (5), one can restrict the set of \underline{q} to the fundamental wedge ($\frac{1}{8}$ of the Brillouin zone) and use the appropriate weight factors and transformation properties in the summations (4) and (8). In this wedge we have taken 312 points.

Finally, it must be mentioned that the lattice sums occurring in equations (3) and (4) have been performed over 42 nearest molecules in the ethylene crystal. The crystal structure is known from X-ray diffraction [22], but the monoclinic cell parameters a, b, c and β and the Euler angles ξ, η, ζ corresponding with the equilibrium orientations of the molecules have been optimized in the calculations (by minimizing the free energy as mentioned above). This minimization was carried out by the program package MINUITs [23]. The calculations have been made also for deuterated ethylene, for which the crystal structure under pressure is known [24].

2.3. Raman intensities

In a sample of randomly oriented crystallites as one has for the Raman measurements on ethylene [25], the polarized Stokes intensity for a non-degenerate lattice mode j with normal coordinate Q_j and frequency ω_j is given by [26]:

$$I_j = \frac{\hbar \omega_s^4}{2\pi c^3 \omega_j [1 - \exp(-\beta\omega_j)]} \sum_{\alpha, \beta} \left| \frac{\partial \chi_{\alpha\beta}}{\partial Q_j} \right|^2 \quad (11)$$

where ω_s is the frequency of the scattered light, $\omega_s = \omega_0 - \omega_j$. The tensor χ describes the (high frequency) electric

susceptibility of the crystal. In the simplest ("oriented gas") model the molecules in the crystal are assumed to be non-interacting and the crystal susceptibility χ is given by the sum of the molecular polarizability tensors $\underline{\alpha}^\sigma$, expressed in the crystal principal axes system. Actually, the susceptibility χ which is the response function of the crystal to external electric fields, is modified by the interactions between the molecules. The principal correction term to the response function is due to the internal field from the induced dipoles, which changes the local field and, thereby, the induced dipole moments. Including this term one obtains [27]:

$$\chi = \frac{4\pi}{v} \sum_{\sigma, \sigma'} (\underline{1} - \underline{\alpha} \cdot \underline{L})_{\sigma\sigma'}^{-1} \cdot \underline{\alpha}^{\sigma'} \quad (12)$$

where v is the unit cell volume, $\underline{\alpha}$ is the $3n \times 3n$ tensor containing the molecular polarizability tensors: $\underline{\alpha}_{\sigma\sigma'} = \delta_{\sigma\sigma'} \underline{\alpha}^\sigma$, \underline{L} is the $3n \times 3n$ Lorentz tensor which is composed of 3×3 Lorentz tensors $\underline{L}_{\sigma\sigma'}$, [27] and n is the number of sublattices. In principle, other correction terms due to higher multipoles, to overlap interactions and to dispersion forces between the molecules should be included as well. We expect the induced dipole field correction term to be dominant, however, as it is for the collision induced (depolarized) Raman intensities in compressed gases [28] and, therefore, we have neglected all other interaction terms.

In crystals where the molecules lie on centers of symmetry (such as ethylene) the optical ($\underline{q} = \underline{0}$) modes are purely translational (u) or purely rotational (g); only the g modes are Raman active. In that case, the susceptibility derivative simplifies to [11]:

$$\frac{\partial \chi}{\partial Q_j} = \sum_{\sigma} \sum_{\alpha} \frac{\partial \chi}{\partial u_{\alpha, \sigma}^r} (\underline{e}_j^r)_{\alpha}^{\sigma} \quad (13)$$

where $(\underline{e}_j^r)_{\alpha}^{\sigma}$ are the (rotational) components ($\alpha=4,5,6$) of the eigenvector for the librational mode j (with $\underline{q} = \underline{0}$) which multiply the rotational displacements, $\underline{u}^r = (\theta_x, \theta_y, \theta_z)$, of the molecules σ . From (12), noting that the Lorentz tensors \underline{L} do not change by rotational displacements (they depend only on the molecular positions), one finds, after some manipulation [11]:

$$\frac{\partial \chi}{\partial u_{\alpha, \sigma}^r} = \frac{4\pi}{v} \sum_{\sigma', \sigma''} (\underline{1} - \underline{\alpha} \cdot \underline{L})_{\sigma', \sigma}^{-1} \frac{\partial \underline{\alpha}^{\sigma}}{\partial u_{\alpha, \sigma}^r} (1 - \underline{L} \cdot \underline{\alpha})_{\sigma \sigma''}^{-1} = \Pi_{\alpha}^{\sigma} \quad (14)$$

The derivatives $\frac{\partial \underline{\alpha}^{\sigma}}{\partial u_{\alpha, \sigma}^r}$ of the molecular polarizabilities (in the crystal axes system) with respect to the rotational displacements of the molecules (about the crystal axes) are completely determined by the rotational transformation properties of the molecular tensors $\underline{\alpha}^{\sigma}$. So, for a given crystal structure the quantities Γ_{α}^{σ} can be calculated from the molecular polarizabilities $\underline{\alpha}^{\sigma}$ and their rotational derivatives (both transformed to the crystal axes system) and from the Lorentz tensors \underline{L} . From the lattice dynamics calculations (see section 2.2.) we have obtained the eigenvectors \underline{e}_j^r and, thus, we can compute the intensity of the (unpolarized) Raman band for each mode j by the formula:

$$I_j = \frac{\hbar \omega_s^4}{2\pi c^3 \omega_j [1 - \exp(-\beta \omega_j)]} \sum_{\alpha, \beta} \left| \sum_{\sigma, \gamma} (\Gamma_{\gamma}^{\sigma})_{\alpha\beta} (\underline{e}_j^r)_{\gamma}^{\sigma} \right|^2 \quad (15)$$

The molecular polarizability of ethylene has been measured [29] and calculated by ab initio methods [8]. For the present calculations we have used the experimental values (which are not very different from the calculated ones): $\alpha_{xx} = 36.4$, $\alpha_{yy} = 26.1$, $\alpha_{zz} = 22.9$ atomic units, in a molecular frame with the x axis along the C-C bond and the molecule lying in the xy plane.

2.4. Infrared intensities

A model for the infrared intensities of lattice vibrations which is consistent with the description of the Raman intensities [11] (section 2.3.), has recently been proposed [12]. The integrated absorption intensity for phonon mode j measured with unpolarized radiation is:

$$\Gamma_j = \frac{2\pi^2 \hbar}{vc \omega_j [1 - \exp(-\beta \omega_j)]} \sum_{\alpha} \left| \frac{\partial Z}{\partial Q_j} \alpha \right|^2 \quad (16)$$

where $\frac{\partial Z}{\partial Q_j} \alpha$ is the dipole moment change induced in the unit cell by the ($\underline{q} = \underline{j} \underline{0}$) mode with normal coordinate Q_j . This normal coordinate is composed of molecular displacements; for ethylene only the translational displacements \underline{u}^t (the u modes) are involved. For molecules without intrinsic dipole moments (such as ethylene) a dipole moment

can be induced by the interactions with the neighbours according to the following three mechanisms: polarization by the electric field of the neighbours (and by external fields), dispersion forces and (short range) overlap effects. In compressed (pure) gases it has been found [31] that the first term yields the main contribution to the collision induced IR absorption (although the overlap effects are non-negligible; in gas mixtures they are even dominant [31-33]). Just as in our model for the Raman intensities, we have neglected the overlap and dispersion interactions. The remaining polarization term yields the following (linear response) expression [12] for the dipole moment induced in a given molecule σ by the displacements \underline{u}^t of other molecules σ'' :

$$\underline{z}^\sigma = - \sum_{\sigma'} \underline{\chi}_{\sigma\sigma'} \cdot \sum_{\sigma''} \underline{B}_{\sigma'\sigma''} \underline{u}_{\sigma''}^t \quad (17)$$

The tensor $\underline{\chi}_{\sigma\sigma'}$ is part of the electric susceptibility tensor of the crystal including the local field corrections, cf. eq. (12):

$$\underline{\chi}_{\sigma\sigma'} = \frac{4\pi}{V} (\underline{1} - \underline{\alpha} \cdot \underline{L})_{\sigma\sigma'}^{-1} \cdot \underline{\alpha}^{\sigma'} \quad (18)$$

and $\underline{B}_{\sigma'\sigma''}$ contains the derivatives of the electric field at site σ' with respect to the displacements of the molecules σ'' . In order to calculate the internal electric field in the crystal the molecules can be represented by continuous charge distributions, by point multipoles or by sets of point charges distributed over the molecules (not necessarily on the nuclei). We have chosen the latter representation, just as for the calculation of the electrostatic contribution to the crystal free energy and force constants (see sections 2.1. and 2.2.). Then, the field derivative matrix \underline{B} takes the form:

$$B_{\alpha\beta}^{\sigma\sigma'} = \sum_{m \in \sigma'} q_{\sigma'}(m) \sum_{\ell} \nabla_{\alpha} \nabla_{\beta} | \underline{R}_{\sigma\sigma'}(\ell) + \underline{R}(m) |^{-1} \quad (19)$$

where $q_{\sigma'}(m)$ are the point charges placed on molecule σ' at positions $\underline{R}(m)$ relative to the center of mass and the vectors $\underline{R}_{\sigma\sigma'}(\ell)$ are defined as in eq. (4). The induced molecular dipole moments (17) can be summed over the unit cell and the dipole moment derivatives appearing in the infrared intensity (16) can be found by using the relation between the normal coordinates Q_j and the molecular displacements \underline{u}_{σ}^t . Thus, we obtain:

$$\begin{aligned} \frac{\partial Z}{\partial Q_j} &= \sum_{\sigma} \frac{\partial Z^{\sigma}}{\partial Q_j} = \sum_{\sigma} \sum_{\sigma', \alpha} \frac{\partial Z^{\sigma}}{\partial u_{\alpha, \sigma}^t} (\underline{e}_j^t)_{\alpha}^{\sigma'} \\ &= - \sum_{\sigma, \sigma', \sigma''} \chi_{\sigma\sigma''} \cdot B_{\sigma''\sigma'} \cdot (\underline{e}_j^t)^{\sigma'} \end{aligned} \quad (20)$$

The susceptibility tensor $\chi_{\sigma\sigma'}$, can be calculated as in section 2.3 from the molecular polarizabilities and the Lorentz tensor for the given crystal structure. For the same structure and a given set of molecular point charges (see table 1) the field derivatives \underline{B} can be evaluated, using Ewald's method [26] (which has been used also for the calculation of the Lorentz tensor). The eigenvectors \underline{e}_j^t are those from the lattice dynamics calculation again, but now for the translational $\underline{q} = \underline{0}$ modes (the u modes).

3. Results and discussion

The results of the crystal structure optimization with the ab initio potential and with an empirical hydrocarbon potential [2] (see section 2.1.) are shown in table 2. In the harmonic model calculation we have minimized the internal energy of the crystal (at T=0), neglecting the zero point vibrations; in the SCP calculations we have minimized the Gibbs free energy for the temperatures and pressures where the experimental structure determinations [24] were done. The overall agreement between the calculated and experimental data is fairly good, which is satisfactory especially for the ab initio potential since it contains no empirical fit parameters. In the SCP calculations (at zero pressure) the lattice appears to dilate relative to the harmonic calculation; this effect is mainly due to the zero point motions. The largest relative increase occurs for the parameter b (which is smaller than the experimental value). The dilation is smaller for the ab initio potential, which is what one would expect since the empirical potential is somewhat softer (it yields lower phonon frequencies, see below). The lattice contraction which is obtained by increasing the pressure to 1.9 kbar is very well reproduced by the SCP calculations.

The phonon frequencies $\omega_j(\underline{q})$ have been calculated for 312 wave vectors \underline{q} in the fundamental wedge of the Brillouin zone, which is necessary for calculating the free energy (4) and the SCP effective force constants (5) via equations (6) and (8). In table 3 the results are shown just for $\underline{q} = \underline{0}$, since only the optical frequencies have been measured so far [25,34]. The agreement between calculations and

Table 2

Crystal structure of C_2D_4 , space group $P2_1/n$ ($Z=2$)

structure parameters		T = 85 K , p = 0					T = 99 K , p = 1.9 kbar		
		calculated (harmonic) ^{a)}		calculated (SCP) ^{b)}		experimental [24]	calculated (SCP) ^{b)}		experimental [24]
		empirical potential [2]	ab initio potential [6]	empirical potential [2]	ab initio potential [6]		empirical potential [2]	ab initio potential [6]	
lattice	a [Å]	4.726	4.730	4.799	4.782	4.613	4.716	4.710	4.506
constants	b [Å]	6.435	6.205	6.610	6.334	6.610	6.546	6.280	6.558
	c [Å]	4.135	4.004	4.212	4.064	4.037	4.121	4.000	3.977
	β [degrees]	93.9	88.5	93.4	88.2	94.5	94.2	89.1	95.2
molecular orientations ^{c)}	ξ [degrees]	-27.0	-31.7	-27.8	-32.2	-27.0	-28.2	-32.0	-26.8
	η [degrees]	-11.7	- 9.3	-11.2	- 9.1	-14.6	-11.6	- 9.4	-14.2
	ζ [degrees]	-31.8	-31.3	-32.0	-31.5	-34.3	-31.9	-31.6	-34.3

a) by minimizing the internal energy (T=0)

b) by minimizing the free energy

c) Euler angles defined as follows: Start with the molecule lying in the ac^* plane, the C-C axis along the a axis, and rotate by ξ, η and ζ about the a, b and c^* axes, respectively.

Table 3

Optical ($q = 0$) phonon frequencies [cm^{-1}] in the C_2D_4 crystal

symmetry		T=30K, p=0				T=99K, p=1.9 kbar	
		calculated (harmonic)		calculated (SCP)		experimental [25,34]	calculated (SCP) ab initio potential [6]
		empirical potential [2]	ab initio potential [6]	empirical potential [2]	ab initio potential [6]		
libra- tional modes	B_g	31.1	41.6	33.4	42.6	60	44.6
	A_g	65.7 ^{a)}	66.9	64.8 ^{a)}	66.6	75	74.1
	A_g	76.3 ^{a)}	87.6	74.3 ^{a)}	84.6	78	90.2
	B_g	111.1	134.5	107.2	130.3	95	139.4
	A_g	116.3	139.5	111.7	136.0	123	146.5
	B_g	120.7	176.3	118.2	172.7	135	181.4
trans- lational modes	A_u	59.1	69.9	54.9	66.6	-	73.1
	A_u	69.9	87.7	65.6	83.2	69.5 ^{b)}	89.0
	B_u	105.2	118.3	99.2	113.4	104.0 ^{b)}	124.8

a) If these modes were assigned by their Raman intensities, their order would have to be reversed (only for the empirical potential, see table 5)

b) Measured at 20K [34]

experiment is reasonable, but somewhat less good than we have recently found [19] for the N_2 crystal, where especially the translational mode frequencies were reproduced almost perfectly by the SCP treatment with an ab initio potential. This is probably due to the ab initio potential for C_2H_4 and, in particular, its analytic (atom-atom) representation, which has been obtained from fewer ab initio calculated points, being somewhat less accurate. (Moreover, the atom-atom model appeared to be more realistic for the N_2-N_2 potential than for the $C_2H_4-C_2H_4$ potential, in the short range region).

In all cases, except for the lowest frequency B_g mode, the SCP anharmonic corrections lower the harmonic frequencies; the effective force constants are smaller than the second derivatives at the potential minimum. For the ab initio potential all SCP corrections improve the agreement with the experimental frequencies, i.e. they point in the right direction, but they are still considerably too small. (If the potential is not completely realistic they can not, of course, fully remove the discrepancy). For the empirical potential [2] the SCP corrections actually make the results worse, in some cases. This must probably be ascribed to the empirically fitted potentials containing already some effects of the anharmonic lattice vibrations implicitly. Increasing the pressure to 1.9 kbar raises all the phonon frequencies, changing the temperature in the range from 0 to 100 K has practically no effect (less than 1 cm^{-1}).

A result which is striking, is that we have found practically no difference between the SCP eigenvectors $\underline{e}_j(\underline{q})$ and the harmonic ones, although the frequencies (the eigenvalues) do differ. So, for the calculations of the Raman and IR intensities we have used the eigenvectors from the harmonic calculations. The Raman intensities are shown in tables 4 and 5, for ethylene and deuterated ethylene. First, we observe from the difference between the absolute intensities in the columns 4 and 5 of table 4 that the local field corrections to the crystal electric susceptibility [11] are quite important. (Note that the Raman intensities depend on the fourth power of the matrix $(\underline{1}-\underline{a}\cdot\underline{L})^{-1}$, see equations (14) and (15)). For the relative intensities, which is what can be reliably extracted from the measurements [25], the "oriented gas" model yields about the same results as the model which includes these corrections.

The relative intensities calculated with the ab initio potential agree reasonably well with experiment, except for the very

Table 4

Raman intensities of optical modes in the C_2H_4 crystal

mode symmetry	calculated ^{a)}						experimental [25]	
	empirical potential [2]		ab initio potential [6]				frequencies [cm ⁻¹]	relative intensities ^{b)}
	frequencies [cm ⁻¹]	relative intensities ^{b)}	frequencies [cm ⁻¹]	absolute intensities ^{c)}	relative intensities ^{b)}	oriented with local gas model field cor- rections		
B _g	38	0.66	50	0.09	0.34	0.35	73	0.19
A _g	79	0.81	80	0.24	0.97	1.00	90	1.00
A _g	90	1.00	105	0.13	0.51	0.53	97	0.42
B _g	131	0.19	157	0.04	0.15	0.15	114	0.20
A _g	163	0.17	196	0.03	0.11	0.11	167	0.006
B _g	170	0.04	249	0.005	0.024	0.025	177	0.002

a) from the harmonic calculations (the eigenvectors are practically the same as the SCP eigenvectors).

b) relative to the most intense mode

c) in arbitrary units

Table 5

Raman intensities of optical modes in the C_2D_4 crystal

mode symmetry	calculated ^{a)}				experimental [25]	
	empirical potential [2]		ab initio potential [6]		frequencies [cm^{-1}]	relative intensities ^{b)}
	frequencies [cm^{-1}]	relative intensities ^{b)}	frequencies [cm^{-1}]	relative intensities ^{b)}		
B_g	31	0.64	42	0.43	60	0.17
A_g	66	0.66	67	1.00	75	1.00
A_g	76	1.00	88	0.52	78	0.50
B_g	111	0.20	134	0.13	95	0.20
A_g	116	0.14	139	0.08	123	0.08
B_g	121	0.014	176	0.015	135	0.013

a) from the harmonic calculations (the eigenvectors are practically the same as the SCP eigenvectors)

b) relative to the most intense mode

low intensities of the two highest frequency modes in ethylene. These modes correspond with almost pure rotational oscillations of the C_2H_4 molecules about their C-C axes (in phase, A_g , or out of phase, B_g). Since the proton mass is low, the amplitudes of these oscillations are relatively large. Apart from possible experimental inaccuracies in these low intensities, the SCP formalism and the model used for calculating the Raman intensities are probably less reliable in this case. For the corresponding modes in C_2D_4 (see table 5) the agreement is much better.

The Raman intensities calculated with the empirical potential [2] show an interesting discrepancy, both for C_2H_4 and for C_2D_4 . If one were to assign the lowest two A_g modes by their intensities, rather than by their frequencies, then their order would be reversed. Looking at the frequencies alone, one could not detect such a discrepancy and the danger of trying to improve the empirical fit parameters by using the measured phonon frequencies [3] is clearly demonstrated here. Also, the overall agreement with the measured relative Raman intensities is less good for the empirical potential than it is for the ab initio potential.

Table 6 shows that the agreement between the calculated relative IR intensities and the measured data [34] is rather bad, both for the ab initio potential and for the empirical one; the latter seems to give slightly worse results. Maybe the ethylene films on which the IR intensity measurements have been made, do not correspond with the model of randomly oriented crystallites for which formula (16) has been derived. Due to the symmetry, the induced dipole moment must lie along the crystal b axis for the A_u modes, while it follows from the calculations that the B_u mode yields a dipole transition moment nearly parallel to the a axis. A comparison with polarized IR spectra would be very informative. On the other hand, the model used for calculating the induced dipole moments is probably too crude. In particular, the neglect of overlap effects on the induced dipoles may lead to inaccuracies. The reason why the calculated IR intensities are worse than the Raman intensities could be that the latter appear already in the "oriented gas" model, i.e. they depend in the first instance just on the molecular polarizability tensors (in particular, on their rotational transformation behaviour). A result which seems to be consistent with experiment is that the lowest frequency A_u mode, which has not been observed until now, is indeed calculated to have a

Table 6

Infrared intensities of optical modes in the C₂H₄ crystal

mode symmetry	calculated ^{a)}				experimental [34]	
	empirical potential [2]		ab initio potential [6]		frequencies [cm ⁻¹]	relative intensities ^{b)}
	frequencies [cm ⁻¹]	relative intensities ^{b)}	frequencies [cm ⁻¹]	relative intensities ^{b)}		
A _u	63	0.10	74	0.16	-	-
A _u	75	0.33	93	0.72	73	1.00
B _u	113	1.00	126	1.00	110	0.66

a) from the harmonic calculations (the eigenvectors are practically the same as the SCP eigenvectors)

b) relative to the most intense mode

low relative intensity.

4. Conclusions

Summarizing the discussions, we conclude that the intermolecular C_2H_4 potential from ab initio calculations [6-9] yields a fairly good structure and reasonably good phonon frequencies for the ethylene crystal. If the anharmonic effects are taken into account by the self-consistent phonon method, the frequencies are systematically improved; the corrections are substantially too small to yield agreement with experiment, however. The effects of pressure on the ethylene crystal structure and on the phonon frequencies are well represented by the SCP calculations. From the calculation of the (relative) intensities of the Raman active optical modes it was found that the calculated polarization vectors of these modes are fairly realistic, too.

An empirical hydrocarbon atom-atom potential [2] also yields a fairly good crystal structure and reasonably good phonon frequencies, but now the harmonic frequencies are not always improved by the SCP corrections. This might be expected since the empirical potential probably contains the effects of the (anharmonic) lattice vibrations implicitly already; so, the results will not be improved by again adding these effects, explicitly. The polarization vectors obtained from this empirical potential are less realistic, as shown by the comparison of the Raman intensities. In particular, it was found in this case that the assignment of two A_g modes by their frequencies is not consistent with their intensity ratio. So, this assignment may have to be reversed, but then the agreement with the measured frequencies is deteriorated.

The model [11] which we have used to calculate the Raman intensities in the ethylene crystal appeared to work quite well; the absolute intensities are strongly affected by the local field corrections, but the relative intensities practically do not change from the "oriented gas" results. The model for the IR intensities [12] has still to be improved, probably by taking the overlap induced dipole moments into account.

Acknowledgement

One of us (A.v.d.A.) is grateful to dr. V.V. Goldman, dr. M.H. Boon and prof. G. Vertogen for useful discussions about the SCP formalism.

References

1. A.I. Kitaigorodski, *Molecular Crystals and Molecules*, (Academic, New York, 1973).
2. D. Hall and D.E. Williams, *Acta Cryst.* A31, 56 (1975).
3. T.L. Starr and D.E. Williams, *Acta Cryst.* A33, 771 (1977).
4. T. Luty and G.S. Pawley, *Chem. Phys. Letters*, 28, 593 (1974).
5. J.C. Raich and N.S. Gillis, *J. Chem. Phys.* 66, 846 (1977).
6. T. Waslutynski, A. van der Avoird and R.M. Berns, *J. Chem. Phys.* 69, 5288 (1978).
7. P.E.S. Wormer and A. van der Avoird, *J. Chem. Phys.* 62, 3326 (1975).
8. F. Mulder, M. van Hemert, P.E.S. Wormer and A. van der Avoird, *Theoret. Chim. Acta*, 46, 39 (1977).
9. P.E.S. Wormer, F. Mulder and A. van der Avoird, *Int. J. Quantum Chem.* 11, 959 (1977).
10. N.R. Werthamer in: *Rare Gas Solids*, M.L. Klein and J.A. Venables, eds., Vol. I, (1976) p. 265 and references therein.
11. T. Luty, A. Mierzejewski and R.W. Munn, *Chem. Phys.* 29, 353 (1978).
12. T. Luty and R.W. Munn, *Chem. Phys.* 43, 295 (1979).
13. A. Beyer, A. Karpfen and P. Schuster, *Chem. Phys. Letters* 67, 369 (1979).
14. E. Clementi, W. Kolos, G.C. Lie and G. Ranghino, *Int. J. Quantum Chem.* 17, 377 (1980).
15. P. Claverie in: *Intermolecular Interactions: From Diatomics to Biopolymers*, B. Pullman ed., Wiley, New York (1978), p. 69.
16. A. van der Avoird, P.E.S. Wormer, F. Mulder and R.M. Berns, in: *Van der Waals systems, Topics in Current Chemistry*, Springer, Berlin 93, 1 (1980)
17. J.C. Raich, N.S. Gillis and A.B. Anderson, *J. Chem. Phys.* 61, 1399 (1974).
18. T. Waslutynski, *Phys. Stat. Sol. (b)* 76, 175 (1976).
19. T. Luty, A. van der Avoird and R.M. Berns, *J. Chem. Phys.* 73, 5305 (1980).
20. R.M. Berns and A. van der Avoird, *J. Chem. Phys.* 72, 6107 (1980).
21. M. Abramowitz and I.A. Stegun, *Handbook of Mathematical Functions*, National Bureau of Standards, Washington (1964).
22. G.J.H. van Nes and A. Vos, *Acta Cryst.* B33, 1653 (1977).
23. CERN Computer Centre Program Library, D506, D516, F. James and M. Ross, authors.
24. W. Press and J.J. Eckert, *J. Chem. Phys.* 65, 4362 (1976).
25. G.R. Elliot and G.E. Leroi, *J. Chem. Phys.* 59, 1217 (1973).
26. M. Born and K. Huang, *Dynamic Theory of Crystal Lattices*, Clarendon, Oxford (1954).
27. C.J.F. Bötcher and P. Bordewijk, *Theory of Electric Polarization*, Vol. 2, 2nd ed., Elsevier, Amsterdam (1978) p. 434.

26. L. Frommhold, *Advan. Chem. Phys.* (1980)
and references therein.
29. N.J. Bridge and A.D. Buckingham, *Proc. Royal Soc. A*295, 334 (1966).
30. G.W. Hills and W.J. Jones, *J. Chem. Soc. Faraday Trans. II*, 71,
812 (1975).
31. J.D. Poll and J.L. Hunt, *Can. J. Phys.* 54, 461 (1976).
32. R.M. Berns, P.E.S. Wormer, F. Mulder and A. van der Avoird,
J. Chem. Phys. 69, 2102 (1978).
33. P.E.S. Wormer and G. van Dijk, *J. Chem. Phys.* 70, 5695 (1979).
34. M. Brith and A. Ron, *J. Chem. Phys.* 50, 3053 (1969).

Ab initio calculations of the collision-induced dipole in He-H₂.I. A Valence Bond approach.[†]

R.M. Berns, P.E.S. Wormer, F. Mulder and A. van der Avoird
Instituut voor Theoretische Chemie
Universiteit van Nijmegen
Toernooiveld, Nijmegen
The Netherlands

Abstract

The collision-induced dipole in the system He-H₂ is calculated in the multistructure Valence Bond method, using the non-orthogonal monomer orbitals. In the region around the collision diameter, which contributes most to the collision-induced IR absorption, the long range results (the leading terms are the quadrupole-induced dipole on He with R⁻⁴ dependence and the dispersion dipole with R⁻⁷ dependence) are modified by overlap effects. The short range behaviour is determined, moreover, by the appearance of other important terms, the exchange dipole and the overlap-induction dipole on H₂, which vanish in the long range. Since all the short range contributions have approximately the same (exponential) dependence on the intermolecular distance, they can be collected and added as a single exponential dipole function to the R⁻⁴ and R⁻⁷ long range terms. Of the latter terms the R⁻⁷ dispersion dipole is of little importance.

[†] Supported in part by the Netherlands Foundation for Chemical Research (SON) with financial aid from the Netherlands Organization for the Advancement of Pure Research (ZWO).

1. Introduction

During a collision between two unlike atoms or molecules the intermolecular interaction generates a dipole moment in the collision complex, which for obvious reasons is called a "collision induced dipole". Because collision induced dipoles are a function of the intermolecular separation, the relative orientation of the molecules and the intramolecular vibrational coordinates, they give rise to absorption and emission of radiation involving all three types of degrees of freedom [1]. The absorption and emission due to translational and rotational motion are observed as broad bands in the far infrared ($100\text{-}600\text{cm}^{-1}$); the collision induced vibrational transitions are associated with much shorter wavelengths, for instance the vibrational transitions of H_2 lie around 4500cm^{-1} .

Much work has been done on the measurements of these spectra, see for instance ref. 2 or the compilation of Rich and McKellar [3] for extensive literature surveys. Since the pioneering work of Van Kranendonk [4] and Poll and Van Kranendonk [5] much effort has also been put into the development of a theory explaining the line-shapes. For a review of these theories we refer to ref. 1.

Considerably less attention has been paid to the mechanism that yields the collision induced dipole itself, and especially the influence of the short range effects, such as exchange and penetration, has rarely been studied; consequently their role in the induction mechanism is at present not well understood. More has been written about the long range forces, and in particular the importance of a permanent multipole on one molecule inducing a dipole on the other has often been stressed, as it gives the leading contribution in a $1/R$ expansion of the dipole moment [6-7]. This effect is of course absent in the collision of two noble gas atoms. Here, the long range induced dipole is caused by the London dispersion forces as has been discussed in refs. 10 and 11.

The few papers that deal with short range forces all consider pairs of atoms. Matcha and Nesbet [12] performed some SCF calculations on noble gas pairs, and Lacey and Byers Brown [13] did first order perturbation calculations on the same systems and a few other atomic pairs. Nobody to date, however, has included the relevant long and short range effects in one single calculation; hence the question of the relative importance of these effects is still undecided.

In this paper we will consider long and short range contributions to the collision induced dipole for the first time within one formalism: the multistructure Valence Bond (VB) method. We have chosen to undertake this study on the He-H₂ system for several reasons: In the first place the induced vibrational spectrum has been interpreted recently [14], enabling a comparison of the calculations with the experiment (although a comparison with the results of this paper is only partially possible, since the translational band has not yet been interpreted and we do not consider changes in the vibrational coordinate. In a second paper we will give a more detailed analysis including vibration). A second reason for the choice of He-H₂ is that we have previously calculated part of its potential energy surface [15], also using the VB formalism so that we had a wave function at our disposal. (It has appeared that the dipole moment could not be directly calculated from this wave function, however, since it is much more sensitive to orthogonalization of the orbital basis than the interaction energy), Finally, mixtures of noble gases with H₂ belong to the most widely investigated systems, and He-H₂ is the simplest example of such a mixture at least from the quantum chemist's point of view.

As has been pointed out before [16], the VB method changes for increasing intermolecular distance into an ordinary perturbation method. One can use this feature of VB as a selection criterion for VB structures, that is, one includes in the calculation only the VB structures that are known to give important contributions in the long range. Doing this, one assumes implicitly that short range forces are not yet so dominant in the region of interest that they make a modelling after long range theory impossible. Our experience with calculations around the Van der Waals minimum is that this assumption holds reasonably well for the energy, and it is interesting to see whether this also works for the dipole moment, especially since the distances of interest are somewhat shorter in this case. The region most sensitively probed by the experiment ranges from 4.5 to 8 bohr and the sensitivity peaks just inside the scattering diameter.

2. Theory

The Valence Bond method is a variational method; therefore it requires the solution of a secular problem with the Hamiltonian ma-

trix elements having the following form:

$$\langle Y \phi_a^A \phi_b^B | H^A + H^B + V | Y \phi_a^A \phi_b^B \rangle$$

Here H^A is the Hamiltonian of monomer A, H^B of monomer B and V describes the interaction between the two. The operator Y is the spin-free equivalent of a singlet spin projector times the antisymmetrizer; it is a linear combination of all electron permutations. In this work Y is an NP-type Young projector and hence our VB structures are the spin-free equivalents of spin-bonded functions [17]. The a-th excited state ϕ_a^A of molecule A is a product of SCF orbitals obtained from a Hartree-Fock calculation on the free monomer; ϕ_b^B is constructed analogously. In accordance with the usual second order perturbation theory for long range forces [18] only singly excited states on each of the monomers are taken into account. This means that we do not take intramolecular correlation into consideration.

Two different spin coupling schemes are possible: A and B can both be excited to a triplet or to a singlet state. Since we have found earlier [15] that the VB structures arising from triplet-triplet coupling hardly mix into the VB ground state of the complex, we do not include these kinds of states.

For larger intermolecular distances the differential overlap between orbitals on A and B becomes negligible, and hence Y factorizes effectively into a product of two singlet Young projectors Y^A and Y^B , with Y^A acting on the electrons of A only and Y^B acting on the electrons of B.

As we have discussed earlier [16], the solution Ψ_{VB} of the secular problem corresponding to the lowest energy, may be thought of as having been obtained in the long range from a perturbation treatment (PT) in a finite basis. Defining the resolvent R_0 of the unperturbed Hamiltonian $H^A + H^B$ in this basis [19]:

$$R_0 \equiv \sum_{a,b} \frac{|ab\rangle\langle ab|}{\Delta E_{ab}}$$

where $|ab\rangle = |Y^A \phi_a^A\rangle |Y^B \phi_b^B\rangle$, and

$$E_{ab} = (E_0^A - E_a^A) + (E_0^B - E_b^B)$$

we can write [19]:

$$|\psi_{PT}\rangle = (1 + R_0 V + R_0 V R_0 V + \dots) |00\rangle$$

Here we have used that the first order interaction is zero in the long range.

The dipole moment of the complex can now be approximated by:

$$\langle \vec{\mu}_{PT} \rangle = \langle \psi_{PT} | \vec{\mu} | \psi_{PT} \rangle$$

where $\vec{\mu} = \vec{\mu}^A + \vec{\mu}^B$ and $\vec{\mu}^A = \sum_{\alpha \in A} \vec{r}_\alpha q_\alpha$ (a sum over the particles α of A, which have charges q_α and position vectors \vec{r}_α). An analogous definition holds for $\vec{\mu}^B$. Using the above perturbation expansion of ψ_{PT} one writes through second order in V for $\langle \vec{\mu}_{PT} \rangle$:

$$\langle \vec{\mu}_{PT} \rangle = \langle 00 | \vec{\mu}^{(0,0)} + \vec{\mu}^{(1,0)} + \vec{\mu}^{(1,1)} + \vec{\mu}^{(2,0)} | 00 \rangle \quad (1)$$

where the effective dipole moment operators are given by:

$$\begin{aligned} \vec{\mu}^{(0,0)} &= \vec{\mu} \\ \vec{\mu}^{(1,0)} &= \vec{\mu} R_0 V + V R_0 \vec{\mu} \\ \vec{\mu}^{(1,1)} &= V R_0 \vec{\mu} R_0 V \\ \vec{\mu}^{(2,0)} &= \vec{\mu} R_0 V R_0 V + V R_0 V R_0 \vec{\mu} \end{aligned} \quad (2)$$

The first contribution to $\langle \vec{\mu}_{PT} \rangle$, which is of zeroth order in V, is the vector sum of the permanent moments on the monomers, this contribution is zero for He-H₂. The term of first order in V corresponds to a permanent moment on A inducing a dipole on B plus a permanent moment on B inducing a dipole on A. We will elaborate the matrix element $\langle 00 | \vec{\mu}^{(1,0)} | 00 \rangle$ in the appendix, where a formula is derived for the induced dipole in a pair of molecules of arbitrary symmetry. For the complex under consideration only part of the (1,0)-contribution occurs, because He does not have any multipole moment. The third and fourth terms have no classical counterparts, we will refer to them as (1,1)-dispersion and (2,0)-dispersion respectively. Byers Brown and Whisnant [10] have named these terms dispersion of type II and type I, respectively.

Although the solution of the secular problem contains in principle a superposition of all orders of perturbation, we can never-

theless separate to a certain extent the different orders of perturbation within the VB framework by relying on the high symmetry of the monomers and assuming that third and higher order effects are negligible. In order to explain the procedure we need a few definitions. The He states of different symmetry species (i.e. of different L-quantum number) and of different symmetry subspecies (i.e. of different M-quantum number) are labelled by λ . The indices λ are in 1-1 correspondence with the set of spherical harmonics or their real form, the tesseral harmonics. Similarly μ labels the H_2 -states of different symmetry; the notation common for homonuclear diatomics is used to denote μ explicitly. We can now write R_0 as follows:

$$R_0 = \sum_{\lambda} \sum_{\mu} R_0(\lambda; \mu), \quad (3)$$

where $R_0(\lambda; \mu)$ includes a sum over all states of symmetry λ on He and a sum over all H_2 -states characterized by μ .

For a linear complex lying along the z-axis the multipole expansion for V through R^{-4} dependence takes the form (for neutral monomers):

$$\begin{aligned} V = & R^{-3} [-2V_3(z;z) + V_3(x;x) + V_3(y;y)] \\ & + 3R^{-4} [-\frac{1}{2}V_4(3z^2-r^2;z) + V_4(xz;x) + V_4(yz;y)] \\ & - 3R^{-4} [-\frac{1}{2}V_4(z;3z^2-r^2) + V_4(x;xz) + V_4(y;yz)] \end{aligned} \quad (4)$$

Here $V_3(z;z)$ stands for $(\sum_{\alpha \in A} q_{\alpha} z_{\alpha})(\sum_{\beta \in B} q_{\beta} z_{\beta})$ and similar definitions hold for the other interactions. In the case of a perpendicular, T shaped, complex, which can be obtained from the linear one by rotating H_2 around the y-axis over 90° , we substitute:

$$V_4(z;3z^2-r^2) = -\frac{1}{2}V_4(z;3x^2-r^2) + \frac{3}{2}V_4(z;z^2-y^2)$$

into the expansion of V, in order to have again only terms which are adapted to the local symmetries (the symmetries of the subsystems).

Using (3) and (4) one can expand the effective dipole operators defined in (2), see tables I and II. In deriving these tables we have translated the operators $\vec{\mu}^A$ and $\vec{\mu}^B$ to the centers of mass of the respective monomers, which is allowed for neutral subsystems.

Now we can define the different dipole moment contributions in

TABLE I

Decomposition of the effective dipole moment operators defined in (2) into symmetry adapted components for the linear case.

$$\vec{\mu}(1,0) = \frac{3}{2} R^{-4} \mu_z^{\text{He}} R_0(z; \sigma_g) V_4(z; 3z^2 - r^2) + \text{hermitean conjugate}$$

$$\begin{aligned} \vec{\mu}(1,1) = & 3 R^{-7} \{ V_3(z; z) R_0(z; \sigma_u) \mu_z^{\text{He}} R_0(3z^2 - r^2; \sigma_u) V_4(3z^2 - r^2; z) \\ & + V_3(x; x) R_0(x; \pi_{x,u}) \mu_z^{\text{He}} R_0(xz; \pi_{x,u}) V_4(xz; x) \\ & + V_3(y; y) R_0(y; \pi_{y,u}) \mu_z^{\text{He}} R_0(yz; \pi_{y,u}) V_4(yz; y) \} \\ - & 3 R^{-7} \{ V_3(z; z) R_0(z; \sigma_u) \mu_z^{\text{H}_2} R_0(z; \sigma_g) V_4(z; 3z^2 - r^2) \\ & + V_3(x; x) R_0(x; \pi_{x,u}) \mu_z^{\text{H}_2} R_0(x; \pi_{x,g}) V_4(x; xz) \\ & + V_3(y; y) R_0(y; \pi_{y,u}) \mu_z^{\text{H}_2} R_0(y; \pi_{y,g}) V_4(y; yz) \} \\ & + \text{hermitian conjugate} \end{aligned}$$

$$\begin{aligned} \vec{\mu}(2,0) = & 3 R^{-7} \mu_z^{\text{He}} R_0(z; \sigma_g) \{ V_3(z; z) R_0(3z^2 - r^2; \sigma_u) V_4(3z^2 - r^2; z) \\ & + V_3(x; x) R_0(xz; \pi_{x,u}) V_4(xz; x) \\ & + V_3(y; y) R_0(yz; \pi_{y,u}) V_4(yz; y) \\ & + V_4(3z^2 - r^2; z) R_0(z; \sigma_u) V_3(z; z) \\ & + V_4(xz; x) R_0(x; \pi_{x,u}) V_3(x; x) \\ & + V_4(yz; y) R_0(y; \pi_{y,u}) V_3(y; y) \} \end{aligned}$$

(continued)

Table I continued

$$\begin{aligned}
 & -3R^{-7} \mu_z^{H_2} R_0(s; \sigma_u) \{ V_3(z; z) R_0(z; \sigma_g) V_4(z; 3z^2 - r^2) \\
 & \quad + V_3(x; x) R_0(x; \pi_{x,g}) V_4(x; xz) \\
 & \quad + V_3(y; y) R_0(y; \pi_{y,g}) V_4(y; yz) \\
 & \quad + V_4(z; 3z^2 - r^2) R_0(z; \sigma_u) V_3(z; z) \\
 & \quad + V_4(x; xz) R_0(x; \pi_{x,u}) V_3(x; x) \\
 & \quad + V_4(y; yz) R_0(y; \pi_{y,u}) V_3(y; y) \}
 \end{aligned}$$

+ hermitean conjugate

TABLE II

Decomposition of the effective dipole moment operators defined in (2) symmetry adapted components for the perpendicular case

$$\vec{\mu}^{\dagger}(1,0) = -\frac{3}{4} R^{-4} \mu_z^{\text{He}} R_0(z; \sigma_g) V_4(z; 3z^2 - r^2) + \text{hermitean conjugate}$$

$$\begin{aligned} \vec{\mu}^{\dagger}(1,1) = & 3 R^{-7} \{ V_3(z; z) R_0(z; \pi_{z,u}) \mu_z^{\text{He}} R_0(3z^2 - r^2; \pi_{z,u}) V_4(3z^2 - r^2; z) \\ & + V_3(x; x) R_0(x; \sigma_u) \mu_z^{\text{He}} R_0(xz; \sigma_u) V_4(xz; x) \\ & + V_3(y; y) R_0(y; \pi_{y,u}) \mu_z^{\text{He}} R_0(yz; \pi_{y,u}) V_4(yz; y) \} \\ - & 3 R^{-7} \{ -\frac{1}{2} V_3(z; z) R_0(z; \pi_{z,u}) \mu_z^{\text{H}_2} R_0(z; \sigma_g) V_4(z; 3z^2 - r^2) \\ & + \frac{3}{2} V_3(z; z) R_0(z; \pi_{z,u}) \mu_z^{\text{H}_2} R_0(z; \delta_{z^2 - y^2; g}) V_4(z; z^2 - y^2) \\ & + V_3(x; x) R_0(x; \sigma_u) \mu_z^{\text{H}_2} R_0(x; \pi_{z,g}) V_4(x; xz) \\ & + V_3(y; y) R_0(y; \pi_{y,u}) \mu_z^{\text{H}_2} R_0(y; \delta_{zy; g}) V_4(y; yz) \} \\ & + \text{hermitean conjugate} \end{aligned}$$

$$\begin{aligned} \vec{\mu}^{\dagger}(2,0) = & 3 R^{-7} \mu_z^{\text{He}} R_0(z; \sigma_g) \{ V_3(z; z) R_0(3z^2 - r^2; \pi_{z,u}) V_4(3z^2 - r^2; z) \\ & + V_3(x; x) R_0(xz; \sigma_u) V_4(xz; x) \\ & + V_3(y; y) R_0(yz; \pi_{y,u}) V_4(yz; y) \\ & + V_4(3z^2 - r^2; z) R_0(z; \pi_{z,u}) V_3(z; z) \\ & + V_4(xz; x) R_0(x; \sigma_u) V_3(x; x) \\ & + V_4(yz; y) R_0(y; \pi_{y,u}) V_3(y; y) \} \end{aligned}$$

(continued)

Table II continued

$$\begin{aligned}
 & - 3 R^{-7} \mu_z^{H_2} R_0(s; \pi_{z,u}) \left\{ - \frac{1}{2} V_3(z; z) R_0(z; \sigma_g) V_4(z; 3x^2 - r^2) \right. \\
 & \quad + \frac{3}{2} V_3(z; z) R_0(z; \delta_{z^2 - y^2, g}) V_4(z; z^2 - y^2) \\
 & \quad + V_3(x; x) R_0(x; \pi_{z, g}) V_4(x; xz) \\
 & \quad + V_3(y; y) R_0(y; \delta_{zy, g}) V_4(y; yz) \\
 & \quad - \frac{1}{2} V_4(z; 3x^2 - r^2) R_0(z; \pi_{z, u}) V_3(z; z) \\
 & \quad + \frac{3}{2} V_4(z; z^2 - y^2) R_0(z; \pi_{z, u}) V_3(z; z) \\
 & \quad + V_4(x; xz) R_0(x; \sigma_u) V_3(x; x) \\
 & \quad \left. + V_4(y; yz) R_0(y; \pi_{y, u}) V_3(y; y) \right\}
 \end{aligned}$$

+ hermitean conjugate

the VB formalism. Let us agree to call a VB structure of local symmetry $(z; \sigma_g)$ which represents He in an excited state and H_2 in its ground state a "He-induction structure", then we see from tables I and II that a calculation on a basis that consists of only the He induction structures and the ground state gives the $(1,0)$ -part of the dipole moment. We also see from tables I and II that He induction structures contribute to the $(1,1)$ - and $(2,0)$ part, but that they only do so in cooperation with "dispersion" VB structures (singly excited on both monomers) of other local symmetry. If, for instance, the dispersion structures of $(z; \sigma_u)$ symmetry are added to the basis the He induction structures will give a contribution to the $(1,1)$ and $(2,0)$ dispersion dipoles on H_2 , and to the $(2,0)$ -dispersion dipole on He, both in the case of the linear complex.

In analogy we call a VB structure representing He in its ground state and H_2 in an excited σ_u -state (linear complex) or $\pi_{z,u}$ -state (perpendicular complex) an " H_2 induction structure". As can be seen from tables I and II these structures alone do not give a long range contribution to the dipole; in the short range they give a dipole moment on H_2 , which is induced by penetration of the He-atom into the charge cloud of the H_2 -molecule, causing incomplete screening of the He nucleus, and by the repulsive exchange force originating from the overlap. We refer to this effect as H_2 overlap-induction.

The total dipole moment $\langle \vec{\mu}_{VB} \rangle = \langle \Psi_{VB} | \vec{\mu} | \Psi_{VB} \rangle$ is obtained from a VB calculation including the ground state, the He induction structures, the H_2 induction structures and the dispersion structures which determine the R^{-7} contribution in the long range (see tables I and II); the latter structures also account for part of the higher (R^{-9} , etc.) dispersion contributions. Such a VB calculation yields the coefficients in the following expansion:

$$|\Psi_{VB}\rangle = \sum_{a,b} |Y \phi_a^A \phi_b^B\rangle C_{ab} \quad (5)$$

The VB dipole moment is split into three parts:

$$\begin{aligned} \langle \vec{\mu}_{VB} \rangle &= C_{00}^2 \langle Y \phi_0^A \phi_0^B | \vec{\mu} | Y \phi_0^A \phi_0^B \rangle + 2 \sum'_{a,b} \langle Y \phi_0^A \phi_0^B | \vec{\mu} | Y \phi_a^A \phi_b^B \rangle C_{ab} C_{00} \\ &+ \sum'_{a,b} \sum'_{a',b'} \langle Y \phi_a^A \phi_b^B | \vec{\mu} | Y \phi_{a'}^A \phi_{b'}^B \rangle C_{ab} C_{a'b'} \end{aligned} \quad (6)$$

Then, summarizing, we define the following contributions:

- (1) The exchange dipole is the expectation value of $\vec{\mu}$ over the ground state VB structure. This contribution, which is due to the antisymmetrization only and vanishes in the long range, is practically equal to the first term of (6) since the coefficient C_{00} is very close to unity.
- (11) The induction dipole on He is the dipole obtained from a VB calculation including all induction VB structures on He, together with the ground state. Analogously for the (overlap-) induction dipole on H₂. These contributions form part of the second term in (6).
- (111) The (2,0) dispersion dipole is obtained from the same term as the induction dipoles, i.e. $2 \sum_a \langle Y \phi_0^A \phi_0^B | \vec{\mu} | Y \phi_a^A \phi_0^B \rangle C_{a0} C_{00}$ for molecule A, but now the coefficients C_{a0} are modified by the admixture of the appropriate (2,0) dispersion structures (see tables I and II) in the VB calculation. Subtracting the induction dipoles defined in (11) yields the (2,0) dispersion dipole. This procedure is justified since the long range expansion of the second term in (6) is the following:

$$2 \langle 00 | \vec{\mu} (R_0 V + R_0 V R_0 V) | 00 \rangle = \langle 00 | \vec{\mu}^{(1,0)} + \vec{\mu}^{(2,0)} | 00 \rangle,$$

which can be proved by substituting the long range results for the VB coefficients:

$$C_{ab} \approx \langle ab | 1 + R_0 V + R_0 V R_0 V | 00 \rangle$$

- (1v) Analogously, if we substitute these coefficients into the third term of (6) and retain only the term in V^2 we find:

$$\langle 00 | V R_0 \vec{\mu} R_0 V | 00 \rangle = \langle 00 | \vec{\mu}^{(1,1)} | 00 \rangle$$

and, so, the (1,1) dispersion dipole in VB is defined as the third term in (6) restricted to those matrix elements that yield the corresponding long range dispersion contribution (tables I and II).

Because in VB the wave functions are antisymmetrized and the exact interaction operator is used instead of only the lowest terms in the multipole expansion, the dispersion terms are modified by exchange and penetration and will no longer have an R^{-7}

dependence for smaller distances. The (1,0) He induction term too will deviate from a strict R^{-4} dependence. H_2 overlap-induction will become an important contribution, as will the exchange dipole. Decreasing R we will also find that more and more matrix elements which are vanishing in the long range will be giving contributions, because of the breakdown of local selection rules, and hence that the separately distinguished contributions (i) to (iv) will no longer completely add up to $\langle \vec{\mu}_{VB} \rangle$.

3. Computations

Two geometries of the He- H_2 are considered: a perpendicular, T shaped, one and a linear conformation. In both cases the intermolecular distance is varied from 4.0 to 10.0 bohr, whereas the H-H distance is kept fixed at 1.40 bohr.

The SCF monomer orbitals, from which the VB structures are constructed, are taken from Geurts et al. [15]. The A.O. basis used in that reference is a H(6,4,1/1,2,1), He(6,2,1/1,1,1) G.T.O. basis, with the exponents of the polarization functions optimized for a calculation of the dispersion energy.

At the start of this work it was our intention to use the VB wavefunctions as well from ref. 15. The VB structures in that work are derived from orthogonalized orbitals, and if one uses these the dipole induced on He by H_2 at a distance of 8.0 bohr in the perpendicular geometry comes out to be $-29.14 \cdot 10^{-5}$ a.u.. The same contribution to the dipole moment of the complex can be calculated classically. Employing the values $\alpha_0^{He} = 1.335$, $\langle Q_2^{H_2} \rangle = 0.4931$, $\langle Q_4^{H_2} \rangle = 0.3639$ and $\langle Q_6^{H_2} \rangle = 0.2365$, all calculated from the basis of Geurts et al., one finds a classical value of $-23.77 \cdot 10^{-5}$ a.u.. Judging from our experience in calculating Van der Waals energies this difference of about 20% between the VB and the long range result was considered too high, so we calculated the same dipole in a basis originating from the pure, and hence non-orthogonal, monomer orbitals. This gave $-23.89 \cdot 10^{-5}$ a.u., a number in perfect agreement with the classical result. It is easy to understand why orthogonalization has such a relatively large effect: by mixing the orbitals on A with those on B, and vice versa, one contaminates the VB structures with charge transfer structures, and an amount of charge of $0.66 \cdot 10^{-5}$ a.u.

transferred from one molecule to the other is already sufficient to explain the above differences. So, because of this sensitivity of the calculated collision induced dipoles to the artificial charge transfer introduced by orthogonalization, all subsequent calculations had to be performed in a basis of VB structures derived from the original non-orthogonal monomer MO's. The method employed by us is described in ref. 20.

Unfortunately such a calculation is rather difficult, and because the Van der Waals energy is hardly affected by orthogonalization, our program handling non-orthogonal orbitals was never developed past a pilot stage. As the main limitation is that it can handle at most eight non-orthogonal, non-doubly occupied, orbitals simultaneously, we were forced to divide up the calculations into smaller pieces.

From the perturbation results given in tables I and II it is clear that in the long range a VB calculation, involving all structures that give an R^{-7} dependence, can be split. In the linear case, for instance, we see that a calculation based on the ground state and structures of (z, σ_g) and $(z; \sigma_u)$ symmetry gives one term of the (1,1) dispersion dipole on H_2 and one term of the (2,0) dipole on He, (and the He induction, of course). Another calculation, based on $(z; \sigma_g)$ - and $(xz; \pi_{x,u})$ -structures, gives a different term of the (2,0) dipole on He and no contribution to the (1,1) dipole. As far as perturbation theory holds, such terms are strictly additive.

Earlier [16] it was noted in energy calculations that a similar additivity also holds for shorter distances. Several tests on the dipole moment of this complex at $R = 5.2$ and 8.0 bohr have shown that here too the additivity predicted by long range theory holds excellently, even though at 5.2 bohr exchange and penetration are far from negligible. This makes it possible to partition the orbital set into subsets of different local symmetry and to divide the complete VB calculation into smaller ones based on choices out of these subsets guided by tables I and II.

However, a complication arises here from the fact that the tables I and II are derived under the assumption of orthogonal states and hence orthogonal orbitals. So, additivity holds only strictly in that case; or, in other words, the orbitals figuring in the resolvents of tables I and II must be interpreted as orthogonalized orbitals. The orthogonalized orbitals can of course be expanded in

terms of the original orbitals. Substituting these expansions into the resolvents, it follows that coupling matrix elements occur that are zero in the long range. The strength of these coupling matrix elements is determined by the intermolecular overlap of the orbitals involved, which is negligibly small in most cases. Such mixing does not occur for orbitals of different global symmetry ($C_{\infty v}$ and C_{2v} for the linear and the perpendicular case, respectively) which have zero overlap, and the corresponding parts of the resolvent are still additive.

The latter property was used when making a first partitioning of the VB calculation with the non-orthogonal orbitals. In the linear case we have included the dispersion structures of (σ, σ) type and those of (π, π) type in two separate VB calculations; in the perpendicular case we had to make a further splitting of the VB calculation. The number of orbitals in each VB calculation was restricted by inspecting the weight of the structures in the VB wave function of Geurts et al. [15] in which these orbitals occur. Moreover, we have performed numerous tests to check that no important overlap contributions were neglected and that additivity holds between the separate VB calculations.

4. Results and discussion

In tables III and IV the different contributions to the dipole moment are given for the linear and the perpendicular case, respectively. Note that the (1,1) contribution is absent for the T shaped complex. Because this contribution is only 10% of the (2,0) dipole for the linear geometry, a number in accordance with the findings of Byers Brown and Whisnant [10,11], and because the (2,0) dispersion itself is already very small, we decided that it was not worth the effort to calculate this small effect in the perpendicular case as well.

As will be shown in a second paper, the region responsible for the collision induced absorption in He- H_2 stretches from 4.5 to 8.0 bohr. We see that the two short range effects, exchange and H_2 overlap-induction, are dominant there, although the dipole moment in He induced by the permanent moments on H_2 is also sizable. This latter term has a strikingly good R^{-4} dependence down to $R = 5.2$ bohr. As far as the absence of higher multipole terms (R^{-6} , R^{-8} , etc.) is con-

TABLE III. Decomposition of the VB dipole moments for the linear geometry^a.
All dipole moments are in 10^{-5} a.u.^b.

R [bohr]	Exchange	H ₂ -overlap induction	He-induction ^c	(2,0)-disp	(1,1)-disp	Rest	$\langle \mu_{VB} \rangle$
4.0	1768.48	2870.56	1020.39 (834.33)	384.21	-25.05	-394.99	5623.60
5.2	249.07	377.87	300.81 (282.87)	51.92	-5.35	-63.93	910.39
5.6	121.96	184.18	214.89 (208.97)	11.14	-3.39	-29.59	499.19
6.0	57.73	87.97	159.07 (157.76)	-5.32	-2.07	-12.81	284.57
7.0	7.57	12.57	83.93 (84.34)	-7.69	-0.71	-1.24	94.43
8.0	0.78	1.53	49.02 (49.17)	-3.33	-0.26	-0.10	47.64
10.0	0.00	0.02	20.00 (20.00)	-0.57	-0.05	0.00	19.40

- a. The decomposition is performed according to the definitions (i) to (iv) given in the text.
- b. Positive direction of the dipole moment corresponds with negatively charged H₂ and positively charged He.
- c. In parentheses the multipole expansion results are given, calculated as a sum of the R⁻⁴, R⁻⁶ and R⁻⁸ terms.

TABLE IV. Decomposition of the VB dipole moments for the perpendicular geometry. All dipole moments are in 10^{-5} a.u. (see captions table III)

R [bohr]	Exchange	H ₂ -overlap induction	He-induction	(2,0)-disp	Rest	$\langle \mu_{VB} \rangle$
4.0	1136.97	1142.02	-219.35 (-364.63)	52.36	-132.96	2249.04
5.2	172.37	176.57	-116.23 (-130.61)	-26.89	-22.57	183.25
5.6	84.21	85.67	-91.98 (-97.55)	-23.87	-11.24	42.79
6.0	39.24	40.70	-72.58 (-74.30)	-18.36	-5.34	-16.34
7.0	4.74	5.64	-40.65 (-40.37)	-7.46	-0.93	-38.66
8.0	0.43	0.65	-23.89 (-23.77)	-2.84	-0.23	-25.88
10.0	0.00	0.00	-9.80 (-9.79)	-0.54	0.01	-10.33

cerned, this can be understood since the hexadecapole and higher permanent moments of H₂ are relatively small [21]. What is surprising, however, is the absence of short range effects, while short range forces become non-negligible at around 7.0 bohr, which can also be seen from the fact that the dispersion terms fail to have an R⁻⁷ dependence for distances shorter than 7.0 bohr. The (2,0)-dispersion even changes sign in that region.

Regarding a comparison with the results of Poll and Hunt [14] obtained from an interpretation of the experimental spectrum, we note that one can write:

$$\mu_{//} = A_{01} - \sqrt{2} A_{21} + \sqrt{3} A_{23}$$

$$\mu_{\perp} = A_{01} + \frac{1}{2} \sqrt{2} A_{21} - \frac{1}{2} \sqrt{3} A_{23}$$

Here the A-values are the ones defined by Poll and Hunt in their parametrization of the dipole moment of an atom-diatom system; $\mu_{//}$ stands for the dipole moment of the linear complex and μ_{\perp} for the dipole moment of the T shaped complex. Clearly, for the isotropic part A_{01} of the dipole moment one has

$$A_{01} \approx \frac{1}{3}(\mu_{\parallel} + 2\mu_{\perp})$$

Since A_{01} has a short range component, as well as a long range component due to dispersion, the following parametrized form for A_{01} is physically reasonable:

$$A_{01} = C \exp[-R/\rho] + DR^{-7}$$

The dispersion part is obtained by fitting $\frac{1}{3}(\mu_{\parallel} + 2\mu_{\perp})$ at large distances (7 to 10 bohr) to the form DR^{-7} , which goes quite well. The short range contribution is obtained by fitting the same expression at short distances, (4.0 to 5.6 bohr) after the dispersion part is subtracted. We then find a good exponential behaviour. In this manner the following values are resulting: $C = 38.8$ a.u., $\rho = 0.58$ bohr, $D = -61.8$ a.u. (The exchange dipole alone yields $\rho = 0.61$ bohr). The value of ρ is in reasonable agreement with the value $\rho = 0.624$ bohr quoted by Poll and Hunt [14]; more detailed fits including variations in the rotational and vibrational coordinates of H_2 are presented in a forthcoming paper.

The parameter A_{23} is mainly due to induction. From the formula derived in the appendix we get:

$$A_{23} = \sqrt{3} \alpha_0^{\text{He}} \langle Q_2^{\text{H}_2} \rangle R^{-4}$$

As we have seen earlier, one gets essentially the same result for the He induction dipole whether we apply this formula or fit the VB He induction results at large distances, both methods give $A_{23} = 1.14/R^4$. Using the accurately computed values of ref. [22] and ref. [23] for α_0^{He} and $\langle Q_2^{\text{H}_2} \rangle$, respectively, one gets $A_{23} = 1.16/R^4$.

Comparing the different contributions to the collision induced dipole, as given in tables III and IV, one finds as the most important conclusion of this paper that a very good description of the collision induced dipole moment is obtained by including exchange, H_2 -overlap induction and, as the only long range effect, the quadrupole induction dipole on the He-atom. The two different short range effects have practically the same, exponential, distance dependence.

When looking at heavier rare gas systems one must keep in mind that the polarizability of the He-atom is extraordinary small. Therefore, one can expect for heavier rare gases the long range effects

to be more important, but also the exchange and penetration to start at larger distances. In any case, it is clear from our results that the effects of short range forces on the collision induced spectra cannot be neglected.

Acknowledgement

We express our thanks to Prof. J.D. Poll for suggesting this problem and for valuable discussions.

APPENDIX

In this appendix the matrix element $\langle 00 | \mu^{\rightarrow(1,0)} | 00 \rangle$ is expressed in a series in $1/R$. No assumption is made regarding the symmetries of the subsystems, the only condition is that they are neutral. Specializing the resulting expression to an atom-diatom system it becomes the well-known classical formula describing an isotropic polarizable charge in the field of permanent multipoles.

We will follow Fano and Racah's notation [24] in writing a Clebsch-Gordan series as an irreducible tensorial product, denoted by square brackets. The spherical harmonics $C_{\ell m}(\hat{r})$ used below have the phase of Condon and Shortley and are normalized to $4\pi/(2\ell+1)$.

We evaluate

$$\langle 00 | \mu^{\rightarrow(1,0)} | 00 \rangle = \langle 00 | (\mu^{\rightarrow A} + \mu^{\rightarrow B}) R_0 V + V R_0 (\mu^{\rightarrow A} + \mu^{\rightarrow B}) | 00 \rangle$$

First the term $\langle 00 | \mu^{\rightarrow B} R_0 V | 00 \rangle$ is considered, the other terms follow then by analogy. Because the monomer B is neutral, we may measure $\mu^{\rightarrow B}$ from any origin; we choose the center of mass of B.

Expanding R_0 , and inserting the multipole expansion for V [17] we get:

$$\begin{aligned} \langle 00 | \mu_{\nu}^{\rightarrow B} R_0 V | 00 \rangle &= \sum_{\ell_a, \ell_b=0}^{\infty} (-1)^{\ell_a} \begin{pmatrix} 2L \\ 2\ell_a \end{pmatrix}^{\frac{1}{2}} (2L+1)^{\frac{1}{2}} R^{-L-1} \sum_b \Delta E_{ob}^{-1} \\ &\times [\langle 0 | \mu_B^{\rightarrow} | b \rangle \times [\vec{C}_L(\hat{R}) \times \langle 0 | \vec{Q}_{\ell_a}^{\rightarrow A} | 0 \rangle \times \langle b | \vec{Q}_{\ell_b}^{\rightarrow B} | 0 \rangle]^{(L)}]^{(0)}_{\nu} \end{aligned} \quad (1)$$

Here: $\mu_{\nu}^{\rightarrow B}$ is the ν -th spherical component of $\mu^{\rightarrow B}$

$$L = \ell_a + \ell_b$$

$R = (R, \hat{R})$ is the vector pointing from the center of mass of A

to the center of mass of B

$$Q_{\ell_a m_a}^A = \sum_{\alpha \in A} q_{\alpha} r_{\alpha}^{\ell_a} C_{\ell_a, m_a}(\hat{r}_{\alpha}) \quad (\text{a summation over the charges } q_{\alpha} \text{ belonging to molecule A and having position vectors } \vec{r}_{\alpha} = (r_{\alpha}, \hat{r}_{\alpha})).$$

$$Q_{\ell_b m_b}^B \quad \text{as for A}$$

Instead of the irreducible product arising in this expression we would rather have the following one:

$$\left[\langle 0 | \vec{\mu}^B | b \rangle \times \langle b | \vec{Q}_{\ell_b}^B | 0 \rangle \right]^{L_b} \times \langle 0 | \vec{Q}_{\ell_a}^A | 0 \rangle^{(\lambda)} \times \vec{C}_L(\hat{R})^{(1)} \quad (2)$$

because here the irreducible tensors on B are coupled first, and hence we may be able to substitute the dipole/ ℓ_b -pole polarizability of B. Furthermore, this irreducible product gives the simplest possible behaviour under rotation of the monomers.

One readily derives that the required recoupling coefficient is $\left[(2\lambda+1)(2L_b+1)(2L+1) \right]^{\frac{1}{2}} \times G$, where G is the graph given in fig. 1. This graph breaks on three lines [25], and so we get for the recoupling coefficient:

$$\left[(2\lambda+1)(2L_b+1)(2L+1) \right]^{\frac{1}{2}} (-1)^{\lambda+1+L} \begin{Bmatrix} \lambda & L & 1 \\ 0 & 1 & L \end{Bmatrix} \begin{Bmatrix} \ell_a & \lambda & L_b \\ 1 & \ell_b & L \end{Bmatrix} =$$

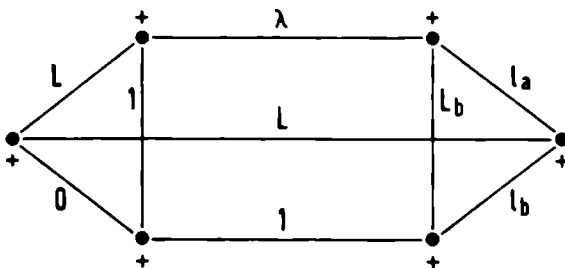


Fig. 1. Graph G representing the recoupling coefficient referred to in the appendix.

$$= \left[\frac{(2\lambda+1)(2L_b+1)}{3} \right]^{\frac{1}{2}} \left\{ \begin{matrix} \lambda_a & \lambda & L_b \\ 1 & \ell_b & L \end{matrix} \right\} \quad (3)$$

where the expressions between curly brackets are the usual Wigner 6j-symbols.

Define the irreducible ℓ_b -pole/ ℓ'_b -pole polarizability of B by:

$$\alpha_{(\ell_b, \ell'_b) L_b}^{\rightarrow B} = \sum_b' \frac{[\langle 0 | \vec{Q}_{\ell_b}^B | b \rangle \times \langle b | \vec{Q}_{\ell'_b}^B | 0 \rangle]}{E_0^B - E_b^B} (L_b) \quad (4)$$

Then:

$$\begin{aligned} \langle 00 | \mu_{\nu}^B R_0 V + V R_0 \mu_{\nu}^B | 00 \rangle &= \frac{1}{\sqrt{3}} \sum_{\lambda_a, \ell_b=0}^{\infty} (-1)^{\lambda_a} \left(\frac{2L_a}{2\ell_a} \right)^{\frac{1}{2}} R^{-L-1} \\ &\times \sum_{\lambda, L_b} [(2\lambda+1)(2L_b+1)(2L+1)]^{\frac{1}{2}} \\ &\times \left\{ \begin{matrix} \lambda_a & \lambda & L_b \\ 2 & \ell_b & L \end{matrix} \right\} (T_{\nu} + (-1)^{\nu} T_{-\nu}^*) \quad (5) \end{aligned}$$

where:

$$T_{\nu} \equiv \left[[\alpha_{(1, \ell_b) L_b}^{\rightarrow B} \times \langle 0 | \vec{Q}_{\ell_a}^A | 0 \rangle]^{(\lambda)} \times \vec{C}_L(\hat{R}) \right]_{\nu}^{(1)}$$

and further one easily shows:

$$(-1)^{\nu} T_{-\nu}^* = (-1)^{-L_b + \ell_b + 1} \left[[\alpha_{(\ell_b, 1) L_b}^{\rightarrow B} \times \langle 0 | \vec{Q}_{\ell_a}^A | 0 \rangle]^{(\lambda)} \times C_L(\hat{R}) \right]_{\nu}^{(1)}$$

To our knowledge this formula for the dipole moment induced on a molecule of arbitrary symmetry by another molecule, also of arbitrary symmetry, has not been given before. The vector T_{ν} has the following physical interpretation: a permanent moment $\langle 0 | \vec{Q}_{\ell_a}^A | 0 \rangle$ on A induces an irreducible tensor of order L_b on B via the dipole/ ℓ_b -pole polarizability of B. These two monomer tensors couple to give a dimer tensor of order λ , which in turn couples with the geometrical tensor $\vec{C}_L(\hat{R})$ to the ν -component of the vector \vec{T} .

If B is an atom (in a state $|\gamma_0 L_0 M_0\rangle$) the polarizability tensor (4) is a scalar:

$$\begin{aligned} \alpha_{(\ell_b, \ell'_b) L_b}^B &= \delta_{\ell_b \ell'_b} \delta_{L_b, 0} (2\ell_b+1)^{-\frac{1}{2}} \sum_{\gamma_1 L_1} (-1)^{L_0+L_1-\ell_b} \{L_0, L_1, \ell_b\} \\ &\times \frac{\langle \gamma_0 L_0 || Q_{\ell_b} || \gamma_1 L_1 \rangle \langle \gamma_1 L_1 || Q_{\ell_b} || \gamma_0 L_0 \rangle}{E_{\gamma_0 L_0} - E_{\gamma_1 L_1}} \quad (6) \end{aligned}$$

where $\{L_0, L_1, l_b\}$ is the triangular delta, and the double barred matrix elements are the usual reduced matrix elements introduced by applying the Wigner-Eckart theorem.

In the case of $l_b=1$ the above definition for the dipole/dipole polarizability of an atom differs by a factor $\frac{1}{3}\sqrt{3}$ from the more usual definition:

$$\alpha_{(1,1)0}^B = \frac{1}{3}\sqrt{3} \alpha_0^B, \text{ where } \alpha_0^B \equiv \frac{2}{3} \sum_b \sum_l \frac{\langle 0 | r_1 | b \rangle \langle b | r_1 | 0 \rangle}{E_b^B - E_0^B}, \text{ } r_1 = x, y, z.$$

If A is a linear molecule in a Σ -state, one easily proves:

$$\langle 0 | Q_{l_a m_a}^A | 0 \rangle = C_{l_a m_a}(\hat{R}_A) \langle Q_{l_a}^A \rangle,$$

where \hat{R}_A is the unit vector that specifies the orientation of A, and $\langle Q_{l_a}^A \rangle$ is the component of the l_a -pole along the molecular axis. If A is a homonuclear diatomic, only even l_a -values occur. One finally arrives at:

$$\begin{aligned} \langle 00 | \mu_V^{\text{He}} R_0 V + V R_0 \mu_V^{\text{He}} | 00 \rangle &= \frac{1}{\sqrt{3}} \sum_{l_a} [(l_a+1)(2l_a+1)(2l_a+3)]^{\frac{1}{2}} \\ &\times R_a^{-l_a-2} \alpha_0^{\text{He}} \langle Q_{l_a}^{\text{H}_2} \rangle [\vec{C}_{l_a}(\hat{R}_{\text{H}_2}) \times \vec{C}_{l_a+1}(\hat{R})]_V^{(1)} \end{aligned} \quad (7)$$

Note that this formula has been derived without using the gradient formula, as is usually done [8,9].

References

1. J. van Kranendonk, *Physica* 73, 156 (1974).
2. H.L. Welsh, M.T.P. *International Review of Science, Physical Chemistry Series I*, Volume 3, p. 33 (1972).
3. N.H. Rich, A.R.W. McKellar, *Canad. J. Phys.* 54, 486 (1976).
4. J. van Kranendonk, *Physica* 23, 825 (1957).
5. J.D. Poll, J. van Kranendonk, *Canad. J. Phys.* 39, 189 (1961).
6. J. van Kranendonk, *Physica* 24, 347 (1958).
7. I. Ozier, K. Fox, *J. Chem. Phys.* 52, 1416 (1970).
8. C.G. Gray, *J. Phys. B* 4, 1661 (1971).
9. E.R. Cohen, *Canad. J. Phys.* 54, 475 (1976).
10. W. Byers Brown, D.M. Whisnant, *Molec. Phys.* 25, 1385 (1973).
11. D.M. Whisnant, W. Byers Brown, *Molec. Phys.* 26, 1105 (1973).

12. R.L. Matcha, R.K. Nesbet, Phys. Rev. 160, 72 (1967).
13. A.J. Lacey, W. Byers Brown, Molec. Phys. 27, 1013 (1974).
14. J.D. Poll, J.L. Hunt, Canad. J. Phys. 54, 461 (1976).
15. P.J.M. Geurts, P.E.S. Wormer, A. van der Avoird, Chem. Phys. Letters 35, 444 (1975).
16. P.E.S. Wormer, A. van der Avoird, J. Chem. Phys. 62, 3326 (1975).
17. P.E.S. Wormer, Intermolecular Forces and the Group Theory of Many-Body Systems, Nijmegen, 1975, thesis.
18. J.O. Hirschfelder, W.J. Meath, Adv. Chem. Phys. 12, 3 (1967).
19. A. Messiah, Quantum Mechanics, Volume II, North Holland, Amsterdam (1965).
20. P.E.S. Wormer, T. van Berkel, A. van der Avoird, Molec. Phys. 29, 1181 (1975).
21. F. Mulder, A. van der Avoird, P.E.S. Wormer, Molec. Phys. 37, 159 (1979).
22. W. Meyer, Chem. Phys. 17, 27 (1976) ($\alpha_0^{\text{He}} = 1.380$ a.u.).
23. W. Kolos, L. Wolniewicz, J. Chem. Phys. 43, 2429 (1965). ($\langle Q_2^{\text{H}_2} \rangle = 0.484$ a.u., ground state vibrational average).
24. U. Fano and G. Racah, Irreducible Tensorial Sets, Academic Press, New York, 1959.
25. E. El Baz and B. Castel, Graphical Methods of Spin Algebras, Marcel Dekker, Inc., New York, 1972.

C H A P T E R V I I I

MACINTOS: THE MANY ATOM CONFIGURATION
INTERACTION PROGRAM FOR ORTHOGONAL SPIN ORBITALS

1. Introduction

One of the methods used in the study of electronic correlation effects is the Configuration Interaction (CI) method [1]. In the CI method the wavefunction is written as a linear combination of predefined (spin adapted) configuration functions and the variational solutions of the Schrödinger equation are obtained by diagonalization of the H-matrix. The possible number of configuration functions increases very rapidly with the number of electrons and orbitals; in practice this means that one very soon runs out of computer storage and execution times become excessively long if no special programming techniques are used.

The program MACINTOS is especially designed for performing large scale CI calculations. The program belongs to the class of conventional CI programs and is based on the concept of a formula tape [1]. It takes a list of configuration with an arbitrary spin value as input, and interprets them as bonded functions [2]. This flexibility in input makes the program slower than, for example, direct CI programs [3], where certain classes of configurations are treated simultaneously.

The advantage of bonded functions over other spinfunctions is that the number of different spin symmetry coefficients is limited to a few and all are powers of two. This keeps the formula tape short. The price one pays, however, is the non-orthogonality of different bonded functions with the same spatial occupancies.

The first version of the program was written in 1972 and the old as well as the new program are essentially based on Reeves' algorithm [2] for H-matrix elements between bonded functions. This algorithm as well as the Yoshimine algorithm [4] for sorting two-electron spin symmetry coefficients stored on the formula tape, have been considerably improved.

The program has the following limits:

- 1) number of orbitals: 107
- 2) number of configurations: 32767
- 3) number of open-shell singlet pairs: 62

In most cases, the capacity of the hardware, not these, will be the real limit. The only input needed for the program is, besides a list of configurations, a list of molecular integrals (ATMOL-format [5]). For a number of cases it is possible to let the program generate this list of configurations, with or without the use of Abelian spatial

symmetry.

The program was developed on and designed for an IBM 370/158 computer and written in standard FORTRAN IV. The program is machine independent except for a few parts, such as the packing of indices, where machine dependent algorithms have been used. Furthermore there are numerous routines in assembly language which provide system facilities not accessible from FORTRAN, such as dynamic core allocation, obtaining date and time, checking allocated datasets, etc. The program consists of a number of independent sections, which can be executed separately and correspond to phases in the solution of the generalized eigenvalue problem. We will first give a brief description of the theory and next describe the various sections.

2. Theory

We give here only a brief description of the theory involved (for more details see Ref. 1).

We are interested in solutions of the Schrödinger equation

$$H\psi = E\psi \quad (1)$$

where H is given by

$$H = \sum_{\mu} h_{\mu} + \sum_{\mu < \nu} g_{\mu\nu} \quad (2)$$

where h and g are one- and two electron operators respectively.

The method we use for the solution of eq. 1 is based on the variation principle, which states that the energy functional

$$E[\psi] = \frac{\langle \psi | H | \psi \rangle}{\langle \psi | \psi \rangle} \quad (3)$$

is stationary with respect to all variations in the function ψ if and only if ψ coincides with the exact eigenfunction of H.

In our case we approximate ψ by a linear combination of predetermined functions ϕ_s , so

$$\psi \approx \sum_s C_s \phi_s \quad (4)$$

and substitution of eq. 4 into eq. 3 gives the well known secular equa-

tion or generalized eigenvalue problem:

$$\underline{H} \underline{c} = E \underline{S} \underline{c} \quad (5)$$

$$\text{where } H_{IJ} = \langle \phi_I | H | \phi_J \rangle \quad (6)$$

$$S_{IJ} = \langle \phi_I | \phi_J \rangle \quad (7)$$

This can be transformed to the standard eigenvalue problem by using the unitary transformation matrix \underline{U} , which diagonalizes \underline{S} :

$$\underline{U}^\dagger \underline{S} \underline{U} = 1 \quad (8)$$

The eigenvalue problem becomes then:

$$\underline{H}' \underline{c}' = E \underline{c}' \quad (9)$$

where

$$\underline{H}' = \underline{U}^\dagger \underline{H} \underline{U} \text{ and} \quad (10)$$

$$\underline{c}' = \underline{U}^\dagger \underline{c} \quad (11)$$

We will take the functions ϕ_s equal to spin bonded functions, which implies that we have to evaluate H-matrix elements between bonded functions [1]. In general the matrix elements can be written as:

$$H_{IJ} = G_{IJ} \left\{ \sum_{i \leq j} h_{ij}^{IJ} \langle i|h|j \rangle + \sum'_{i,j,k,l} g_{ijkl}^{IJ} \langle ik|g|jl \rangle \right\} \quad (12)$$

where the prime denotes a summation over canonically ordered indices only.

After the secular equation (5) has been solved properties can be calculated. This can be very easily done, in the case of one-electron properties, by using the first order density matrix or natural orbitals. The first order density matrix is defined as

$$\rho_{ij} = \sum_{PQ} c_P^* c_Q G_{PQ} h_{ij}^{PQ} (2 - \delta_{ij})^{-1}, \quad (13)$$

where c_P, c_Q are the expansion coefficients defined in eq. 4. Natural

orbitals are the eigenvectors of the matrix $\underline{\rho}$. Molecular one-electron properties can now given by

$$\langle \psi | Q | \psi \rangle = \sum_{i \leq j} \rho_{ij} \langle i | Q | j \rangle = \sum_{\nu} n_{\nu} \langle \nu | Q | \nu \rangle \quad (14)$$

where ν indicates natural orbitals with eigenvalues (occupation numbers) n_{ν} .

3. Generation of a list of configurations

To start a CI calculation it is necessary to have a list of configurations. This list can optionally be generated by a section of the program, which is able to produce the following classes of configurations: full valence space, full valence space with all single excitations and full valence space with all single and double excitations. For this purpose the orbitals are divided in three classes:

- a) frozen: always doubly occupied.
- b) valence: from these orbitals the full CI valence space is built.
- c) virtual: excitations from the valence space are made to this class of orbitals.

The number of configurations is of course dependent on the number of orbitals and electrons in each class and the total spin value.

The generator can use spatial symmetry, but the corresponding group has only one-dimensional real representations (the largest such group being D_{2h}).

The generator is based on the distinct row table, which is used in unitary group theory [3]. The distinct row table is generated for the input values, number of electrons, orbitals and spin, and then traced for all paths. Each path has a one-to-one correspondence to a bonded function. The spatial symmetry is used when a bonded function is generated.

4. Reordering the list of configurations

This step is necessary because during the actual calculation of the matrix elements in the next section it is assumed that bonded functions with the same spatial occupancy are adjacent and furthermore it makes the whole CI calculation much more efficient. As a result, the transformation matrix in eq. 8 becomes block diagonal, which means

that the transformation of the H-matrix (eq. 10) can be done very efficiently.

The reordering is done by constructing a binary tree, which next is traversed in postorder [6]. For this purpose the representation of the configuration is changed to orbital occupancies. The resulting order of the configurations is according to increasing weight (orbital occupancy).

5. Generation of spin symmetry coefficients

This section is concerned with the calculation of the spin symmetry coefficients G_{IJ} , h_{ij}^{IJ} and g_{ijkl}^{IJ} appearing in eq. 12. See for the theoretical background of the method Ref. [7] and [8]. A recent rederivation of the formulae by the use of Jucys diagrams has been given in Ref. [9].

The section is based on Reeves' algorithm [2] for matrix elements between bonded functions (eq. 12). The algorithm, dating from 1966, has been improved in several aspects:

- 1) The determination of the number of non-coincidences (= NONCO) between bra and ket is done only once for each block of H-matrix elements (all involving the same pair of orbital products in bra and ket). The time for determining NONCO and for the pairing of orbitals in bra and ket is linear in the number of electrons, rather than quadratic, as it was in the original algorithm. This has been achieved by representing a bonded function as an ordered orbital product and a permutation defined such that it returns the bonded function when acting on the orbital product.
- 2) The construction of the Pauling superposition pattern (Rumer diagram) has been separated into two consecutive steps. First the odd and even chains are determined by starting traces at the unpaired electrons. If no even chains are present one has to scan through the unpaired electrons only once; if even chains (which come in pairs) are present this is done twice. Then the cycles are determined by scanning with steps of two (rather than one) through the paired electrons.
- 3) during the pattern construction the positions of mismatching orbitals are recorded. This makes it unnecessary to move the non-coincidences to the end of the list of the orbitals.
- 4) The coefficients g_{ijkl}^{IJ} multiplying a two electron integral has the

form:

$$t \times u \times C$$

where the quantities t and u are occupation numbers $0 < t, u < 2$ and C is a coefficient that can take on seven values $(\pm 2, \pm 1, \pm \frac{1}{2}, 0)$.

- 5) The quantity $G_{I,J}$ depends only on the index of bra and ket (not on any integral index) and is given by:

$$G_{I,J} = \pm(\sqrt{2})^{\pm g_{I,J}}$$

where $g_{I,J}$ is an integer.

We store on a separate file the exponent $g_{I,J}$ together with the two signs, all packed in one byte. This g -file has the same block structure as the H -matrix file (only $\text{NONCO} \leq 2$ blocks are stored together with the block index). The "jk-coefficients" $t \times u \times C$ are stored rowwise together with the pertinent integral index and the H -matrix column index; this takes six bytes per coefficient. Row indices are superfluous since diagonal H -matrix elements are non zero, and hence an end-of-row mark is all that is needed. The coefficient h_{ij}^{IJ} multiplying an one electron integral can take only three values (0, 1 and 2). The coefficient h_{ij}^{IJ} is packed in four bytes together with the integral index and the H -matrix column index. Again only an end-of-row mark is needed to indicate the row index.

6. Generation of orthogonalization matrix

This section is concerned with the calculation of the matrix \underline{U} defined in eq. 8, needed for the solution of the generalized eigenvalue problem.

The method used is a Löwdin-orthonormalization. The S -matrix is constructed and has block diagonal form, so each block can be treated separately. For each block the $\underline{S}^{-\frac{1}{2}}$ matrix is constructed, which has the advantage of being symmetric.

7. Sorting of two-electron spin symmetry coefficients

Generation of the two-electron spin symmetry coefficients g_{ijkl}^{IJ} by Reeves' algorithm was outlined in section 5. The coefficients

depend on both the configuration and molecular integral indices. They are generated such that the configuration indices I and J are ordered canonically, but the integral indices i,j,k and l are not in the canonical order. As long as all two-electron integrals fit in main storage this would cause no problems. However, with large basis sets this is no longer possible. In most cases it is possible to have only a fraction of the integrals in storage and all references to integrals not in storage can not be resolved. This is why the two-electron coefficients need to be reordered. The sorting is done using an idea of Yoshimine [4] but with a modified method of tracing the records containing the coefficients. In the original Yoshimine algorithm back chaining on indices stored on disc is performed, which makes it later necessary to construct the two-electron part of the H-matrix backwards. In the new algorithm, however, an array is reserved for storing record indices in such a way that it is possible to trace forward through the file. The two-electron part of the H-matrix can be constructed in the same way as the one-electron part. The main advantage of this is that bases truncated from above can easily be dealt with, without having to construct a new formula tape for each truncation.

8. Construction of H-matrix

In this section the H-matrix (or rather only the lower triangle) is constructed out of the spin symmetry coefficients from section 5 and the molecular integrals. The H-matrix is usually a rather sparse matrix (only 10% non zero elements) and it is efficient to use this structure during storage of the matrix. The H-matrix has to be built in steps. Namely, the molecular integral file is segmented in loads such that each load fits in core. In the i-th step all the integrals of the i-th load are multiplied by the pertinent spin symmetry coefficients and added to the two-electron part of the H-matrix. The modified Yoshimine sort of the formula tape ensures that a coefficient g_{ijkl}^{IJ} and its corresponding integral (ij|kl) are simultaneously in core. Furthermore the processing of the H-matrix in each step is in canonical order in I and J, i.e. $I \geq J = 1, \dots, NCONF$. Hence the lower triangle of the H-matrix is constructed rowwise. The one-electron part is then added to the two-electron part, finally the matrix elements are multiplied by the coefficient G_{IJ} , according to formula 12.

9. Orthogonalization of H-matrix

This is the first phase of the solution of the generalized eigenvalue problem. The H-matrix constructed as in section 8 is transformed using the transformation matrix described in section 6 and formula 10.

The transformation matrix has block diagonal form and the H-matrix has many blocks of zero matrix elements. The transformation uses information about the block structure, in order to avoid multiplications with blocks containing zeros.

10. Diagonalization of H-matrix

This is the second step in the solution of the eigenvalue problem. The program has two different diagonalization routines available. The first routine is a standard full storage diagonalization. The routine calculates all eigenvalues and eigenvectors of a symmetric matrix. The matrix is first reduced to tridiagonal form by a sequence of Householder transformations [10] and the eigenvalues and eigenvectors found by the QR method [10]. Finally the eigenvectors of the original matrix are obtained by transforming the vectors, which yielded the tridiagonal form.

The second routine is specially written for obtaining the lowest eigenvalue and eigenvectors of large matrices, which do not fit in storage. The eigenvalues and eigenvectors are calculated iteratively using the method of optimized relaxations (MOR) [11] with successive over-relaxation [12]. The relaxation is applied simultaneously to the several trial vectors. Each iteration is followed by the diagonalization of the iteration matrix [13] in order to improve the separation of the eigenvector components in the trial vectors.

11. Back transformation of eigenvectors to original basis

This is the last phase of the solution of the secular equation. The eigenvectors from section 10 are transformed according to eq. 11 by using the transformation matrix described in section 6.

12. Construction of the first order density matrix and natural orbitals

From the eigenvector of section 11 the density matrix is constructed using the one-electron spin coefficients, described in section 5, according to formula 13. The natural orbitals are obtained by diagonalizing the density matrix.

13. Calculation of energy contributions

This section is concerned with configuration selection. Configuration selection is often necessary because as the number of basis functions is increased, there comes a point where the number of (spin-adapted) configuration functions becomes too large to be handled as one secular problem. Here one method of shortening the CI expansion of the wavefunction is described briefly. First a reference space is defined, which contains the most important configurations. Next all remaining configurations are investigated separately, by adding each configuration to the reference space and computing the lowest eigenvalue in the extended reference space. If the addition of a configuration lowers the energy by more than a certain threshold, that configuration is selected. After a complete scan of the configuration space a CI calculation on basis of the selected configurations is performed. The eigenvalue is calculated, in the extended reference space, by the use of a formula derived by partitioning [14] of the H-matrix. This formula is more efficient than performing a diagonalization for the extended reference space. For this purpose a preliminary CI calculation on the basis of the reference space is performed and all eigenvalues and eigenvectors are saved. For every configuration the following equation has to be solved:

$$H_{aa} + \sum_{\lambda} \frac{Y_{\lambda} Y_{\lambda}^*}{\epsilon - \epsilon_{\lambda}} - \epsilon = 0$$

where $Y_{\lambda} = \sum_i H_{ai} c_{i\lambda}$,

$\epsilon_{\lambda}, c_{i\lambda}$ are the eigenvalues and eigenvectors, respectively of the reference space. H_{aa} is the diagonal H-matrix element of the added configuration, H_{ai} is the matrix element between the added configuration and the i^{th} configuration in the reference space. This equation is solved using the Newton-Raphson [15] scheme. In order to obtain conver-

gence, it is important to choose a proper starting value for ϵ . It is easy to prove that for

$$\epsilon_0 - \frac{2Y_0^2}{H_{aa} - \epsilon_0} < \epsilon < \epsilon_0,$$

the process converges towards the lowest eigenvalue ϵ .

14. Example

Some characteristics of a typical large-scale CI calculation are given as an example. This calculation was performed in order to obtain the dipole polarizability of CN^- [16]. The configuration space used has the dimension 17748. It consists of a full CI basis within valence orbitals (dim. 230) and all single excitations from the valence orbitals to the virtual orbitals. The total CI basis is generated by the use of the configuration generation subprogram, with the following specifications:

- number of electrons : 14
- number of frozen orbitals : 3
- number of valence orbitals: 7
- number of virtual orbitals: 44
- spin : singlet
- spatial symmetry group : C_S
- symmetry of configurations: A_1

Run statistics

CPU Time (in minutes on
IBM 370/158)

- | | |
|--|----------------|
| 1) Generation of spin symmetry coefficients: | 432 |
| number of $G_{I,J}$ coefficients | : 15, 157, 731 |
| number of $h_{i,j}^{I,J}$ coefficients | : 1, 408, 645 |
| number of S-matrix coefficients: | 34, 516 |
| number of $g_{i,j,k,l}^{I,J}$ coefficients: | 48, 829, 649 |
| 2) Sorting of spin symmetry coefficients: | 80 |
| 3) Construction of H-matrix: | 57 |
| (3 integral loads) | |

4) Orthogonalization of H-matrix:	44
5) Diagonalization of H-matrix:	195
start vector: eigenvector of valence space extended with zero's only lowest eigenvalue and eigenvector are calculated, with an iteration thres- hold of 10^{-6} on the vector time per iteration	15
6) Backtransformation of lowest eigenvector, construction of density matrix and calculation of natural orbitals:	3

Total CPU time is 811 minutes. However, for calculations with the same configuration space, such as geometry optimizations or finite field calculations, 299 minutes are necessary, because the same sorted spin symmetry coefficients can be used.

References

1. I. Shavitt in *Methods of Electronic Structure Theory*, edited by H.F. Schaefer III, *Modern Theoretical Chemistry, Volume 3* (Plenum Press, New York, 1977).
2. C.M. Reeves, *Comm. of the ACM*, 9, 276 (1966).
3. *The Unitary Group, Lectures Notes in Chemistry*, 22, editor J. Hinze, (Springer, Berlin, 1981).
4. M. Yoshimine, *IBM Report, RJ 555 (No. 1, 1634)*, 1969.
5. V.R. Saunders, *ATMOL3 4-index transformation program*, Daresbury Research Laboratory, Warrington, United Kingdom.
6. D. Knuth, *The Art of Computer Programming*, vol. 1-3, (Addison-Wesley, London, 1969).
7. I.L. Cooper and R. McWeeney, *J. Chem. Phys.* 45, 226 (1966).
8. B.T. Sutcliffe, *J. Chem. Phys.* 45, 235 (1966).
9. P.E.S. Wormer and J. Paldus, *Int. J. Quantum Chem.* 18, 841 (1980).
10. J. Stoer and R. Bulirsch, *Einführung in die Numerische Mathematik*, (Springer, Berlin, 1973), vol. II.
11. I. Shavitt, C.F. Bender, A. Pipano and R.P. Hosteny, *J. Comput. Phys.* 11, 90 (1973).
S. Falk, *Z. Angew. Math. Mech.* 53, 73 (1973).
12. R.M. Nisbet, *J. Comput. Phys.* 10, 614 (1972);
A. Ruhe, *Math. Comp.* 28, 695 (1974);
H.R. Schwarz, *Comp. Meth. Appl. Mech. Eng.* 3, 11 (1974).

13. M. Clint and A. Jennings, *Comput. J.* 13, 76 (1970);
R.C. Raffenetti, *J. Comput. Phys.* 32, 403 (1979);
I. Shavitt, unpublished.
14. E.U. Condon and G.H. Shortley, *The Theory of Atomic Spectra*,
(University Press, Cambridge, 1959 section 11²).
15. J. Stoer, *Einführung in die Numerische Mathematik*,
(Springer, Berlin, 1972). vol. I.
16. R.M. Berns and P.E.S. Wormer, to be published.

Finite Field Configuration Interaction Calculations on the Distance
Dependence of the Hyperpolarizabilities of H₂[†]

Rut M. Berns and Paul E.S. Wormer
Institute of Theoretical Chemistry
University of Nijmegen
Toernooiveld
6525 ED Nijmegen
The Netherlands

Abstract

We present the results of finite field full CI calculations of the first three non-vanishing (hyper)polarizabilities of the hydrogen molecule: the dipole-field α_{11} , the quadrupole-(field)² β_{211} and the dipole-(field)³ γ_{1111} polarizability. The internuclear distance is varied from 0.2 to 6.0 bohr. Correlation effects on the (hyper)polarizabilities and their derivatives are investigated.

[†]Supported in part by the Netherlands Foundation for Chemical Research (SON) with financial aid from the Netherlands Organization for the Advancement of Pure Research (ZWO).

1. Introduction

Electric hyperpolarizabilities are important for the understanding of non-linear optical phenomena [1]. However, measurements of the higher order polarizabilities are difficult, and little experimental information on these quantities currently exists. On the other hand, these properties are easily calculated by the common quantum chemical methods developed over the last two decennia. But, because experimental results are scarce, it is difficult to assess whether the ordinary quantum chemical methods such as LCAO-SCF [2] and CI (configuration interaction) [3] are reliable enough for these higher order electric properties.

Fortunately, in the case of H_2 very accurate computational results are available [4,5,6,7], which surpass in quality the existing experimental data. In one of the more recent ones of these publications [6] it is pointed out that the computed hyperpolarizabilities are extremely sensitive to the quality of the wavefunctions used. Since in that work explicitly correlated wavefunctions of the James-Coolidge type have been employed, it is not clear how this conclusion applies to an approach based on orbitals. Transferred to the LCAO-SCF-CI method, this conclusion may mean that correlation effects are predominant, that high quality atomic orbital basis sets are required, or even that both factors are equally important. Finding the cause of this sensitivity will enhance our experience necessary for gauging the quality of calculations on heavier molecules, where James-Coolidge type calculations are impossible, and orbital approaches are at present the only viable option.

In this paper we present higher order polarizabilities of H_2 obtained by means of the common LCAO-SCF-CI technique [2,3] and compare the results, where possible, with the high quality calculations of Ref.'s 4,5,6 and 7. Since the errors in our results are very small (the largest being 4.5%), we thought it worthwhile to calculate the full distance dependence of the components of the first three non-vanishing polarizability tensors. Only the distance dependence of the second order polarizability has been published before [4].

In order to define the quantities presented in this paper, we note that all calculations have been performed with the H_2 -molecule placed in a homogeneous electric field \vec{F} [8]. In that case a Taylor

expansion in the field yields the energy expression [9][†]:

$$\begin{aligned}
 E(\vec{F}) = E(\vec{0}) &- \sum_{m_1} Q_1^{m_1}(\vec{0}) F_{m_1} - \frac{1}{2!} \sum_{m_1 m_2} \alpha_{11}^{m_1 m_2} F_{m_1} F_{m_2} \\
 &- \frac{1}{3!} \sum_{\substack{m_1 m_2 \\ m_3}} \beta_{111}^{m_1 m_2 m_3} F_{m_1} F_{m_2} F_{m_3} \\
 &- \frac{1}{4!} \sum_{\substack{m_1 m_2 \\ m_3 m_4}} \gamma_{1111}^{m_1 m_2 m_3 m_4} F_{m_1} F_{m_2} F_{m_3} F_{m_4} + \dots
 \end{aligned} \tag{1}$$

and for the 2^ℓ -pole moment [9] the expression:

$$\begin{aligned}
 Q_\ell^m(\vec{F}) = Q_\ell^m(\vec{0}) &+ \sum_{m_1} \alpha_{\ell 1}^{m m_1} F_{m_1} + \frac{1}{2!} \sum_{m_1 m_2} \beta_{\ell 11}^{m m_1 m_2} F_{m_1} F_{m_2} \\
 &+ \frac{1}{3!} \sum_{\substack{m_1 m_2 \\ m_3}} \gamma_{\ell 111}^{m m_1 m_2 m_3} F_{m_1} F_{m_2} F_{m_3} + \dots
 \end{aligned} \tag{2}$$

Explicit formulae for the symmetrized polarizability tensors appearing in these equations have been derived by Gray and Lo [9], who have used Rayleigh-Schrödinger perturbation theory. We will deviate from these authors by using tesseral (real) harmonics rather than spherical (complex) harmonics, thus, for $\ell = 1$ the values 1, 0, -1 of m refer to x, z and y respectively.

[†] Atomic units are used throughout this paper:

$$1 \text{ a.u. of length (bohr)} = a_0 \approx 5.29177 \times 10^{-11} \text{ m.}$$

$$1 \text{ a.u. of energy} = E_H \approx 4.3598 \times 10^{-18} \text{ J} \approx 2.6255 \times 10^6 \text{ J/mol.}$$

$$1 \text{ a.u. of electric charge} = e \approx 1.60219 \times 10^{-19} \text{ C.}$$

$$1 \text{ a.u. of dipole moment} = ea_0 \approx 8.4784 \times 10^{-30} \text{ Cm.}$$

$$1 \text{ a.u. of quadrupole moment} = ea_0^2 \approx 4.48658 \times 10^{-41} \text{ Cm}^2.$$

$$1 \text{ a.u. of dipole polarizability} = 4\pi\epsilon_0 a_0^3 \approx 1.64878 \times 10^{-41} \text{ C}^2 \text{ m}^2 \text{ J}^{-1}.$$

$$1 \text{ a.u. of dipole hyperpolarizability} = (4\pi\epsilon_0)^3 a_0^7 / e^2 \approx 6.2353 \times 10^{-65} \text{ C}^4 \text{ m}^4 \text{ J}^{-3}.$$

$$1 \text{ a.u. of quadrupole hyperpolarizability} = (4\pi\epsilon_0)^2 a_0^6 / e \approx 1.6967 \times 10^{-63} \text{ C}^3 \text{ m}^4 \text{ J}^{-2}.$$

In the case of centrosymmetric molecules one has $\alpha_{\ell 1} = \gamma_{\ell 111} = 0$ for even ℓ , and $Q_{\ell}(\vec{0}) = \beta_{\ell 11} = 0$ for odd ℓ . So, the first three non-vanishing tensors for H_2 are α_{11} , β_{211} (the tensor $B_{\alpha\beta,\gamma\delta}$ in Buckingham's notation [10]) and γ_{1111} . These are the tensors presented in this paper.

Finally, we want to point out that in the derivation of Eq. (2) the Hellmann-Feynman theorem has been applied. Therefore, the tensors α_{11} and γ_{1111} obtained from (1) will be equal to those obtained from (2) so far as the Hellmann-Feynman theorem holds. This forms an extra test on the accuracy of the wavefunctions used.

2. Computations

All calculations have been performed with an AO-basis of Cartesian Gaussian-type orbitals. On each hydrogen atom the 10s basis of Ref. 11 has been placed, with the exponents scaled by a factor 1.2. The rather loose contraction (4,2,2,1,1) has been applied in order to have sufficient flexibility among the diffuse orbitals. On each atom four uncontracted p-orbitals were added, with exponents ranging from 2.0 to 0.068, and also two uncontracted d-orbitals with $\alpha_d = 1.69$ and $\alpha'_d = 0.06$. The compact p- and d-orbitals improve the ground state, whereas the more diffuse orbitals are necessary for a correct description of the hyperpolarizabilities [12]. The resulting 58-dimensional $H[5s,4p,2d]$ basis yields an SCF energy $3.3 \cdot 10^{-5}$ a.u. above the Hartree-Fock limit [13], at an interatomic distance (R) of 1.4 bohr. This basis has been used for all interatomic distances, no rescaling or recontraction has been performed.

The orthonormal orbitals, necessary for a configuration interaction (CI) calculation, have been provided for each value of R by an SCF calculation with field zero. As a full CI wavefunction is invariant under an orthogonal transformation of the orbitals, it is not necessary to use finite field SCF MO's. However, in order to study the electronic correlation effects we have performed finite field SCF calculations for several values of R.

The CI program used [14] is a conventional one, which is to say that it is based on a full formula tape and an explicitly calculated H-matrix. The formula tape is generated by an improved version of Reeves' algorithm [15], and sorted by Yoshimine's bucket sort [16]. The latter algorithm has been modified by keeping the chaining

indices in core, rather than storing them with the buckets. This enables forward chaining of the buckets, which in turn facilitates the construction of the H-matrix, because this matrix can now be constructed in increasing row order and stored directly onto tape. Furthermore, the CI basis can be truncated from above without recalculation of part of the formula tape.

The secular problem is solved by Shavitt's version [17] of the method of overrelaxation (M.O.R.). The integrals come from the ATMOL four-index transformation program [18]. The maximum number of spin-adapted configuration functions that can be handled is mainly a function of the available random access storage (disc), so far we have gone up to dimension 18000 [19].

In order to extract the (hyper)polarizability tensors from the computed energy, dipole and quadrupole values we have applied a homogeneous electric field \vec{F} in three different directions: parallel, perpendicular and under an angle of 45° to the bond. Using group theory [20,10] (cf. also the Appendix) one can show for $D_{\infty h}$ symmetry that α_{11} has two, β_{211} has four and γ_{1111} has three linearly independent components. We find from Eq.'s (1) and (2) the 13 different polynomials given in Table I, which after differentiation at $F = 0$ give rise to 20 linear equations, (see below). Hence we have 11 more equations than unknowns. This overcompleteness gives a check on the numerical stability of the results and the validity of the Hellman-Feynman theorem. In all cases the results proved to be consistent.

Initially we have tried to find the coefficients in the polynomials given in Table I by a least squares polynomial fitting procedure. However, the results appeared to be very sensitive to the interval of F used, especially the components of γ_{1111} were unstable. Therefore we decided to differentiate numerically the computed induction energies and induced moments. To that end we have written the required derivatives as 10 term expansions in powers of the central-difference operator [21]. Because the energy and quadrupole are symmetric and the dipole is antisymmetric under inversion of the field direction (cf. Table I), only ten function values have to be calculated.

A point of concern is the step size ΔF . A value of $\Delta F = 4 \cdot 10^{-3}$ a.u. proved to be optimal. Smaller values give effects too small to be numerically significant. Using larger values we experienced convergence problems in the M.O.R. diagonalization method, particularly for the largest F -values.

TABLE I

Explicit forms of the polynomials in the homogeneous field
 $\vec{F} = (F_1, F_0, F_{-1})$ considered in this work

$$\vec{F} = (0, F, 0):$$

$$-\Delta E = \frac{1}{2} \alpha_{11}^{00} F^2 + \frac{1}{24} \gamma_{1111}^{0000} F^4$$

$$\Delta Q_1^0 = \alpha_{11}^{00} F + \frac{1}{6} \gamma_{1111}^{0000} F^3$$

$$\Delta Q_2^0 = \frac{1}{2} \beta_{211}^{000} F^2$$

$$\vec{F} = (F, 0, 0):$$

$$-\Delta E = \frac{1}{2} \alpha_{11}^{11} F^2 + \frac{1}{24} \gamma_{1111}^{1111} F^4$$

$$\Delta Q_1^1 = \alpha_{11}^{11} F + \frac{1}{6} \gamma_{1111}^{1111} F^3$$

$$\Delta Q_2^0 = \frac{1}{2} \beta_{211}^{011} F^2$$

$$\Delta Q_2^2 = \frac{1}{2} \beta_{211}^{211} F^2$$

$$\vec{F} = (F, F, 0):$$

$$-\Delta E = \frac{1}{2} (\alpha_{11}^{00} + \alpha_{11}^{11}) F^2 + \frac{1}{24} (\gamma_{1111}^{0000} + \gamma_{1111}^{1111} + 6\gamma_{1111}^{1100}) F^4$$

$$\Delta Q_1^0 = \alpha_{11}^{00} F + \frac{1}{6} (\gamma_{1111}^{0000} + 3\gamma_{1111}^{1100}) F^3$$

$$\Delta Q_1^1 = \alpha_{11}^{11} F + \frac{1}{6} (\gamma_{1111}^{1111} + 3\gamma_{1111}^{1100}) F^3$$

$$\Delta Q_2^0 = \frac{1}{2} (\beta_{211}^{000} + \beta_{211}^{011}) F^2$$

$$\Delta Q_2^1 = \beta_{211}^{110} F^2$$

$$\Delta Q_2^2 = \frac{1}{2} \beta_{211}^{211} F^2$$

In total we have performed full CI calculations for 30 different field values and for 34 different interatomic distances ranging from $R = 0.2$ to 6.0 bohr. Clearly in a case as this a CI approach based on a formula tape offers great advantages. We had to prepare only three different formula tapes: one for the field parallel to the bond (in the Abelian subsymmetry C_{2v} the problem has dimension 631), one for the field perpendicular to the bond (dimension 534) and one for the field under an angle (dimension 1039).

In order to get sufficient significant digits in the final results we had to choose very low thresholds in all computational steps. This caused the M.O.R. diagonalization to become very slowly convergent: usually 25 to 30 cycles were needed, even though the starting vector was always a very good approximation to the final vector, as it came from the previous field strength. (One should realize, however, that the H-matrix is not sparse at all, since no matrix elements are zero, because of the presence of three or more mismatching orbitals in bra and ket).

In a conventional CI program, where the H-matrix is precalculated, the large number of cycles does not soon form a serious bottleneck, and indeed we were able to run all the calculations interactively (under VM/CMS on an IBM 4341).

3. Results and discussion

In order to establish to which extent the present calculations are reliable, we compare in Table II our results with the very accurate data derived from explicitly correlated James-Coolidge type wavefunctions [4,5,6,7], as far as they are available. We see a very good agreement, both for the interatomic distance close to the equilibrium, as well as for $R = 4.0$ bohr, where all (hyper)polarizability components are large.

In the presentation of the correlation effects and the distance dependence of the complete tensors α_{11} , β_{211} and γ_{1111} it is convenient to distinguish isotropic and anisotropic components. The latter are defined in such a way that they vanish in the case of spherical symmetry, that is, in the united and in the separated atom limit. The former, denoted by A_0 , B_0 and G_0 , respectively, are the only components arising for S-state atoms. The different components are defined in Table III, and in the Appendix the group theoretical

TABLE II

Comparison of quadrupole moment and (hyper)polarizabilities with accurate computational data. All quantities are expressed in a.u.

	R	This work) ^a	Literature	Dif. (%)
Q_2^0	1.4	0.45035	0.45646) ^b	1.3
Q_2^0	4.0	0.65789	0.69061) ^c	4.7
$A_0)^d$	1.4	5.1556	5.1813) ^e	0.5
$A_0)^d$	4.0	11.6284	11.6697) ^f	0.3
$A_2)^g$	1.4	1.8822	1.8080) ^e	3.9
$A_2)^g$	4.0	7.1711	7.1230) ^f	0.6
β_{211}^{000}	1.4	-90.8	-89.8) ^b	1.1
γ_{1111}^{0000}	1.4	686	674) ^b	1.7

)^a Full CI results

)^b Ref. 6

)^c Ref. 5

)^d $A_0 = \frac{1}{3}\alpha_{//} + \frac{2}{3}\alpha_{\perp}$

)^e Ref. 7

)^f Ref. 4

)^g $A_2 = \alpha_{//} - \alpha_{\perp}$

TABLE III

Definition of components of the (hyper)polarizabilities such that they are invariant under $D_{\infty h}$. Indices on the tensor components refer to tesseral (real) harmonics in Racah's normalization. Subscripts on the invariants refer to the irreps of $SO(3)$ they belong to. Components not listed are zero.

$$A_0 = \frac{1}{3}(\alpha_{11}^{00} + 2\alpha_{11}^{11})$$

$$A_2 = (\alpha_{11}^{00} - \alpha_{11}^{11})$$

$$\alpha_{11}^{11} = \alpha_{11}^{-1-1} = A_0 - \frac{1}{3}A_2$$

$$\alpha_{11}^{00} = A_0 + \frac{2}{3}A_2$$

$$B_0 = \frac{1}{5}[2\sqrt{3}(\beta_{211}^{211} + \beta_{211}^{110}) + (\beta_{211}^{000} - \beta_{211}^{011})]$$

$$B_2 = -\sqrt{3}(2\beta_{211}^{211} - \beta_{211}^{110}) + (\beta_{211}^{000} - \beta_{211}^{011})$$

$$\tilde{B}_2 = \beta_{211}^{000} + 2\beta_{211}^{011}$$

$$B_4 = -\frac{2}{7}\sqrt{3}(\beta_{211}^{211} - 4\beta_{211}^{110}) - \frac{6}{7}(\beta_{211}^{000} - \beta_{211}^{011})$$

$$\beta_{211}^{211} = \beta_{211}^{-2-1-1} = -\beta_{211}^{2-1-1} = \sqrt{3}\left(\frac{1}{3}B_0 - \frac{2}{21}B_2 - \frac{1}{30}B_4\right)$$

$$\beta_{211}^{110} = \beta_{211}^{-1-10} = \sqrt{3}\left(\frac{1}{3}B_0 + \frac{1}{21}B_2 + \frac{2}{15}B_4\right)$$

$$\beta_{211}^{011} = \beta_{211}^{0-1-1} = -\frac{1}{3}B_0 - \frac{2}{21}B_2 + \frac{1}{5}B_4 + \frac{1}{3}\tilde{B}_2$$

$$\beta_{211}^{000} = \frac{2}{3}B_0 + \frac{4}{21}B_2 - \frac{2}{5}B_4 + \frac{1}{3}\tilde{B}_2$$

$$G_0 = \frac{1}{27}(8\gamma_{1111}^{1111} + 12\gamma_{1111}^{1100} + 3\gamma_{1111}^{0000})$$

$$G_2 = \frac{1}{9}(-4\gamma_{1111}^{1111} + 3\gamma_{1111}^{1100} + 3\gamma_{1111}^{0000})$$

$$G_4 = \gamma_{1111}^{1111} - 6\gamma_{1111}^{1100} + \gamma_{1111}^{0000}$$

$$\gamma_{1111}^{1111} = \gamma_{1111}^{-1-1-1-1} = 3\gamma_{1111}^{11-1-1} = \frac{3}{35}G_4 - \frac{6}{7}G_2 + \frac{9}{5}G_0$$

$$\gamma_{1111}^{1100} = \gamma_{1111}^{00-1-1} = -\frac{4}{35}G_4 + \frac{1}{7}G_2 + \frac{3}{5}G_0$$

$$\gamma_{1111}^{0000} = \frac{8}{35}G_4 + \frac{12}{7}G_2 + \frac{9}{5}G_0$$

rationale of these definitions is given. Note that, as is usual, A_0 is proportional to the trace of the polarizability tensor, and also that A_2 is the common anisotropy factor.

The correlation effects on the quadrupole moment and the (hyper) polarizabilities are listed in Table IV for two distances: $R = 1.4$ and 3.2 bohr. As is to be expected, the closed-shell Hartree-Fock method breaks down completely for the larger distance. However, for the near equilibrium value of R the correlation effects are surprisingly small, and accordingly the SCF results, too, are not far from the accurate values quoted in Table II. No values for B_4 , G_2 and G_4 have been given for $R = 1.40$ bohr. At this distance, which is relatively close to the united atom limit, the computed hyperpolarizability components are very nearly linearly dependent. As a result of this the higher anisotropy factors become very small, so that correlation effects cannot be given with enough accuracy.

The largest correlation error occurs in the SCF quadrupole moment Q_2^0 , it is 7.5%. Since the Møller-Plesset theorem [22] applies to first order properties, but not to higher order properties, one would expect the correlation error in Q_2^0 to be smaller than in the (hyper)polarizabilities. Remarkably enough this is in contrast with the computational results.

The (hyper)polarizability derivatives (differentiated with respect to R) are given in Table V again with the influence of correlation indicated. These derivatives have been computed by a two-term expansion in the central-difference operator [21] with a step size of $\Delta R = 0.05$ bohr, thus four grid points were required: $R = 1.30, 1.35, 1.45$ and 1.50 bohr. From Table II of Kolos and Wolniewicz [4] one obtains the estimate $A_0' = 4.35$ a.u. and $A_2' = 3.38$ a.u., both values agree very well with our CI results and show that the corresponding SCF results have an error of about 8%. Note that correlation effects are not so large as to make the SCF results meaningless.

The distance dependence of the non-vanishing components of α_{11} , β_{211} and γ_{1111} is given in Table VI, VII and VIII, respectively. The same results are presented graphically in Figs. 1, 2 and 3. The anisotropy factors, having been defined in such a way that they are zero for $R = 0$ and for large R , must have one or more extrema in between. And indeed, one observes that A_2 has a maximum, B_2 , B_2 and G_4 have a maximum and a minimum, and that B_4 and G_2 have again only one extremum. Note that the phases of the tensor components have been chosen

TABLE IV

CORRELATION EFFECTS.

All quantities are expressed in a.u.

	R = 1.4			R = 3.2		
	SCF	CI	DIF. %	SCF	CI	DIF. %
Q_2^0	0.49357	0.45035	8.8	1.76477	0.95476	45.9
A_0	5.2231	5.1556	1.3	18.1731	12.1008	33.4
A_2	1.8396	1.8822	2.3	18.9249	9.3081	50.8
B_0	-109.305	-107.972	1.2	-881.581	-433.295	50.9
B_2	-57.188	-62.122	7.9	-1035.79	-317.625	69.3
\tilde{B}_2	-21.732	-22.951	5.3	-515.04	-26.190	94.9
B_4				-21.139	-91.501	76.9
G_0	321.	335.	4.2	2979.	2426.	18.6
G_2				1117.	2416.	53.8
G_4				-986	3780	126.

TABLE V

Derivatives of hyperpolarizabilities with respect to R (at $R = 1.40 a_0$).
All quantities are expressed in a.u.

	SCF	CI	Dif. (%)
A_0'	4.76	4.33	9.0
A_2'	3.64	3.49	4.1
B_0'	-176	-158	10.2
B_2'	-114	-115	0.9
\tilde{B}_2'	-56	-53	5.3
G_0'	574	550	4.2

TABLE VI

Distance dependence of the isotropic polarizability A_0 and the anisotropy factor A_2 . See Table III for the definition of these quantities. All values are expressed in a.u.

R	A_0	A_2	R	A_0	A_2
0.20	1.5399	0.0300	3.00	11.8100	9.1175
0.40	1.8844	0.0958	3.20	12.1008	9.3081
0.60	2.3490	0.2298	3.40	12.1974	9.1569
0.80	2.9153	0.4540	3.60	12.1236	8.6998
1.00	3.5765	0.7911	3.80	11.9188	8.0082
1.20	4.3274	1.2602	4.00	11.6284	7.1711
1.30	4.7315	1.5530	4.20	11.2956	6.2743
1.35	4.9413	1.7127	4.40	10.9556	5.3884
1.40	5.1556	1.8822	4.60	10.6328	4.5619
1.45	5.3743	2.0612	4.80	10.3417	3.8223
1.50	5.5969	2.2500	5.00	10.0887	3.1806
1.60	6.0533	2.6556	5.20	9.8747	2.6360
1.80	7.0010	3.5734	5.40	9.6973	2.1816
2.00	7.9731	4.6073	5.60	9.5526	1.8066
2.20	8.9350	5.7073	5.80	9.4359	1.4995
2.40	9.8445	6.7999	6.00	9.3427	1.2494
2.60	10.6551	7.7945	∞	9.0014	0.0
2.80	11.3219	8.5951			

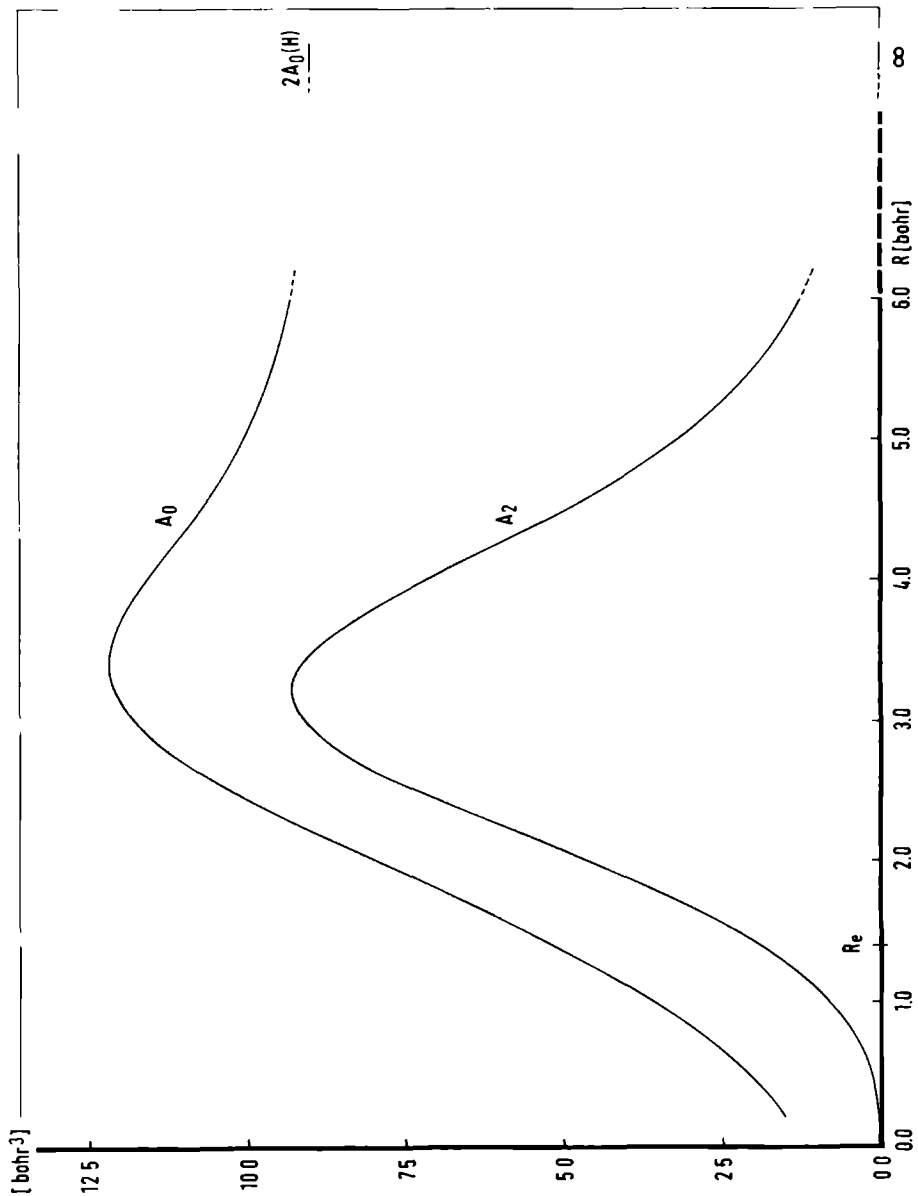


Fig. 1. The isotropic (A_0) and anisotropic (A_2) component of the dipole-field polarizability as a function of the H-H distance.

TABLE VII

Distance dependence of the invariant components of the hyperpolarizability tensor β_{211} . See Table III for the definition of the quantities. All values are expressed in a.u.

R	B_0	B_2	\tilde{B}_2	B_4
0.20	-12.101	-7.055	-0.556	-0.790
0.40	-17.544	-9.458	-0.980	-1.000
0.60	-26.301	-13.453	-2.069	-1.203
0.80	-39.023	-19.630	-4.253	-1.371
1.00	-56.468	-28.920	-8.029	-1.507
1.20	-79.298	-42.593	-14.034	-1.599
1.30	-92.888	-51.536	-18.093	-1.618
1.35	-100.242	-56.611	-20.419	-1.616
1.40	-107.972	-62.122	-22.951	-1.613
1.45	-116.076	-68.077	-25.695	-1.608
1.50	-124.551	-74.497	-28.648	-1.603
1.60	-142.587	-88.775	-35.184	-1.604
1.80	-182.687	-123.180	-50.538	-1.780
2.00	-227.120	-164.774	-67.924	-2.615
2.20	-273.893	-211.182	-84.959	-5.072
2.40	-320.118	-257.829	-97.841	-10.673
2.60	-362.300	-298.146	-101.863	-21.169
2.80	-396.897	-325.064	-92.552	-38.048
3.00	-421.055	-332.514	-67.176	-61.852
3.20	-433.295	-317.625	-26.190	-91.501
3.40	-433.950	-281.968	26.161	-124.077
3.60	-425.052	-231.252	82.747	-155.417
3.80	-409.676	-173.504	135.658	-181.405
4.00	-391.082	-116.591	178.467	-199.177
4.20	-372.021	-66.402	207.601	-207.672
4.40	-354.393	-26.127	222.447	-207.466
4.60	-339.227	3.445	224.737	-200.189
4.80	-326.874	23.179	217.184	-187.880
5.00	-317.240	34.767	202.870	-172.504
5.20	-309.993	40.133	184.540	-155.691
5.40	-304.721	41.077	164.373	-138.671
5.60	-301.007	39.110	143.950	-122.281
5.80	-298.482	35.402	124.317	-107.047
6.00	-296.840	30.808	106.106	-93.246
∞	-297.414	0.0	0.0	0.0

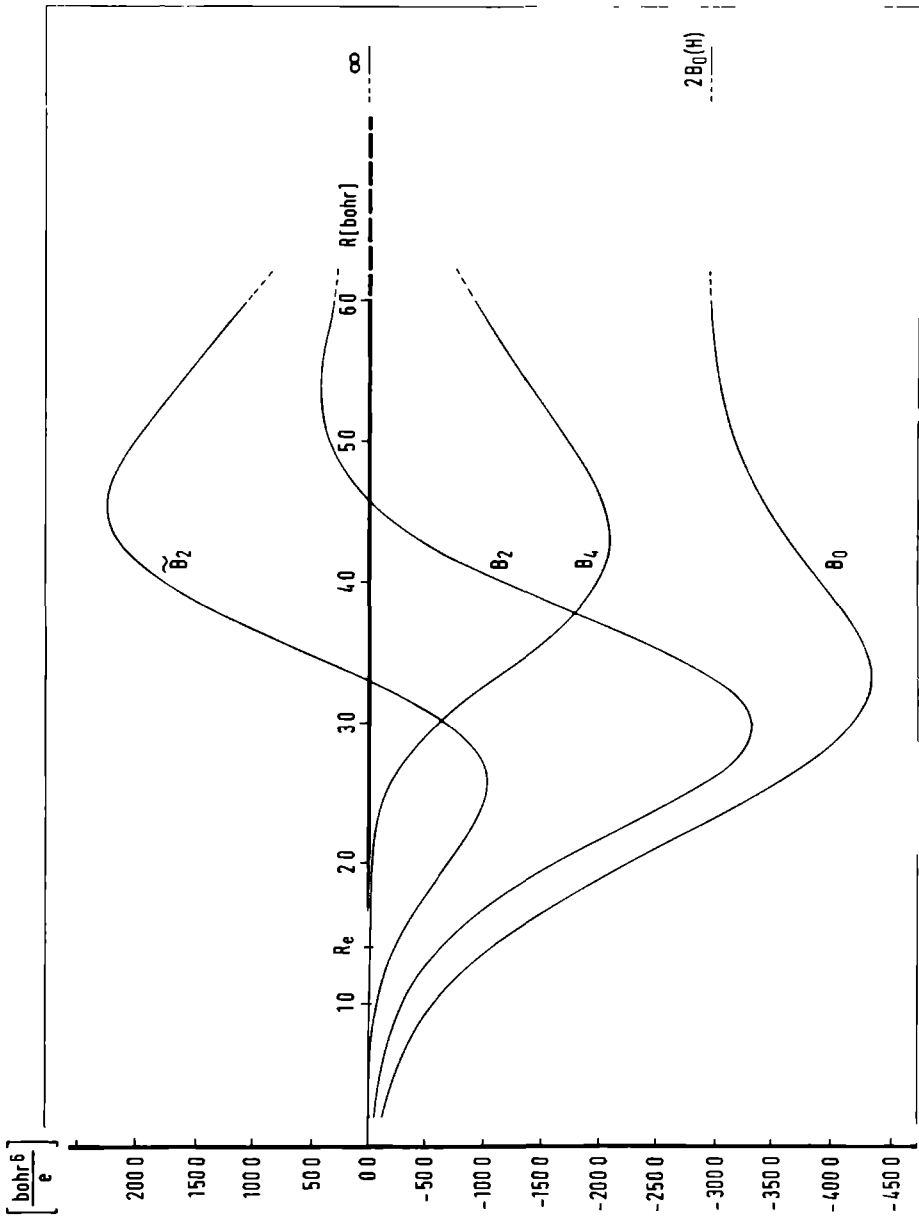


Fig. 2. The isotropic (B_0) and anisotropic (B_2 , \tilde{B}_2 and B_4) components of the quadrupole-(field)² hyperpolarizability as a function of the H-H distance.

TABLE VIII

Distance dependence of the invariant components of the hyperpolarizability tensor χ_{1111} . See Table III for the definition of the quantities. All values are expressed in a.u.

R	G ₀	G ₂	G ₄
0.20	28.2	4.05	-6.48
0.40	43.1	5.63	-8.25
0.60	68.4	8.49	-10.0
0.80	107	13.2	-11.7
1.00	162	20.7	-13.8
1.20	237	32.5	-16.8
1.30	283	40.8	-18.6
1.35	308	45.7	-19.5
1.40	335	51.2	-20.4
1.45	363	57.4	-21.2
1.50	393	64.4	-21.9
1.60	457	80.9	-22.5
1.80	605	128	-15.9
2.00	779	203	18.1
2.20	981	325	116
2.40	1213	517	331
2.60	1477	809	751
2.80	1773	1224	1452
3.00	2095	1770	2475
3.20	2426	2416	3780
3.40	2739	3094	5243
3.60	3000	3711	6649
3.80	3180	4180	7790
4.00	3266	4444	8511
4.20	3260	4490	8770
4.40	3177	4347	8594
4.60	3040	4064	8091
4.80	2872	3693	7377
5.00	2693	3284	6562
5.20	2516	2872	5715
5.40	2351	2479	4906
5.60	2201	2120	4162
5.80	2070	1800	3499
6.00	1956	1522	2915
∞	1394	0.0	0.0

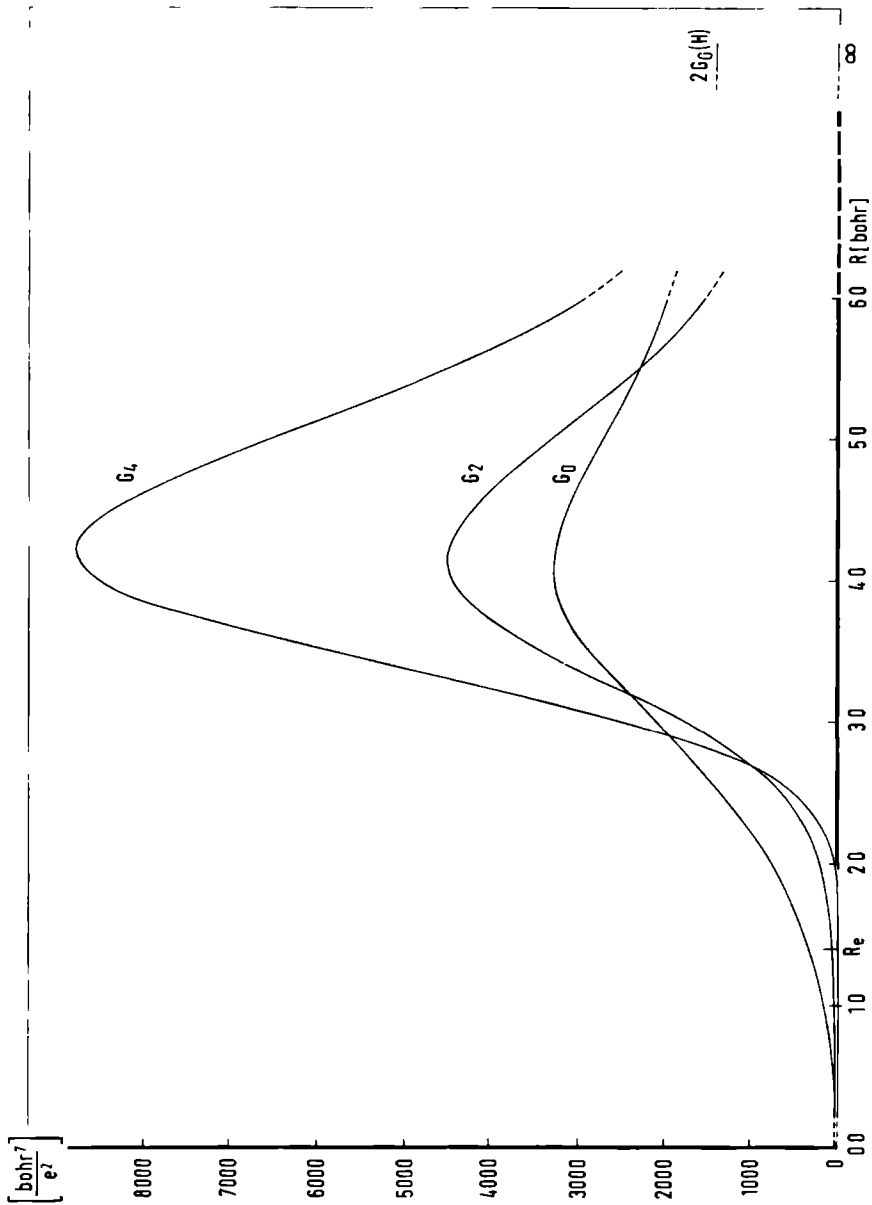


Fig. 3. The isotropic (G_0) and anisotropic (G_2 and G_4) components of the dipole-(field)³ hyperpolarizability as a function of the H-H distance.

arbitrary, so it is not physically significant whether an extremum is a maximum or a minimum.

In the region of the extrema, between 3 and 5 bohr, the deviation of H_2 from spherical symmetry is the largest, the hydrogen molecule resembles an atom the least in that region. One also sees illustrated in the figures that the hydrogen molecule in its equilibrium structure is fairly spherical: $R = 1.4$ is relatively close to the united atom limit. The three isotropic (hyper)polarizability curves show more or less the same qualitative behaviour as a function of R . All three go through an extremum. Kolos and Wolniewicz [4] attribute the occurrence of the extremum in A_0 to an expansion in the electronic charge cloud, which arises when two hydrogen atoms approach each other from infinity. This expansion is followed by a contraction when the hydrogen atoms penetrate deeper into each other. This seems a likely explanation for the behaviour of B_0 and G_0 as well.

4. Conclusions

The most important conclusion of this work is that the finite field LCAO-SCF-CI method, which is based on orbitals, is capable of yielding results which are very near the accurate values obtained from explicitly correlated functions. This gives hope for applications to larger molecules, where at present only orbital approaches are feasible.

Furthermore we have found that correlation effects for H_2 in its equilibrium structure are not predominant. (The situation is of course different for larger bond distances, where the restricted Hartree-Fock approach yields meaningless results). Admittedly, many of the more interesting correlation effects, such as the coupling of pair clusters and the occurrence of higher clusters [23], are absent in two-electron systems, and their importance for polarizability calculations remains to be assessed, but nevertheless our results suggest that it is necessary to spend much attention on the SCF calculations before CI is contemplated. The choice of an A.O. basis is of crucial importance; the errors introduced by an inadequate basis cannot be corrected by a CI calculation, and may easily exceed the size of the correlation effects. In this connection it may be pointed out that the present results are obtained with an extremely large orbital/electron ratio. Application of the same ratio to a simple molecule as N_2

implies the use of a 406-dimensional A.O. basis. Although the use of such a very large basis can hopefully be avoided by a careful optimization, it remains probably true that basis sets which are large by today's standards, are required for reliable SCF computation of (hyper)polarizabilities. This will make the calculation of the remaining correlation errors also a challenging task.

APPENDIX

On the symmetry adaptation of hyperpolarizability tensors

In this appendix we will mention the group theoretical considerations which have led to the definition of the quantities given in Table III.

By definition the components of a (hyper)polarizability tensor span a symmetrized outer product of irreducible representation (irreps) of the full rotation-reflection group $O(3)$. These irreducible representations are real and orthogonal, as we are dealing with tesseral harmonics in this work. As pointed out by Jahn [20], a logical first step in the symmetry adaptation of a tensor to a molecular symmetry group is a reduction with respect to $O(3)$. Irreducible representations of $O(3)$ which are not symmetric under permutation of equal indices do not occur in this reduction. For instance, the polarizability tensor α_{11} does not contain the $L=1$ representation, because this irrep is antisymmetric. In the same way it follows that χ_{1111} contains irreps of even L only. In the case of two or more l -values being equal to unity, it is convenient to apply the isomorphism of the tensor with the space of homogeneous polynomials in x, y and z . Thus, for example, the irreducible components of χ_{1111} are immediately written down from a table of tesseral harmonics. These irreducible components correspond to the homogeneous polynomials C_4^m ($m=-4, \dots, 4$), $\frac{1}{3} r^2 C_2^m$ ($m=-2, \dots, 2$), and $\frac{1}{9} r^4$. In the case of β_{211} we first adapt by this correspondence the second and third index to $O(3)$, and then by vector coupling adapt the remaining indices to $O(3)$.

The second step in the symmetry adaptation is the subduction of the $O(3)$ irreps to the point symmetry group G of the molecule. It is easy to see that only the tensor components which span the totally symmetric representation of G are non-vanishing, all the other components are zero. In our case of $D_{\infty h}$ symmetry the components adapted to $O(3)$ are automatically adapted to the point group of the molecule,

i.e. if we choose the bond along the z axis, and so only the components belonging to Σ_g^+ survive. In our case of gerade representations the tensor components of even L and with M equal to zero belong to this irrep. These components are given explicitly in Table III.

An additional advantage of the preliminary adaptation to O(3) is that in the case of a symmetry raising from $D_{\infty h}$ to O(3), which occurs in the united as well as in the separated atom limit of a diatomic, the only non-vanishing $D_{\infty h}$ -invariants are those belonging to the L=0 irrep of O(3). The other invariants are therefore genuine anisotropy factors.

Finally it must be remarked that the factors multiplying the resulting invariants cannot be determined by group theory. We have made choices which make the expressions look simple.

Acknowledgements

We are most grateful to Dr. F. Mulder for suggesting the problem and valuable discussions. We want to thank U. Giese and F. de Vries of the university computer center for valuable help with the use of the VM/CMS system. Also we express our thanks to Prof. A. van der Avoird for reading the manuscript.

References

1. M.P. Bogaard and B.J. Orr in: MTP International Rev. of Science, Physical Chemistry, Series Two, Vol. 2, Ed. A.D. Buckingham, (Butterworths, London, 1975).
2. R. McWeeny and B.T. Sutcliffe, Methods of Molecular Quantum Mechanics (Academic Press, London, 1969).
3. I. Shavitt in: Methods of Electronic Structure Theory, Ed. H.F. Schaefer, (Plenum Press, New York, 1977).
4. W. Kolos and L. Wolniewicz, J. Chem. Phys. 46, 1426 (1967).
5. J.D. Poll and L. Wolniewicz, J. Chem. Phys. 68, 3053 (1978).
6. D.M. Bishop and L.M. Cheung, Phys. Rev. A20, 1310 (1979).
7. D.M. Bishop and L.M. Cheung, J. Chem. Phys. 72, 5125 (1980).
8. H.D. Cohen and C.C.J. Roothaan, J. Chem. Phys. 43, S34 (1965).
9. C.G. Gray and B.W.N. Lo, Chem. Phys. 14, 73 (1976).
10. A.D. Buckingham, Adv. Chem. Phys. 12, 107 (1967).
11. S. Huzinaga, J. Chem. Phys. 42, 1293 (1965).
12. F. Mulder, private communication. We thank dr. Mulder for putting at our disposal this basis, which is a condensed version of the fully optimized basis of F. Mulder, A. van der Avoird and P.E.S. Wormer, Mol. Phys. 37, 159 (1979).

13. W. Kolos and C.C.J. Roothaan, *Rev. Mod. Phys.* 32, 219 (1960).
14. R.M. Berns and P.E.S. Wormer, (1979).
15. C.M. Reeves, *Comm. A.C.M.* 9, 276 (1966).
16. M. Yoshimine, IBM Report RJ555, IBM Research San José, California (1969).
17. I. Shavitt, The subroutine SIMEIG (1978).
We thank dr. Shavitt for making this program available to us.
18. V.R. Saunders, ATMOL 3 4-index transformation program, Daresbury Research Lab. Warrington, U.K.
19. R.M. Berns and P.E.S. Wormer, to be published.
20. H.A. Jahn, *Acta Cryst.* 2, 30 (1949).
21. C.-E. Fröberg, *Introduction to Numerical Analysis*, 2nd ed., (Addison-Wesley, Reading, 1974).
22. C. Møller and M.S. Plesset, *Phys. Rev.* 46, 618 (1934).
23. J. Paldus, J. Cizek and I. Shavitt, *Phys. Rev.* A5, 50 (1972).

A comparison of different CI methods
for the calculation of polarizabilities:
The Be atom and the CN⁻ anion as examples[†]

R.M. Berns and P.E.S. Wormer
Institute of Theoretical Chemistry
University of Nijmegen
Toernooiveld, Nijmegen
The Netherlands

[†] Supported in part by the Netherlands Foundation for Chemical Research (SON) with financial aid from the Netherlands Organization for the Advancement of Pure Research (ZWO).

1. Introduction

Nowadays the Hartree-Fock method is used extensively -not only by theorists, but also by experimentalist- for the calculation of molecular properties, such as bonding distances and angles, dipole and higher moments, polarizabilities, etc. In the case of closed-shell molecules in their equilibrium geometry, the Hartree-Fock model is fairly reliable, giving errors usually less than 10%. However, in certain situations the independent particle model is known to yield much larger errors. One such case is exemplified by the Be atom, where the Hartree-Fock state $(1s)^2 (2s)^2$ gives a poor description of the ground state because of the near degeneracy of the 2s- and the 2p-orbitals. Clearly, the configuration $(1s)^2 (2p)^2$ mixes strongly with the Hartree-Fock ground state. This gives rise to uncommonly large correlation effects on the energy and other properties of the Be atom.

A notorious example of a complete breakdown of the restricted Hartree-Fock model regards the dissociation of bonds into open-shell fragments. Basically, one has to distinguish two different errors here. One is introduced by the restricted Hartree-Fock method, which can only describe electron configurations where none of the orbitals are singly occupied. This introduces artificial charge transfer into the wavefunction. The unrestricted Hartree-Fock method corrects this deficiency, as does the CI (Configuration Interaction) method with an appropriately chosen expansion basis. The second error is adherent to a model based on orbitals: the raising of spatial symmetry occurring during the breaking of a bond is not reflected in the orbital energy spectrum. Even in the very elaborate MCSCF (Multi-Configuration Self-Consistent Field) calculations of Roos et al. on the dissociation of N_2 [1], the p-orbitals do not converge to three-fold degenerate sets, as they should in the case of non-interacting nitrogen atoms.

In the case where the Hartree-Fock method fails, one has to apply other methods for the calculation of wave functions. One of the methods most often used to improve upon the independent particle model is the Configuration Interaction (CI) method. In this method an orbital loses its physical meaning as (the square root of) a one-particle density. However, the concept of an orbital being such a fruitful one, one often calculates orbitals from the CI wave func-

tion: the so-called natural orbitals. These are defined [2] as the eigenvectors of the one-particle density matrix, and give, when employed in an independent particle type wave function, the best possible approximation to the CI state from which they are derived [2].

A common procedure, first introduced by Bender and Davidson [3] is to iterate the CI calculations, using as the input orbitals the natural orbitals obtained in the previous step. One iterates until finally the natural orbitals entering the CI calculation are the same as those calculated. One then speaks of INO's (Iterative Natural Orbitals).

In this chapter we will investigate the applicability of the CI-INO method for the determination of dipole polarizabilities. These polarizabilities are obtained from the calculated dipole moments of atoms or molecules placed in small but finite electric fields. The finite field method has proved to be an accurate method, not only for second order polarizabilities but also for higher order polarizabilities [4].

The procedure has been applied to the Be atom and the results are compared with full CI calculations, which give exact solutions within the given orbital basis. Furthermore, calculations have been started on a study of the CN^- anion, or more specifically on a study of its dipole polarizability as a function of the interatomic distance. Here we have an example of the breaking of a bond into open-shell atoms. The choice of CN^- has been motivated by calculations in this institute on the potential energy surface of the KCN molecules [5]. The polarizability of CN^- plays an important rôle in a correct description of this surface.

Unfortunately, due to lack of time, only the equilibrium distance of CN^- has been computed in full detail, so that no conclusions regarding the bond breaking can be given.

2. Method

We have used the finite field method on the CI level, combined with the iterative natural orbital (INO) method. The CI-INO method is applied for obtaining the dipole moment of a molecule in a uniform electric field, from which the dipole polarizability is calculated. The iterative natural orbitals were first used by Bender and

Davidson [3] and later by many other workers [6-13]. By all these workers the INO method was applied for the calculation of energies. We will use it in this work for the determination of properties. For completeness we list here briefly the computational steps:

- 0) perform a Hartree-Fock calculation, this yields molecular orbitals (MO's).
- 1) transform the integrals from the atomic orbital (AO) to the MO basis.
- 2) perform a CI calculation using the Hartree-Fock orbitals as the input orbitals.
- 3) determine the natural orbitals of the ground state by diagonalizing the one-particle first order density matrix.
- 4) determine the natural orbitals on basis of AO's and calculate properties.
- 5) repeat steps (1)-(4), with the same configuration basis and use the natural orbitals of (4) as the input orbitals, until convergence.

The iteration process is stopped if the natural orbital matrix in step (3) becomes the unit matrix, because this matrix of natural orbitals can be seen as the matrix transforming the orbitals of the $(i-1)^{\text{th}}$ into those of the i^{th} iteration.

So far nothing has been said about the configuration bases considered. If we choose the CI space equal to the full CI space, no iterations are necessary, because in that case the formalism is invariant under a transformation of the orbitals. However, for most systems this is not possible, as the full configuration space is too large to be amenable. So one has to reduce the dimension of the CI expansion. There are many possibilities to do so, we have studied two common choices. The corresponding spaces are generated by:

- I) all single and double excitations from the Hartree-Fock ground state.
- II) all single excitations from a full valence space. This valence space is a full CI space and built from orbitals with the highest occupancies (in the case of INO's) or lowest orbital energies (in the case of Hartree-Fock MO's). Furthermore we have chosen for CN^- the orbitals in such a way that dissociation into the proper atomic states is possible.

Space I was chosen because this space gives good results for the dipole polarizabilities and is widely used. The first cycle in the

INO method is called Single and Double CI (SDCI). Space II has the main advantage of being able to describe the proper asymptotic behaviour of a diatomic wave function for increasing internuclear separations. INO-CI with this basis can be regarded as an extension of the full valence super-CI MCSCF method of Roos and coworkers [1]. The space contains higher than double excitations relative to the Hartree-Fock ground state. The first cycle in the INO method with basis II is equivalent to Schaefer's [7] FOCI (First Order CI) method.

3. Results

Because the INO method has not been used previously for the calculation of polarizabilities, the method was first tested on the Be atom, where full CI results can be obtained. Additionally the results of the two CI expansions can be compared. In the case of CN^- comparison with a full CI result is not possible.

3.1. The Be atom

The atomic basis set used was a Be (10,4,1/7,4,1) CGTO set. The basis has been derived from the Van Duijneveldt 9s-6s basis [14]. We have extended the basis with a s-GTO with an exponent of 0.02. The uncontracted p- and d- functions have exponents of 6.3, 0.4, 0.141, 0.05 and 0.1, respectively. The ATMOL3 package [15] is used for performing the integral, Hartree-Fock and four-index transformation calculations. The CI calculations are performed by the use of a conventional CI program developed in this institute [16], and based on bonded functions.

The dimensions of the space I and II, generated by the basis set of 25 contracted orbitals, are 1128 and 850, respectively. No spatial symmetry has been considered. The valence space, which was built from the first two s-orbitals and the first p-set, consists of 50 configurations. The full CI space derived from 25 orbitals has the dimension of 9415 (reduced by C_{2v} symmetry). The results of the calculations are given in table 1. From table 1 we see that INO-I is slightly better than INO-II. The INO-I does not change much during the iteration process, whereas the INO-II result reduces drastically during the iteration. Note that the FOCI (first cycle) result for the dipole moment is off by a factor of almost two. We

Table 1

Results for Be-atom

Space I			Space II		
	$E(F=10^{-3})$	α		$E(F=10^{-3})$	α
SCF	-14.57243124	44.964	SCF	-14.57243124	44.964
SDCI	0.07808	37.877	FDCI	0.02979	65.285
INO: 2	0.07811	37.133	INO: 2	0.04222	60.522
3	0.07811	37.031	3	0.04415	45.753
4	0.07811	37.019	4	0.04438	39.575
5	0.07811	37.017	5	0.04441	36.877
			6	0.04441	35.886
			7	0.04442	35.530
			8	0.04442	35.402
FULL CI	0.08109	36.525	FULL CI	0.08109	36.525

also see an increase in energy (for INO-I only) after a few cycles, an effect which has been reported by other authors [9,11] as well. The number of diagonalization iterations increases considerably during the INO iterations (from 16 to 89) for the same accuracy in the eigenvector. It is likely that this is due to the occurrence of larger off-diagonal elements in the CI matrix [17].

3.2. The CN⁻ ion

The atomic basis sets are a C(11,6,2/6,3,2) and N(11,6,2/6,3,2) CGTO sets. The basis sets are the same as used in Ref. [5] for the calculation of the interaction potential of KCN. The internuclear distance was kept at $2.186a_0$, which is the Hartree-Fock equilibrium distance [5]. During the CI calculations the three MO's with the lowest orbital energies are kept frozen. The polarizability tensor was obtained by applying a field under an angle of 45° to the axis and with a field strength of $10^{-4}\sqrt{2}$. The dimensions of the spaces I and II, generated by the 54 contracted orbitals, are 9487 and

Table 2

Results for CN^- -ion with space I

	$E(F=0)$	$\mu_{//}(F=0)$	$E(F=10^{-4})$	$\alpha_{//}$	α_{\perp}
SCF	-92.33854733	0.215129	-92.33856907	27.3	17.696
SDCI	0.23018	0.07021	0.23019	27.6	18.245
INO: 2	0.22951	0.08134	0.22952	27.7	18.395
3	0.22933	0.08396	0.22933	27.8	18.452
4	0.22929	0.08455	0.22929	27.8	18.475
5	0.22928	0.08468	0.22928	27.8	18.483
6	0.22928	0.08470	0.22928	27.8	18.487

17748, respectively. The valence space was generated by the seven orbitals following the three frozen orbitals, and consists of 230 configurations. During the generation of these spaces C_s point group symmetry has been taken into account (this is the only symmetry remaining when CN^- is in the field). The utilization of symmetry reduces the dimensions of the different CI spaces, but at the same time introduces a technical difficulty. For it can happen that during the INO iterations NO's of different spatial symmetry become degenerate, i.e. have the same occupation number. In such a case the eigenvectors of the first order density matrix are not automatically adapted to the spatial symmetry (in this case C_s), and a symmetry projection followed by a renormalization of the NO's becomes necessary. As already noticed in the calculations on Be the required number of diagonalization iterations increases during the INO iterations. The final results are given in table 2 and 3.

4. Conclusions

In all cases considered in this work the final INO result derived from the CI space I is not much different from the single and double CI result obtained during the first cycle of the INO procedure. This is true for the correlation energy as well as for the dipole moment (and hence for the polarizability). So, it seems un-

Table 3

Results for CN⁻-ion with space II

	E(F=0)	$\mu_{//}(F=0)$	E(F=10 ⁻⁴)	$\alpha_{//}$	α_{\perp}
SCF	-92.33854733	0.215129	-92.33856907	27.3	17.696
VALCI) ^a	0.01939	0.10403			
FDCI	0.08330	0.16284	0.08318	53.9	224.030
INO: 2	0.14135	0.05985	0.14128	50.0	174.359
3	0.15529	0.04860	0.15532	31.6	69.264
4	0.15749	0.05690	0.15752	28.3	34.330
5	0.15781	0.06205	0.15783	27.8	23.388
6	0.15786	0.06448	0.15788	27.6	20.027
7	0.15787	0.06568	0.15788	27.5	18.932
8	0.15785	0.06631	0.15787	27.5	18.560
9	0.15786	0.06666	0.15787	27.5	18.429
10	0.15786	0.06694	0.15787	26.6	18.382
11	0.15786	0.06700	0.15787	27.0	18.365
12	0.15786	0.06704	0.15787	27.2	18.358
13	0.15786	0.06708	0.15787	27.2	18.356
14	0.15786	0.06709	0.15787	27.3	18.355

) ^a Result derived from H.F. orbitals and valence space only

necessary to have a SDCI calculation be followed by an INO analysis, which is costly and time consuming.

However, if one is interested in dissociative processes SDCI is not an adequate method, because the corresponding wave function does not dissociate into the correct atomic states and the SDCI energy is not an extensive (in the thermodynamic sense) property. It can be expected that a CI method based on space II is much better suited to describe the dissociation of a diatomic molecule, because the CI expansion includes the full valence space. But, the present calculations show clearly that in that case the INO iterations are a necessity. The polarizability after the first cycle can differ from the final result by more than an order of magnitude! This makes this method very expensive.

In the case of the Be atom the two INO polarizabilities are not far from the full CI results, with the space I value being somewhat closer. The full CI value itself is in remarkably good agreement with the nearly exact value $36.58 a_0^3$ of Sims and Rumble [18]. As is to be expected from the near degeneracy of the 2s- and 2p-orbitals, the influence of correlation on the polarizability is large (18.8%). This is different for the CN^- anion where the correlation effects on the polarizability are extremely small. If one compares the FFSCF (Finite Field SCF) results with the FFSCF results of Gready et al. [19] ($\alpha_{//} = 30.05$, $\alpha_{\perp} = 19.975 a_0^3$), one must conclude that the actual choice of atomic orbital basis is of more importance for the final result than the inclusion of correlation effects.

References

1. B.O. Roos, P.R. Taylor and P.E.M. Siegbahn, Chem. Phys. 48, 157 (1980).
2. A.J. Coleman, Rev. Mod. Phys. 35, 668 (1963).
3. C.F. Bender and E.R. Davidson, J. Chem. Phys. 70, 2675 (1966).
4. R.M. Berns and P.E.S. Wormer, Submitted for publication to Mol. Phys., reprinted as chapter IX of this thesis.
5. P.E.S. Wormer and J. Tennyson, J. Chem. Phys., to appear September 1981.
6. C.F. Bender and E.R. Davidson, J. Chem. Phys. 47, 4972 (1967).
7. H.F. Schaefer III, J. Chem. Phys. 54, 2207 (1971).
8. C.F. Bender and E.R. Davidson, Phys. Rev. 183, 23 (1969).

9. E.R. Davidson in: *The World of Quantum Chemistry* (R. Daudel and B. Pullman, eds.), p. 17, Reidel, Dordrecht, Holland (1974).
10. S.R. Langhoff and E.R. Davidson, *Int. J. Quantum Chem.* 7, 759 (1973).
11. I. Shavitt in: *Energy, Structure and Reactivity* (D.W. Smith and W.B. McRae, eds.), p. 188, Wiley, New York (1973).
12. H.F. Schaefer III, R.A. Klemm and F.E. Harris, *Phys. Rev.* 181, 137 (1969).
13. H.F. Schaefer III and C.F. Bender, *J. Chem. Phys.* 55, 1720 (1971).
14. F.B. van Duijneveldt, IBM Report RJ 945, (1971).
15. ATMOL3, V.R. Saunders and M.F. Guest, Computational Science Group, Science Research Council, Daresbury Laboratory, Daresbury, Warrington, U.K.
16. R.M. Berns and P.E.S. Wormer (1979).
17. I. Shavitt, B.J. Rosenberg and S. Palalikit, *Int. J. Quantum Chem.* S10, 33 (1976).
18. J.S. Sims and J.R. Rumble, *Phys. Rev.* A8, 2231 (1973).
19. J.E. Gready, G.B. Backskay and N.S. Hush, *Chem. Phys.* 31, 467 (1978).

Voor de bestudering van moleculaire gassen, vloeistoffen en vaste stoffen is kennis van de intermoleculaire potentiaal van essentieel belang. Deze intermoleculaire potentiaal is een functie van de afstand tussen de moleculen en de oriëntatie van de moleculen ten opzichte van elkaar.

In het verleden, werd de potentiaal uitsluitend bepaald uit experimentele gegevens, door het aannemen van een modelpotentiaal (Lennard-Jones of Buckingham (atoom-atoom) type), met een beperkt aantal parameters zodanig gekozen dat de experimentele gegevens goed gereproduceerd werden. In een aantal gevallen leidde deze procedure tot potentialen die een aantal experimentele gegevens goed weergaven, maar andere gegevens welke niet in de fit zijn meegenomen slecht. Dit kan veroorzaakt worden door een slechte vorm van de potentiaal, het experiment is gevoelig voor een ander gebied van de potentiaal dan de gebruikte metingen of door tekortkomingen in de gebruikte modellen voor de interpretatie van de experimenten. Om dit probleem op te lossen is het noodzakelijk om meer informatie te verkrijgen uit andere bronnen.

Tegenwoordig is het mogelijk om redelijk nauwkeurige intermoleculaire potentialen te verkrijgen, door de Schrödinger-vergelijking benaderd op te lossen, door toepassing van zogenaamde ab initio quantummechanische methoden. Dit is niet alleen een gevolg van theoretische verbeteringen van de quantum-chemische methoden, maar ook van het toegenomen vermogen van moderne computers. Toch liggen systemen zoals N_2-N_2 en $C_2H_4-C_2H_4$ nog aan de grens van de mogelijkheden.

In dit proefschrift wordt de Schrödingervergelijking toegepast in de Born-Oppenheimer benadering: de electronische vergelijking wordt opgelost voor een vaste geometrie van de kernen; variatie van de geometrie van de kernen levert de intermoleculaire potentiaal op. Het is nu mogelijk om de modelpotentiaal parameters te verkrijgen door het aanpassen van een modelpotentiaal aan de resultaten van de ab initio berekeningen voor een aantal oriëntaties en afstanden (voor stikstof en etheen resp. in hfdst. II en V). Vervolgens kunnen de potentialen gebruikt worden in bijvoorbeeld roosterdynamica berekeningen aan moleculaire kristallen, om vergelijking met experimentele gegevens mogelijk te maken (hfdst. IV, V en VI).

Deze (atoom-atoom) model potentialen hebben het nadeel dat ze moeilijk systematisch verbeterd kunnen worden. Een andere analytische voorstelling van de intermoleculaire potentiaal, de sferische expansie,

heeft dit nadeel niet. De potentiaal wordt geëxpandeerd in hoekfuncties, die afhangen van de oriëntaties van de moleculen; de expansiecoëfficiënten zijn alleen afhankelijk van de intermoleculaire afstand. Deze (Fourier) coëfficiënten kunnen geschreven worden als integralen van de intermoleculaire potentiaal vermenigvuldigd met de hoekfuncties en ze kunnen berekend worden met behulp van numerieke integratie technieken (Gauss type integraties) (voor het N_2 -dimeer in hfdst. II en III).

De ab initio berekeningen zijn erg duur, zelfs voor vrij kleine systemen (voor de $(N_2)_2$ potentiaal: 3 uren op IBM 370/158 per geometrie). Evaluatie van goedkopere, maar nog wel nauwkeurige methoden is daarom belangrijk voor het berekenen van de potentialen van grotere systemen. Een van deze methoden, de zogenaamde Gordon-Kim methode, die gebaseerd is op uitdrukkingen uit de electronengas theorie voor atomen en moleculen, is getest op het N_2 -dimeer (hfdst. III).

Voor de verklaring van een aantal verschijnselen is niet alleen de intermoleculaire potentiaal belangrijk, maar ook het effect van moleculaire botsingen op andere eigenschappen. Bijvoorbeeld bij de interpretatie van botsingsgeïnduceerde infrarood absorptiespectra (CIA) van gassen met hoge dichtheid, is kennis van het dipoolmoment nodig. Dit dipoolmoment ontstaat wanneer twee of meer verschillende of meer dan twee soortgelijke atomen met elkaar wisselwerken. Evenals de intermoleculaire potentiaal is de dipool een functie van de intermoleculaire afstand en de oriëntaties van de moleculen. De interactiedipool is nog moeilijker te berekenen dan de potentiaal; daarom kunnen alleen kleine systemen beschouwd worden. In hoofdstuk VII wordt de interactiedipool berekend van het He- H_2 systeem. Naar men aanneemt is het de botsingsgeïnduceerde IR absorptie in dit systeem die verantwoordelijk is voor het broeikas-effect dat wordt waargenomen op zware planeten met een atmosfeer die grotendeels uit helium en waterstof bestaat.

Voor grotere afstanden tussen de moleculen kan de potentiaal benaderd worden door de multipoolexpansie. De termen in deze expansie hangen alleen af van de eigenschappen van de afzonderlijke moleculen: permanente en overgangs-multipoolmomenten en polariseerbaarheden. Met andere woorden, men kan nu het probleem reduceren tot de berekening van de eigenschappen van de monomeren. De berekening van deze eigenschappen wordt meestal uitgevoerd op Hartree-Fock ("independent particle") niveau. In een aantal gevallen echter, zijn de resultaten niet nauwkeurig genoeg om een betrouwbare potentiaal te construeren en zijn er dus verfijndere methoden nodig.

Een van deze methoden om het effect van electronencorrelatie te bepalen is de Configuratie Interactie (CI) methode. De golf functie wordt geschreven in termen van (spin aangepaste) configuratiefuncties en de variationele oplossingen van de Schrödinger vergelijking worden verkregen door diagonalisatie van de Hamiltoniaan-matrix. Voor grote moleculen wordt de methode gecompliceerd. Bijvoorbeeld, niet alle spin-symmetrie coëfficiënten, nodig voor de constructie van de H-matrix uit de moleculaire integralen, passen tegelijkertijd in het centrale geheugen van de computer, evenmin als de moleculaire integralen. Ook past niet de volledige H-matrix in het centrale geheugen, gedurende de constructie en diagonalisatie, en het berekenen van alle eigenwaarden en eigenvectoren is onmogelijk. Dit impliceert dat bijzondere methoden nodig zijn. In hoofdstuk VIII is een computerprogramma beschreven, dat speciaal ontworpen is voor grote CI berekeningen.

Als een toepassing van de CI methode, zijn de hyperpolariseerbaarheden van waterstof berekend als functie van de internucleaire afstand (in hoofdstuk IX). De berekening is uitgevoerd op het "full CI" niveau (d.w.z. alle singlet configuraties, die geconstrueerd kunnen worden binnen een gegeven orbital basis, zijn meegenomen). Omdat blijkt dat de hyperpolariseerbaarheden zeer gevoelig zijn voor de kwaliteit van de gebruikte basis, zijn grote basissets nodig, waardoor de berekening zelfs voor dit twee electronensysteem gecompliceerd wordt.

Voor meer-electronen systemen wordt een "full CI" berekening onuitvoerbaar: De expansie van de golf functie moet bekort worden. Dit kan bereikt worden door het gebruiken van een betere basis ("natural orbitals") of door het verkleinen van de configuratieruimte of beide, elk met voor- en nadelen. In hoofdstuk X worden er twee onderzocht: De Iterative Natural Orbital (INO) methode met een configuratie ruimte die alle enkele en dubbele excitaties bevat vanuit de Hartree-Fock grondtoestand en INO met een "first-order" golf functie (bevat alle enkele excitaties vanuit een volledige CI ruimte, geconstrueerd uit de valentie orbitalen). De methoden worden getest op het Be-atoom, waar de electronencorrelatie effecten op de polariseerbaarheid relatief groot zijn. De methoden worden daarna gebruikt om de polariseerbaarheid van het CN-ion te berekenen.

C U R R I C U L U M V I T A E

De schrijver van dit proefschrift werd op 2 juni 1954 te Heerlen geboren. Na het volgen van het basisonderwijs werd in 1966 begonnen met de HBS-B opleiding te Kerkrade waarvan het eindexamen (cum laude) op 19 mei 1971 behaald werd. In datzelfde jaar werd een begin gemaakt met de chemiestudie aan de Katholieke Universiteit te Nijmegen. Het kandidaatsexamen (S4) en doctoraalexamen theoretische chemie, met bijvakken capita uit de natuurkunde en capita uit de wiskunde, werden respectievelijk op 18 februari 1974 en 27 juni 1977 behaald. Het laatstgenoemde doctoraal bijvak werd grotendeels aan de TH te Eindhoven (1975) verricht. In het kader van het hier beschreven promotieonderzoek op de afdeling Theoretische Chemie te Nijmegen volgde een aanstelling als wetenschappelijk medewerker, eerst in dienst van de KUN (1-9-77 tot 1-9-78) en vervolgens in dienst van SON/ZWO (sinds 15-10-1978).

STELLINGEN

I

Brooks en Schaefer vinden bij uitbreiding van de valentieorbital set in hun CI berekeningen onfysische resultaten. In tegenstelling tot de door hen geopperde veronderstelling dat de vergroting van de valentie set de oorzaak zou zijn, moet dit worden toegeschreven aan het gebruik van de INO methode

B R Brooks en H F Schaefer, J Am Chem Soc , **101**, 307 (1979)

II

De aanduiding atoomenergie op antikernenergiestickers getuigt van weinig inzicht in de fysica, maar misschien wel van enig inzicht in de psychologie

III

De analytische uitdrukking voor de vermogensafhankelijkheid van de absorptie van CO₂-laser straling door SF₆-clusters, zoals die door Geraedts et al wordt gegeven, is onbevredigend omdat deze uitdrukking met geen acceptabel fysisch absorptiemodel correspondeert.

J Geraedts, S Setiadi, S Stolte en J Reuss,
Chem Phys Letters, **78**, 277 (1981)

IV

De door Anderson gebruikte methode voor het berekenen van intermoleculaire potentialen is zowel methodologisch als fysisch onverantwoord

A B Anderson, J Chem Phys , **64**, 2266 (1976)

V

De door Schaefer en Meyer getabelleerde waarden voor de C₅ coëfficiënten van het H₂-H₂ systeem moeten op theoretische gronden onjuist zijn

J Schaefer en W Meyer, J Chem Phys , **70**, 344 (1979)

VI

Doordat Handy en Carter bij het evalueren van matrixelementen in hun variatieprobleem een te grof integratierooster toepassen, wordt het door hen beschreven stelsel expansiefuncties niet volledig gebruikt.

N C Handy en S Carter, Chem Phys Letters, **79**, 118 (1981)

VII

Een computersysteem is hoogstens zo goed als zijn documentatie

VIII

Het is onlogisch en onrechtvaardig verschil te maken tussen echtgenoten die wel of niet in dienst van een werkgever zijn geweest bij het bepalen van pensioenaanspraken bij het overlijden van een van hen.

IX

Pople et al , Purvis en Bartlett hebben onlangs onafhankelijk van elkaar een methode voor het oplossen van grote stelsels niet homogene lineaire vergelijkingen voorgesteld. Deze methoden zijn in feite onhandige versies van de „conjugate gradient” methode. Als bovengenoemde auteurs kennis hadden genomen van de standaardwerken over numerieke wiskunde, dan hadden ze zich en hun lezers veel werk kunnen besparen.

J A Pople, R Krishnan, H B Schlegel en J S Binkley,
Int J Quantum Chem , S13, 225 (1979)

G D Purvis en R J Bartlett, J Chem Phys , 75, 1284 (1981)

A S Householder, The theory of matrices in numerical analysis,
Blaisdell Publishing Company, New York, 1964
Dover, New York, 1975

J K Reid, Large sparse sets of linear equations,
Academic Press, London, 1971

J Stoer en R Bulirsch, Einführung in die Numerische Mathematik II,
Springer Verlag, Berlin, 1973

X

Zo nu en dan ontsnapt er één van de 200 000.000 FLOPS van de bij de weervoorspellingen gebruikte CRAY-1 computer naar het weerbericht.

16 oktober 1981

R.M. Berns

Ab initio calculations of
intermolecular forces and
related properties.

